universität wien

MAGISTERARBEIT

Titel der Magisterarbeit

Structural and petrological investigations along a low-angle normal fault on Kythnos, Greece

angestrebter akademischer Grad

Magistra der Naturwissenschaften (Mag.rer.nat.)

Verfasserin: Iris Lenauer, Bakk.
Studienkennzahl lt. Studienblatt: A 066 815
Studienrichtung lt. Studienblatt: Erdwissenschaften
Betreuer: Univ. Prof. Mag. Dr. Bernhard Grasemann

Wien, im Januar 2009

Contents

Acknowledgements **4**

Abstract **5**

Zusammenfassung **6**

1 Introduction **7**

2 Geological Setting **9**

2.1 Overview of the Geology of Greece 9

2.2 The Attic Cycladic Crystalline Complex 10

2.3 Geodynamic Setting 12

3 Kythnos Island **17**

3.1 Previous Works 18

3.2 Mapping Area 18

3.3 Lithostratigraphy 20

3.3.1 Metabasic Rocks 23

3.3.2 Greenschists 23

3.3.3 Ferromanganoan Metasediments 27

3.3.4 Mylonitic Marble 29

3.3.5 Albite-Gneiss 29

3.3.6 Carbonate-rich Albite-Chlorite-Sericite Schist 33

3.3.7 Impure Marble 33

3.3.8 Ultramylonitic Marble 34

3.3.9 Cataclasites 34

3.3.10 Protocataclastic Quartzites 38

3.4 Deformation History 41

3.4.1 Foliation and Lineation 41

3.4.2 Folding 44

3.4.3 Boudinage 46

3.4.4 Shear Sense Indicators and Mineral Grain Deformation 46

3.4.5 Marble-Ultramylonite Shear Zone 46

3.4.6 Brittle-Ductile Deformation 51

3.4.7 Brittle Deformation 51
3.4.8 Summary of Deformation History 53
3.5 Geochemical and Microprobe Investigations 57
3.5.1 Whole Rock Chemistry 58
3.5.2 Mineral Chemistry 61

4 Discussion **68**

5 Conclusions **70**

References **72**

Appendix **80**

Acknowledgements

First of all I would like to thank my supervisor Bernhard Grasemann for the great opportunity to work on this project. Especially his assistance in the field was an enrichment and brought many new insights. Furthermore, his support and patience is much appreciated.
A very special thanks to my friend and colleague Gabi Laner, who has accompanied me since the beginning of my studies and with whom I spent a wonderful time in the field. Without her perseverance and steady words of encouragement, work would not have been the same.
I am greatly indebted to various members of project ACCEL, who devoted time and energy to support this work. I would further like to acknowledge the assistance of the staff at the Center for Earth Sciences, all of whom were willing to offer their help.
Many thanks also to all my friends and colleagues with whom I spent lots of precious hours.
A warm thank you to the members of my family for offering their constant support and encouragement.

Abstract

The island of Kythnos lies in the Western Cyclades, a group of islands south of Athens (Greece). The Cycladic islands are characterized by Miocene extension, which overprints earlier thrust and extrusion tectonics.

Geological and structural investigations on southwestern Kythnos have revealed a hitherto undescribed major normal fault zone. A dominant feature of this large SW-dipping extensional shear zone is a several meters thick layer of an extremely fine-grained marble ultramylonite, along with an up to half a meter thick ultracataclasite.

Lithologies on Kythnos are mostly metasedimentary rocks, such as chlorite-epidote schists and albite-chlorite-mica schists intercalated with marble horizons. Furthermore, there are isolated outcrops of metagabbroic rocks.

The schists and marbles show intense ductile deformation, with penetrative schistosity and mineral lineation. Several folding phases, especially in the gneisses and mylonitic marbles, can be observed. Generally, this appears as large-scale isoclinal subhorizontal folding, overprinted by upright folds. Isolated lenses of metabasites, enveloped within layers of talc-schists, are present within the greenschist-facies footwall rocks. These metagabbroic rocks preserve an original magmatic microstructure and appear largely undeformed.

Ductile to brittle deformation produced calcite mylonites and calcite to quartzite cataclasites. The brittle overprint is pronounced in open fractures and joints associated with ore deposition.

Shear sense indicators within the shear zone, predominantly scc'-fabrics and clast geometries, point to top to SSW-directed kinematics. This evidence of SSW-directed extensional kinematics is in accordance with the neighboring Western Cycladic islands.

Whole-rock chemistry of the metabasites allows these lithologies to be classified in respect of their original composition. Mineral chemistry investigations on ferromanganoan metasediments enables characterization and a comparison with similar lithologies on adjacent islands.

A detailed description of the tectonometamorphic history of Kythnos gives insight into the regional geodynamics in the Aegean Sea and to exhumation processes in general.

Zusammenfassung

Die in den westlichen Kykladen liegende griechische Insel Kythnos ist geprägt von Extensionsbewegungen miozänen Alters, die eine ältere Kompressions- und Extrusionsphase überprägen. Strukturgeologische Untersuchungen im südwestlichen Bereich der Insel Kythnos zeigen eine bisher unbeschriebene Abschiebung. Die große, nach SW einfallende, Störungszone wird durch mehrere Meter mächtige, extrem feinkörnige ultramylonitische Marmore und bis zu einem halben Meter mächtige Ultrakataklasite charakterisiert.
Die lithologischen Einheiten auf Kythnos bestehen überwiegend aus einer metasedimtären Abfolge, die sich aus Chlorit-Epidot-Schiefern und Albit-Chlorit-Glimmerschiefern mit dazwischengeschalteten Marmorlagen zusammensetzt. Untergeordnet erscheinen auch metagabbroische Gesteine.
Schiefer- und Marmorlagen zeigen eine intensive duktile Deformation, die in einer penetrativen Foliation und Minerallineation bemerkbar ist. Weiters können mehrere Faltungsphasen beobachtet werden. Diese bestehen vorwiegend aus einer subhorizontal Isoklinalverfaltung, welche durch eine aufrechte Faltung überprägt wird. Linsenförmige, von Talkschiefern umgebene, Metabasitkörper erscheinen hingegen wenig deformiert, denn diese Einheiten weisen noch Relikte eines primär magmatischen Gefüges auf.
Deformation im spröd-duktilen Übergang zeichnet sich durch die Ausbildung von kalzitischen Marmorultramyloniten und kalzitisch- bis quarzitischen Kataklasiten aus. Eine spröde Deformationsphase wird von offenen und teils durch Erz verfüllten Klüften gekennzeichnet.
Schersinnindikatoren entlang der Abschiebung, vorwiegend scc'-Gefüge und Klastgeometrien, weisen auf eine nach SSW gerichtete Bewegung hin. Die Bewegungsrichtung lässt sich mit ähnlichen Geometrien auf den benachbarten Inseln vergleichen.
Eine Betrachtung des Gesamtgesteinschemismus der Metabasite erlaubt eine Klassifizierung und Zuordnung dieser Gesteine. Die Bestimmung der Zusammensetzung einzelner Mineralphasen aus Fe-Mn-reichen Metasedimenten ermöglicht deren Charakterisierung und einen Vergleich mit ähnlichen Lithologien auf benachbarten Inseln.
Einer ausführliche Beschreibung der tektonischen und kinematischen Geschichte der Scherzone auf Kythnos leistet daher ein Beitrag sowohl zur Erfassung der regionalen geodynamischen Situation im Ägäischen Raum, als auch für das Verständis von Exhumationsprozessen im Allgemeinen.

1 Introduction

Work on Kythnos started within the framework of a project focusing on pilot studies in the Western Cyclades. Within the Austrian Science Fund project ACCEL (Aegean Core Complexes along an Extended Lithosphere) information on the development of the regional geodynamic setting within the Aegean was sought by studying the structural and geological inventory of the western Cycladic islands of Kea, Kythnos and Serifos.
The geodynamic history of the Aegean was previously based primarily on the numerous investigations from Eastern and Northern Cyclades. Studies on the eastern Cycladic islands of Syros, Naxos, Ios, Tinos and Andros and Mykonos provide evidence for an extensional setting with exhumation along low-angle normal faults (Okrusch and Bröcker, 1990; Lee and Lister, 1992; Lister et al., 1984). Low-grade metamorphic rocks were placed in direct contact with high-grade rocks by the evolution of metamorphic core complexes. Crustal-scale detachment faults along which highly metamorphic lithologies were exhumed were found to take place on north- and southward dipping fault planes, showing top to the N and NNE-directed kinematics.
Subsequent investigations of the island of Serifos by the means of three diploma theses (Iglseder, 2005; Zámolyi, 2006; Rambousek, 2007) led to the recognition of a metamorphic core complex associated with at least two S-directed detachment shear zones, a higher and a lower grade. Furthermore, exhumation and extension were accompanied by granodioritic plutonism. A major detachment-type shear zone is also proposed by ACCEL for the island of Kea, on which non-metamorphic klippen were mapped (Davis, 1972). Detailed studies by further three diploma theses by Voit (2008), M. Müller and M. Rockenschaub, extensive mapping by A.H.N. Rice and ongoing work by C. Iglseder unveiled major ductile to brittle low-angle normal faults in the northern and southern areas of the island.
The discovery of major extensional faulting on the islands of Serifos and Kea led to the assumption that there ought to be evidence of this tectonic activity also on Kythnos. A preliminary scouting excursion by B. Grasemann, D. Schneider and E. Draganits unearthed an ultramylonitic marble shear zone in the extreme south of the island. As a result two more masters' theses were initiated in the course of which G. Laner and I took a closer look at the deformation history on South Kythnos at Agios Dimitrios. Next to detailed mapping of the area, the work focused on fluid-rock interactions within the shear zone and the relation between the extensional faulting and lenses of metabasic

lithologies.

Detailed investigations along the major shear zones have now led to both a better understanding of the regional plate tectonic and geodynamic setting and have shed light on the exhumation processes along ductile to brittle shear zones. The manner in which exhumation takes place on low-angle normal faults is not yet completely understood, as the formation of brittle faults with low initial dips cannot be mechanically explained (Axen, 2007). It is therefore highly interesting to observe which mechanisms are at work during the formation of low-angle normal fault zones.

2 Geological Setting

2.1 Overview of the Geology of Greece

The geology of Greece is dominated by the nappes of the Hellenides, an Alpine-Himalayan orogenic belt that provides a link between the Balkan to the North and Turkey to the East (Jacobshagen, 1986). The Hellenide orogen developed over several tectonic cycles, which took place from the Late Paleozoic up to the present. The orogen includes ophiolites, Upper Mesozoic and Tertiary flysches, and Cenozoic molasse basins. Repeated events of metamorphism and related granite intrusions are also a main element of the Hellenides. The orogen is made up of large nappes building a fold-and-thrust belt propagating toward the foreland. Orogenesis involved convergence and nappe tectonics of several zones with distinct facies successions, (Argand, 1924; Clément et al., 2000).

The evolution of the Hellenides is associated with the closing of the Tethyan ocean, which in turn is concordant with the opening of the central Atlantic ocean in the Late Jurassic. The opening of the Atlantic initiated the convergence of Africa and Europe and thus Alpine deformation. The Hellenides are thought to have formed from several microplates between Apulia (Adriatic microplate) and Rhodopia (Jacobshagen, 1994), for which the Moesian platform represents the stable hinterland.

The Hellenides can be divided into several zones according to their paleogeographic position in respect to the passive continental margin of the Neotethys during the Mesozoic. Further division is made regarding depositional environment, facies, magmatic evolution and tectonic position. This enables a distinction between the Western Hellenic nappes, Central Hellenic nappes, Median Crystalline Belt (see 2.2) and Interhellenic nappes (Fig. 1). These nappes are usually separated by ophiolitic remnants indicating the development of oceanic crust.

Whereas in mainland Greece much of the orogenic nappe stacks are preserved, the Aegean region has been affected by extension tectonics (Gautier et al., 2001; Lister et al., 1984). Both syn- and post-orogenic extension have led to the exhumation of deeper crustal material, characterized by high-pressure metamorphic rocks. Synorogenic (with ongoing thrusting further south) extension in the Cyclades and the adjacent Menderes and Lycian nappes in Turkey, commenced during the Eocene and led to the partial exhumation of eclogites and blueschists (Sokoutis et al., 1993; Jolivet et al., 2003). During the Oligocene and early Miocene (24–20 Ma) the Cycladic region was dominated

by post-orogenic extension in a back-arc setting leading to the final exhumation of high-pressure metamorphic rocks (Gautier and Brun, 1994).
The subduction, synorogenic extension and back-arc extension subsequently migrated southwards. The stretching direction points toward NNE, and involves extension of approximately 580 km since the Mid-Eocene (45 Ma) (Brun and Faccenna, 2008).

2.2 The Attic Cycladic Crystalline Complex

The Attic Cycladic Crystalline Complex is part of the Median Crystalline Belt of the Central Hellenides and can be divided into three main tectonic units (Fig. 2). The basal unit shows pre-Alpine metamorphism and represents the continental basement of the Crystalline Complex. It is made up mostly of ortho- and paragneisses formed by Hercynian high temperature metamorphism and relics of Caledonian intrusives. Limestone layers and metabauxites also form part of the basal unit. The intermediary unit is marked by multiphase metamorphic overprint and progressive deformation. Characteristic for the intermediate unit are marble layers, metapelites, metasediments (flysch), metamorphic equivalents of volcanic sequences and metamorphic slices of ophiolites. The Upper Unit of the Attic Cycladic Crystalline consists of a basal ophiolitic mélange and overlying remnants of an ophiolite nappe. Within the mélange there are Permo-Triassic limestones, greenschists, granitoid intrusions and crystalline slices affected by Upper Cretaceous low pressure, high temperature metamorphism. These are overlain by a partial ophiolite sequence consisting of serpentinites, and non-metamorphic Cretaceous limestones and Oligo- to Miocene molasse sediments (Okrusch and Bröcker, 1990; Dürr, 1986). The Upper Unit sequences crop out as klippen and show no evidence of metamorphism.
The Attic Cycladic Crystalline Complex has been subjected to numerous deformation events. The timescale of metamorphism ranges from Variscan (M0) up to recent (M4). The first metamorphic phase (M0) is observable in the pre-alpine continental basement. These are mainly Variscan gneisses cropping out on the islands of Naxos, Ios, Paros, Sikinos and Syros. During the following metamorphic phase (M1) in the Cretaceous (100–70 Ma) (Bröcker and Pidgeon, 2007) to Eocene (50–40 Ma) (Okrusch and Bröcker, 1990) high pressure - low temperature conditions were reached. Metamorphism took place at eclogite to blueschist facies conditions at 14 kbar and 500 +/- 30 °C (Putlitz

Figure 1: Major geological units in Greece. In the Ionian Sea the island of Zakynthos and parts of Kefalonia and Lefkada belong to the Pre-Apulian Zone, which represents an undeformed part of the Adriatic plate. Further to the East follow the nappes of the Hellenides, beginning with the External Hellenides which include the Ionian, Gavrovo-Tripolitza, Pindos and Plattenkalk zones. The Attico-Cycladic massif and its continuation to the Menderes massif are the major elements of the Central Hellenides. The Internal Hellenides are composed of the Sub-Pelagonian, Pelagonian, and Vardar zones in Greece and the Ankara-Izmir and Sakarya zones in Turkey. Further toward Bulgaria follow the Rhodopes and the Paleozoic foreland. Modified after Barr et al. (1999); Ring et al. (1999); Schmid et al. (2008).

et al., 2000). The high-pressure rocks in the Aegean are a product of subduction-related metamorphism (Ring and Layer, 2003). Blueschist-facies rocks crop out on Andros, northern Tinos, Syros (eclogites), Sifnos, Kythnos, N-Serifos, Milos, Ios, Amorgos, and southeastern Naxos (van der Maar and Jansen, 1983). Retrograde medium pressure - medium temperature metamorphic conditions (M2) date back to the Oligocene-Miocene (30–20 Ma) (Schliestedt et al., 1994). On Syros, Ios, Serifos, Kythnos, Kea, Andros, Tinos and Paros lithologies showing greenschist-facies conditions predominate. On the island of Naxos amphibolite-facies rocks can be observed (Avigad, 1998). The metamorphic stages M1 and M2 can further be subdivided into numerous separate events (Forster and Lister, 2005). On Lavrio, Ikaria, Mykonos, Delos, Tinos, Serifos, Naxos and Keros granitic to granodioritic intrusions during the Miocene (15–8 Ma) (Altherr and Siebel, 2007) induced local low pressure contact metamorphism (M3). The final overprint (M4) is related to volcanic activity linked to subduction or deeper mantle processes and lasts from 5 Ma ago up to now. Active volcanism can be observed along the South Aegean Volcanic Arc which lies between the Saronic Gulf and Nisyros and includes the islands of Aegina, Methana, Milos, Kimolos, Santorini, Antiparos, Kos, and Nisyros (Fytikas et al., 1984).

2.3 Geodynamic Setting

The Aegean region can be regarded as a microplate, which is surrounded by the African plate to the south, the Eurasian plate to the north, the Apulian plate to the northwest and the Anatolian plate to the northeast. Surface displacement data show the Aegean microplate moving 3–4 cm/year SSW-wards relative to stable Eurasia and 1 cm/year northwards relative to Africa, resulting in an overall convergence rate of 4–5 cm/year for the Aegean region (McClusky et al., 2000). To the south of the Aegean microplate lies the Hellenic trench and the Mediterranean ridge, at which subduction localized 30–25 Ma ago (Jolivet and Faccenna, 2000). To the northeast lies the North Anatolian Fault, which accommodates the westwards movement of the Anatolian plate (Fig. 3). The modern North Anatolian Fault nucleated in central Anatolia in the Eocene, approximately at 15 Ma (Gautier et al., 2001), has propagated to the northern Aegean Sea and now moves at 2–3 cm/year (McClusky et al., 2000; Clarke et al., 1998; Hollenstein et al., 2008).

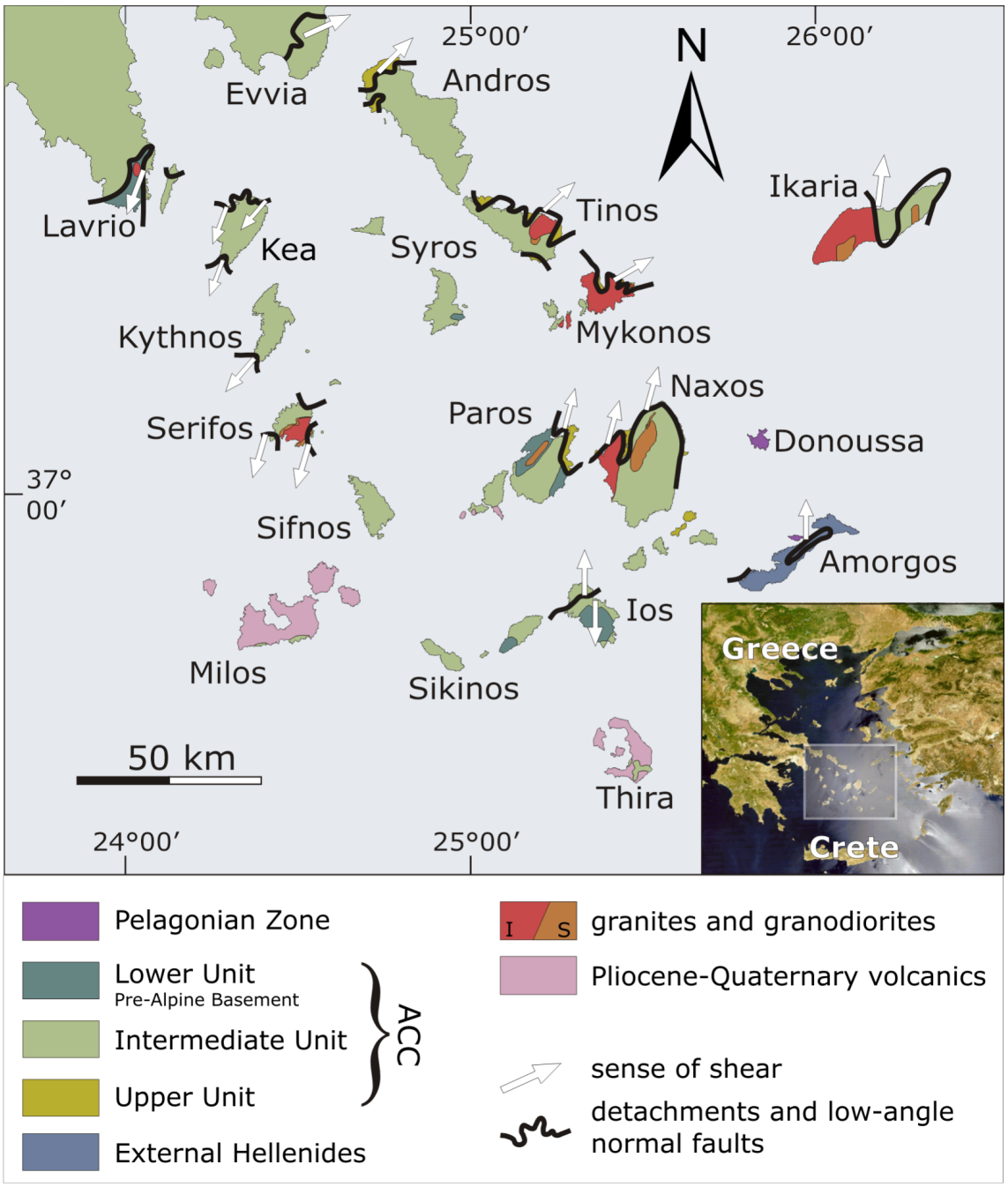

Figure 2: Major units of the Cyclades (modified after Iglseder et al. (in press)). The majority of the Cycladic islands and some areas of the Greek mainland around Lavrio consist of metamorphic rocks associated with the Median Crystalline Belt. The Lower Unit of the ACC crops out on Lavrio, Syros, Paros, Ios and Sikinos. Lithologies of Attic Cycladic Upper Unit are often associated with a detachment-type tectonic contact and can be found on Andros, Tinos, Paros and Naxos. There are also isolated occurrences of External and Internal Hellenides (Pelagonian Zone). Intrusion of Miocene granites and granodiorites occur on Lavrio, Serifos, Tinos, Mykonos, Ikaria, Naxos and Paros. The southern islands (Milos, Thira) are dominated by Pliocene to recent volcanic activity. Kinematics of displacement directions show bilateral symmetry: whereas on the Northern and the Eastern Cyclades movement is NNE-directed, the Western Cyclades show evidence of SSW-directed kinematics.

The Aegean region is the most seismically active region in Europe (Fig. 4). The distribution of earthquake hypocentres shows numerous shallow earthquakes which are concentrated around the Hellenic trench at the presumed active plate boundary. Along with deeper earthquakes they define a Wadati-Benioff zone dipping 30° toward the north and northeast up to a depth of about 150–200 km (Papazachos et al., 2000). Along with tomographic studies (e.g. Spakman et al. (1988)), the Wadati-Benioff zone marks the African plate subducting beneath the European plate. As a result of slab retreat associated with back-arc extension, rigid extrusion of Anatolia and post-orogenic collapse of an overthickened crust, the Aegean microplate is subjected to extension tectonics (Jolivet, 2001; Bohnhoff et al., 2001).

Furthermore, the Aegean region shows mean lithospheric thickness values of 24–30 km (Makris, 1978; Li et al., 2003; Tirel et al., 2004), which, together with high heat flow values and a shallow Moho depth (Makris and Stobbe, 1984; Endrun et al., 2005), can be interpreted as a thinned continental crust. Thinning of the continental crust is put down to gravitational collapse of the orogen during the Oligocene and middle Miocene, induced by the southwards of the subducting African slab.

The subduction zone at the Hellenic Arc is associated with calc-alkaline volcanism, especially prominent at the islands of Milos, Santorini and Kos (Fytikas et al., 1984). The composition of the volcanic material suggests a mantle source contaminated by lower crustal material (Pe-Piper and Piper, 2006).

Both the southward rollback by a retreating of the subduction zone at the Hellenic trench and the lateral extrusion of Anatolia led to widespread extension within the Aegean. Extension is associated with plutonism and low-angle detachment faulting (Lister et al., 1984).

In the Eastern Cyclades metamorphic core complexes exhumed Miocene metamorphic rocks along N- to NE-directed low-angle normal faults (Lister et al., 1984; Jolivet and Faccenna, 2000). South-directed kinematics involving metamorphic core complex formation has been observed in the Western Cyclades on the island of Serifos (Grasemann et al., 2004; Iglseder et al., 2006). On Kea exhumation occurs along a large-scale ductile-brittle shear zone involving low-angle normal faulting (Voit, 2008; Iglseder et al., 2008).

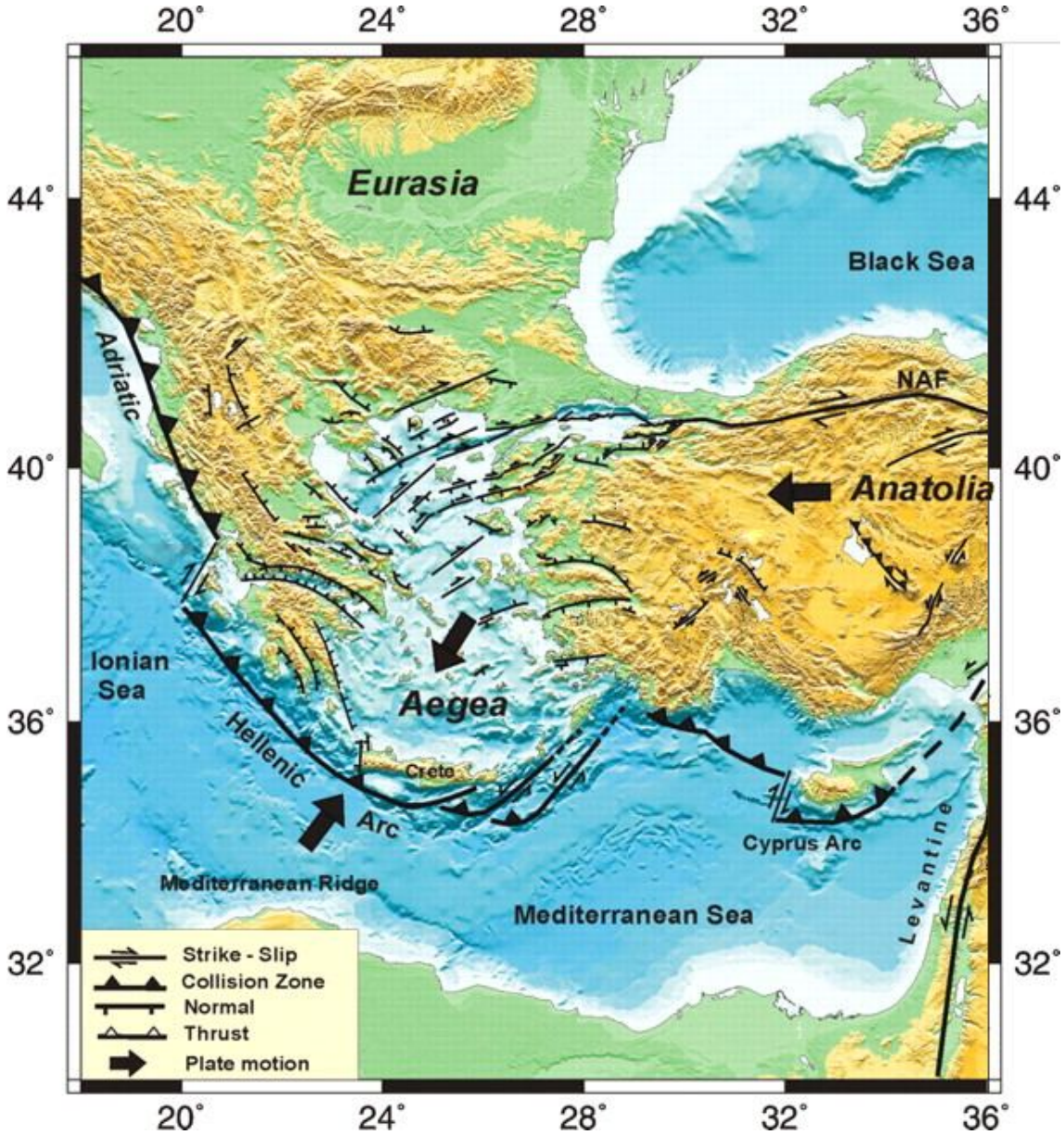

Figure 3: Summary of faulting in the Eastern Mediterranean region by Taymaz et al. (2007). NAF = North Anatolian Fault.

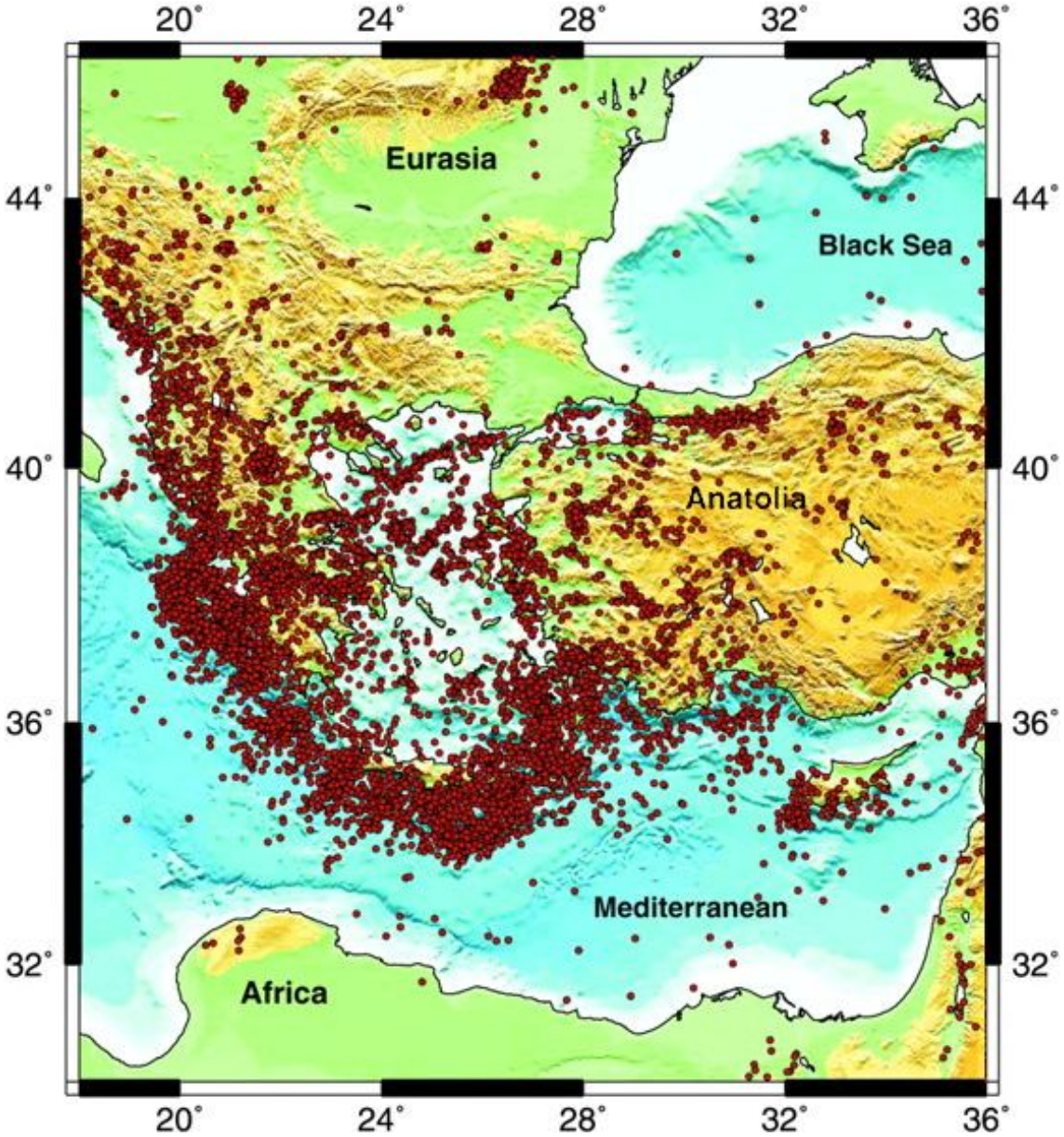

Figure 4: Seismicity with magnitudes for M >3 of the Eastern Mediterranean region and surroundings as reported by USGS during the years 1973–2007. Map after Taymaz et al. (2007).

3 Kythnos Island

The Greek island of Kythnos lies in the Aegean Sea southeast of the capital Athens. It is part of the Cycladic archipelago and lies between the islands of Serifos in the south and Kea in the north. The island comprises 100 km^2 and shows a N-S elongation (22 km N-S versus 5 km E-W). Topographically, Kythnos is dominated by two major ridges striking NNE-SSW. The smaller northern one has its highest elevation at Kakavolo with 356 m, while the longer southern ridge has its highest point on Profitis Ilias at 325 m. Separating these two major ridges is a large flat-lying area at approximately 100 m elevation around the main town of Kythnos.

Earliest signs of settlement on Kythnos island, which are dated to the Mesolithic period (10 000 to 8 000 years BP) have been found in the north at Maroulos (near Loutra). During the 12th century BC the tribe of the Dryopians settled on Kythnos Island as a consequence of being displaced by the Doric tribes from Evvia. It was the Dryopian tribes that gave the island its name, as the root 'kyth' or 'keyftho' relates to a hidden dark place in Phoenician or Dryopian language. This interpretation of the name arraigns to some physical attribute of the island such as shadowy forests, deep valleys, caves or mines. In due course the name changed to Thermia, adhering to the thermal springs in the island's north.

Major early Bronze Age smelting sites were found on the east coast near Skouries, which led to the conclusion that the island of Kythnos must have been a major supplier of copper and iron throughout the Bronze Age. The highly organized smelting site was one of the earliest of such industrial smelting sites in the whole Aegean region (Alram-Stern, 2004). Copper ore was extracted from surrounding areas on the east coast around Agios Ioannis and near Zhogaki and Milyes (east and south of Driopida, respectively). The copper mineralization on Kythnos is generally weak and consists mostly of malachite found within quartz veins or iron oxides (Zacharias et al., 2006). These iron oxides represent the main mineralization on the island. Additional ore was imported from Sifnos for copper production in Skouries (Gale and Stos-Gale, 1984) as the copper ores on Kythnos were of limited extent. The low supply of ore led to Lavrion taking over the role as main copper supplier to the Cyclades by the start of the Lower Cycladic Period (Gale and Stos-Gale, 1984). Major changes took place in the 13th century AD when the Venetians built the settlement of Kastro in the North, which was later invaded by the Turks. In 1830 Kythnos became a member of the Greek Union, with fishing and

agriculture providing the main sources of income on the island. Between the beginning of the 20th century and the Second World War the mining of iron ore once again provided a further income source. After a decline in the 60s and 70s, when the island was effectively desolate, only recently tourism has led Kythnos to prosperity. Currently, there are 1500 permanent residents on the island.

3.1 Previous Works

In the past Kythnos Island has received little attention from geologists. Preliminary geological observations were made by Fiedler (1841) and Philippson (1901) during their travels throughout the Greek islands. The first and so far only extensive mapping was conducted by J.B. De Smeth during the years 1972–1973 and published as the geological map of Kythnos Island by the Greek National Institute of Geological and Mineral Researches (IGME) in 1975 (Fig. 6). The diploma theses by M. Carl and V. Bartsch and a subsequent publication by Schliestedt et al. (1994) provide a detailed petrographic description of major lithologies and an estimation of a P-T-path of greenschist-facies rocks. In 2003 A.I. Chrysanthaki and E.M.M. Baltatzis published geochemical investigations on ferromanganoan metasediments from the Panagia Kanala area on the southeastern coast and the Episkopi area in the west. A summary of the structural evolution of Kythnos island has been provided by the recent publication by Keiter et al. (2008). Furthermore, the thermal springs in Loutra are been subject of several investigations (e.g. Loehnert (1988); Augustithis (1976); Lambrakis and Kallergis (2005)). Pre-historic finds from the north of the island (e.g. Gale and Stos-Gale (1984)) and Bronze Age copper smelting sites (e.g. Alram-Stern (2004)) have received archaeological attention and have been described in detail.

3.2 Mapping Area

The focus of this work lies in the southernmost part of Kythnos Island, near the bay of Agios Dimitrios (Fig. 5). The mapping area includes the settlements of Agios Dimitrios, Karavokyris and Petroussa. The bay area around Agios Dimitrios is flat-lying, the area further south is dominated by two ridges up to 100 m in elevation running from west to east. They are divided by a steep valley marked by a perennial stream. The coastline in the southern area of Kythnos is rugged and uneven. A small island lies offshore of a promontory north of the town of Agios Dimitrios.

Figure 5: Quickbird satellite image of the southernmost region of Kythnos Island. The settlement in the bay is known as Agios Dimitrios. Coordinates are given in UTM Northing and Easting.

3.3 Lithostratigraphy

Kythnos Island is mainly made up of metasedimentary rocks, predominately epidote-chlorite-schists, albite-chlorite-mica schists intercalated with marbles - and a metagabbroic unit (DeSmeth, 1975), (Fig. 6).

Evidence greenschist facies metamorphism is prevalent throughout the island. Relics of an earlier high pressure metamorphism, such as glaucophane minerals and pseudomorphs of jadeite and garnet (Bartsch, 1993; Schliestedt et al., 1994), and the widespread greenschist facies overprint place lithologies on Kythnos into the Intermediate Unit (as in Dürr (1986)) of the Attic Cycladic Crystalline belt.

White mica K-Ar dating constrain the greenschist facies metamorphism at around 26 - 20 Ma (Schliestedt et al., 1994), which corresponds with Oligocene to Miocene ages of similar rocks on other Cycladic islands (Bröcker et al., 2004).

Apart from the abundant greenschists and marbles, there are occurrences of ferromanganoan metasediment layers, as described by Chrysanthaki and Baltatzis (2003), in which garnets and sodium-rich amphiboles are present. Additionally, small lenses of metabasic lithologies crop out. The boudin-like lenses of metagabbroic rocks are commonly enveloped in layers of serpentinitic talc-schists with asbestos veins.

Above layers of epidote-, chlorite-, and albite-schists with intercalated marble follows a conspicuously fine-grained calcitic marble mylonite. This layer is found to be up to 10 m thick. In other areas of the island, this structurally higher position is occupied by coarser-grained impure marble.

Adjacent to this ultramylonitic marble are various cataclastic layers, ranging in deformation grade from protocataclasites to ultracataclasites. Both the underlying marble and the overlying quartzite act as protoliths. Within the cataclasites, a variation of component composition from only marble clasts to only quartzitic clasts can be observed. The structurally uppermost unit is a strongly brecciated and hydrothermally altered quartzite (Fig. 7).

Outside the mapping area (e.g. near Kanala), there are outcrops of garnet-magnetite-amphibole quartzites, which occupy a similar structural position within the greenschists as the tourmaline-epidote gneisses. Furthermore, a massive layer of coarse-grained marble crops out in morphologically higher-lying areas, especially in the north.

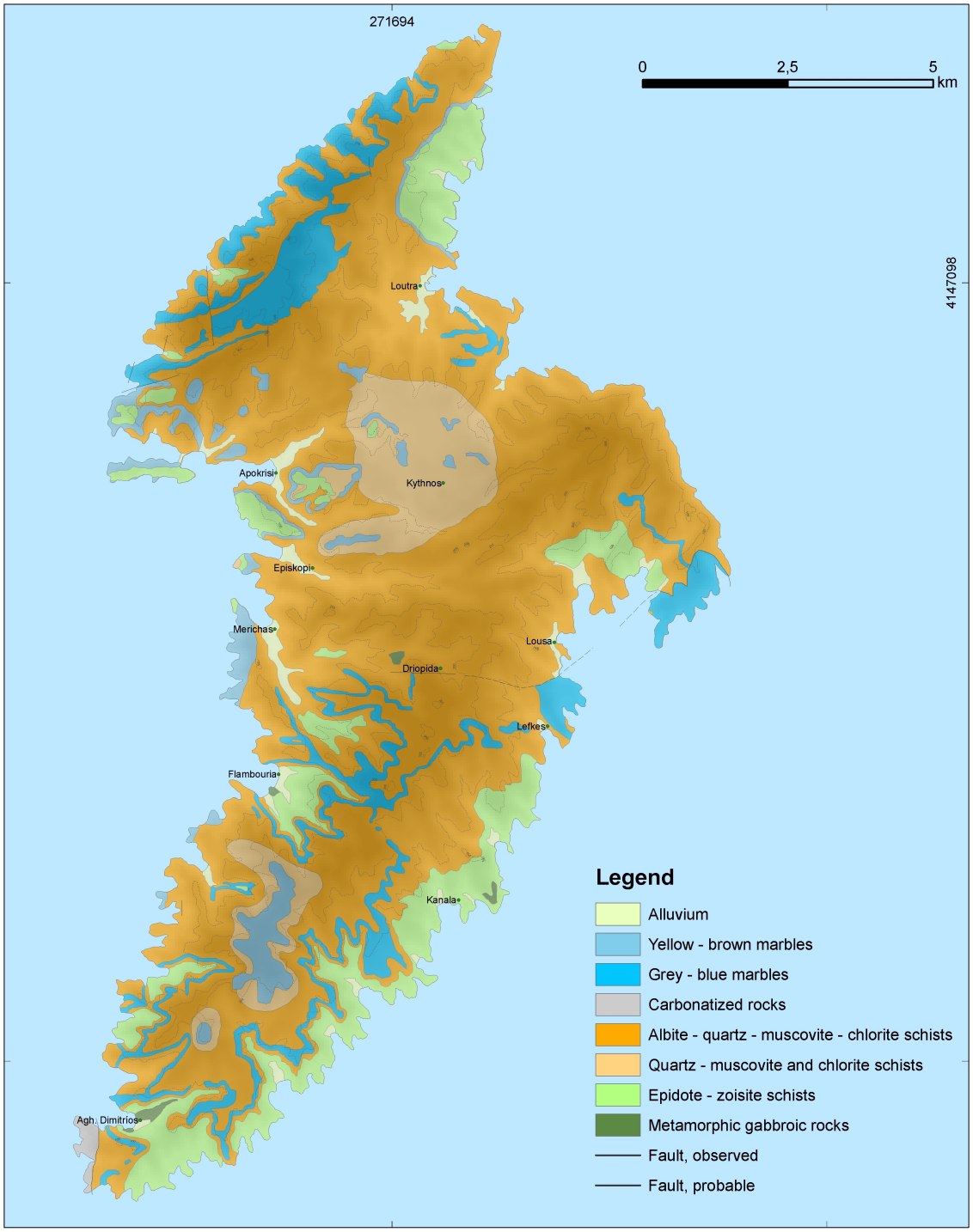

Figure 6: Geological Map of Kythnos Island, modified after DeSmeth (1975).

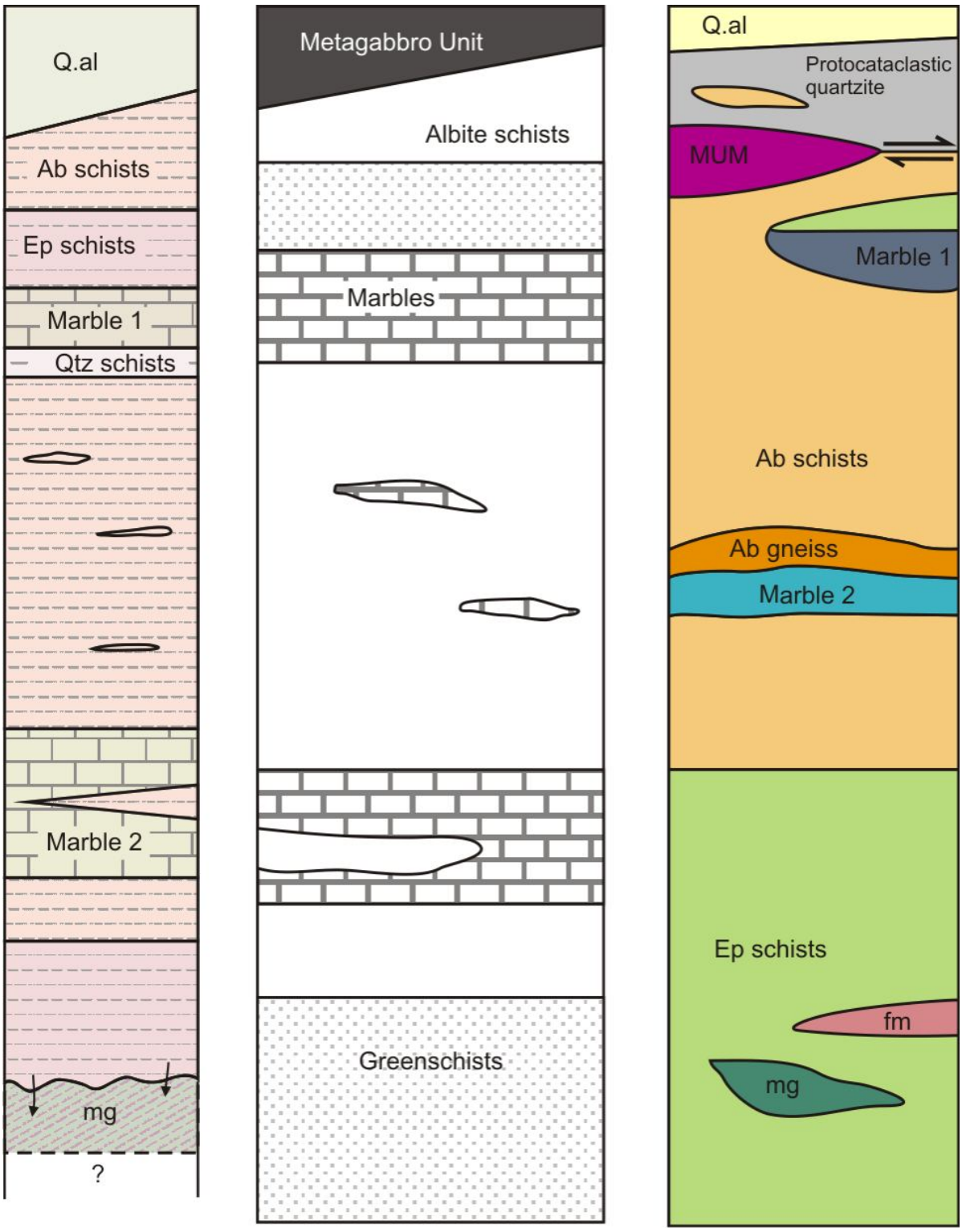

Figure 7: Lithostratigraphic columns by DeSmeth (1975) (left), Schliestedt et al. (1994) (middle) and own (right). Q.al stands for quarternary alluvium, Marble 1 is a yellow-brown marble, Marble 2 a blue-grey marble, mg a metagabbroic unit, MUM an ultramylonitic marble.

3.3.1 Metabasic Rocks

Within the epidote schists, isolated lenses of metabasic lithologies can be found. Only a small number of outcrops are described: near the town of Kanala, Episkopi and Agios Dimitrios. The metamorphic gabbroic rocks cropping out at Agios Dimitrios have a boudin-like lensoid shape of approximately ten by two meters. They are marked by conspicuous rounded weathering forms (Fig. 10) and are enveloped by layers of serpentine-talc schists. The metabasic rocks show relics of an original magmatic fabric, from which pyroxene crystals weather out.

The mineral assemblage includes brown amphibole, magnetite, orthopyroxene, albite, sodium amphibole, calcite, and chlorite. One sample (from Kanala) shows large areas of serpentinization, in which antigorite and chrysotile are found both as fine-grained intergrowth with tremolite and as pseudomorphs after olivine (Fig. 10). Round inclusions within amphibole and pyroxene crystals (Fig. 8) may also have been olivine crystals, now altered to tremolite (within the brown hornblende) and serpentine. Amphibole crystals show marginal alteration from brown hornblende to pale tremolite (Fig. 9). Needles of blue amphibole occur both within the matrix and also as inclusions in feldspar crystals. The metabasic rocks appear massive, showing little to no foliation planes, nor can any evidence of folding or deformation be observed.

3.3.2 Greenschists

Chlorite-sericite-actinolithe-epidote-albite-schists to -gneisses are ubiquitous on Kythnos island. Some portions of these rocks show pervasive growth of calcite between mineral grains, possibly as a result of hydrothermal overprint with carbonate-rich fluids.

The main minerals composing the greenschist are chlorite, sericite, actinolite, epidote, quartz, calcite and albite. The greenschist facies rocks are partially highly fine-grained, showing strong foliation, and generally show subhorizontal dip. Other portions are more massive and contain larger amounts of quartz and feldspar and less phyllosilicates. Conspicuous large epidote crystals weather out on foliation planes and define a lineation toward NNE (Fig. 11). Some epidote crystals show relics of an older internal foliation (Fig. 23).

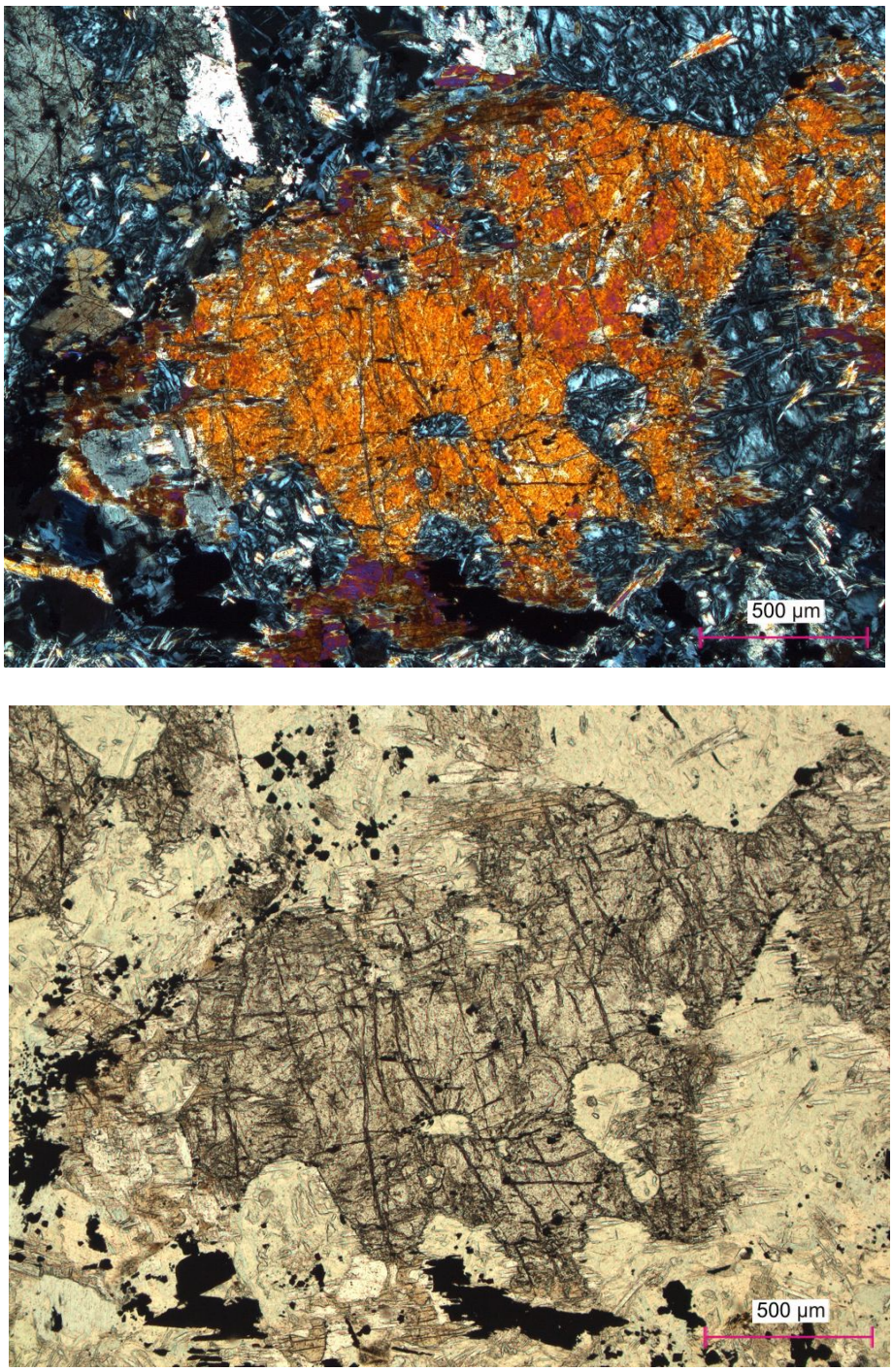

Figure 8: Thin section of metabasite in normal (top) and crossed (bottom) polarized Nicols', unoriented sample. Fine-grained intergrowth of tremolite and serpentine minerals. Large orthopyroxene crystals are partially resorbed and show serpentinized rounded inclusions. Amphiboles show needle-like growth on the margins of the pyroxenes.

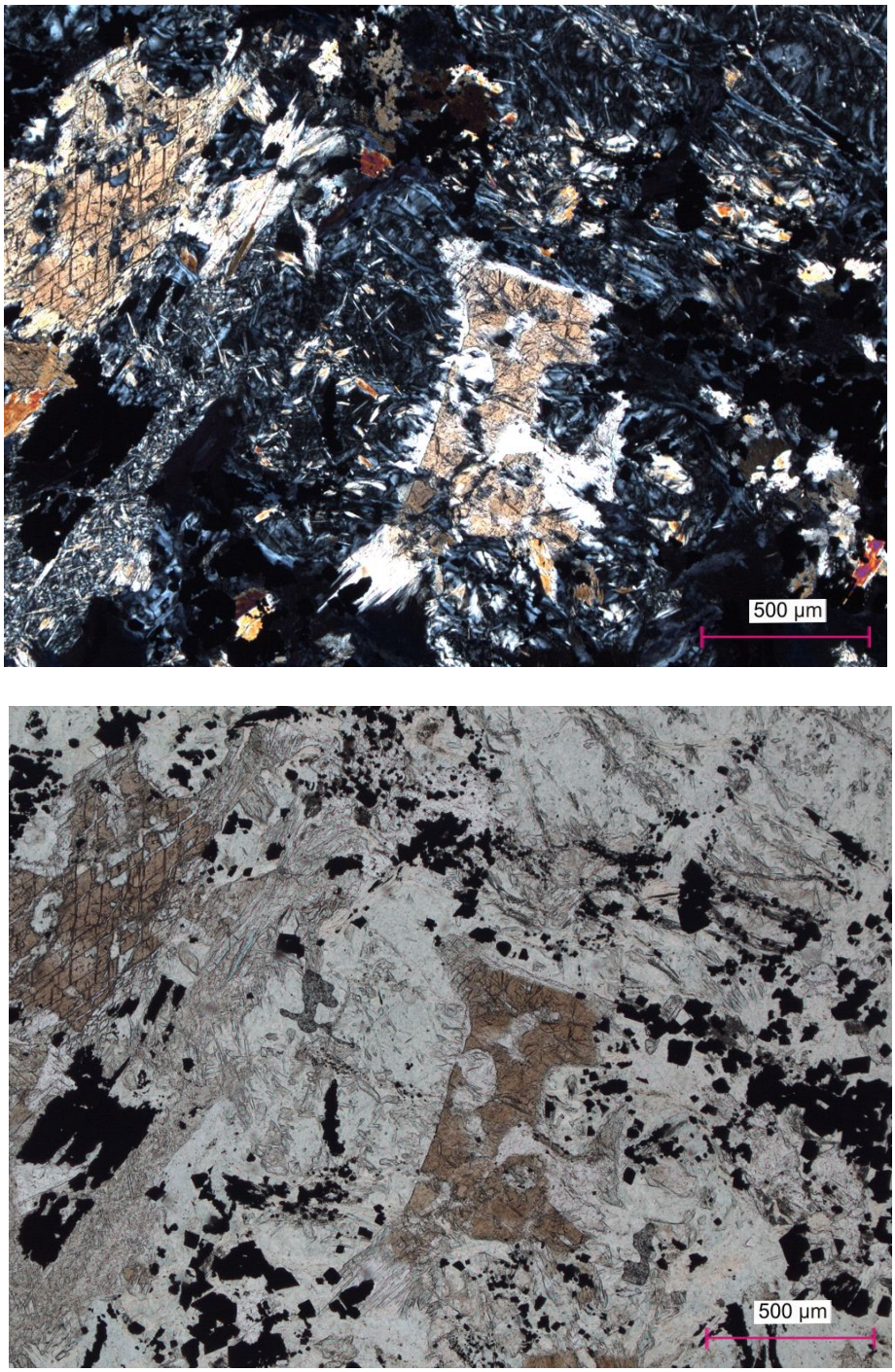

Figure 9: Thin section of metabasite in normal (top) and crossed (bottom) polarized Nicols', unoriented sample. Large crystals of brown hornblende show characteristic cleavage pattern and a tremolite fringe. Opaque Fe-oxide phases are ubiquitous.

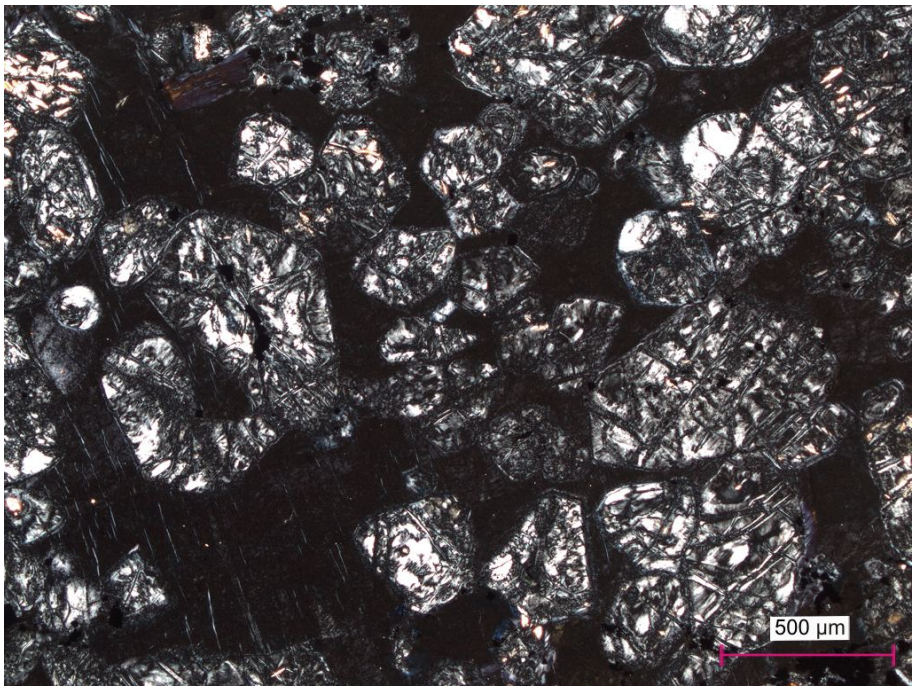

Figure 10: Serpentine (chrysotile/antigorite) pseudomorphs, possibly after olivine (top). Outcrop of metabasic rocks showing rounded weathering forms and original magmatic fabric (bottom).

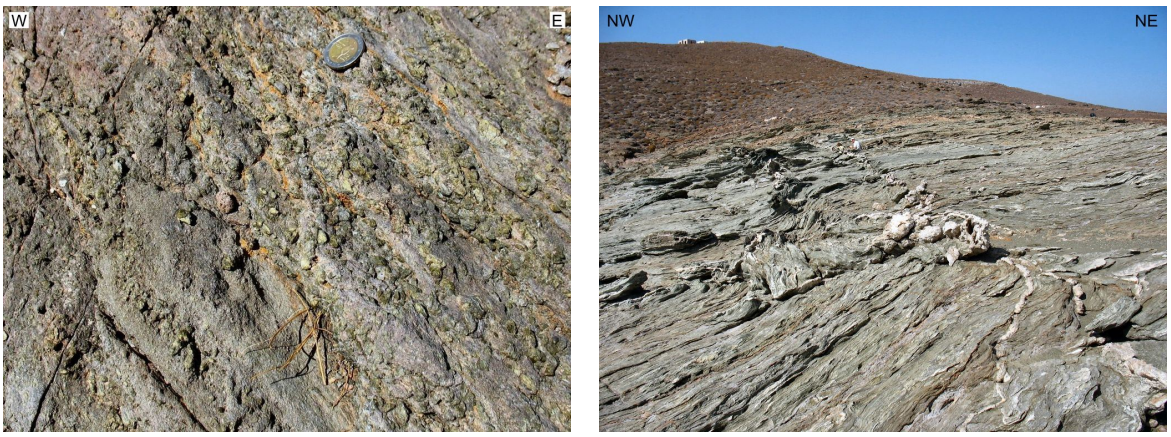

Figure 11: Large epidote crystals weathering out on foliation plane (left). Greenschist with kinked foliation plane (right).

3.3.3 Ferromanganoan Metasediments

Ferromanganoan metasediments, or riebeckite-spessartine-magnetite gneisses, crop out as dark, strongly foliated rocks. The mineral assemblage is composed of spessartine, magnetite, "riebeckite", quartz, albite, muscovite, chlorite, and minor amounts of titanite, titano-magnetite, apatite and rutile.

These dark, black rocks are clearly foliated (mylonitic foliation) and show an alternation between lighter, quartz-rich and darker, magnetite-rich layers. Mineral lineation is defined by the preferential orientation of amphibole needles and strikes shallowly toward NE. Mica minerals and some elongated magnetite grains grow along the foliation plane, whereas garnet and magnetite act as clasts. Syntectonic Ab-blastesis indicates top to SSW-directed shear (Fig. 12).

The garnet-magnetite-amphibole quartzite samples were obtained at a location near Kanala (W-Kythnos) and are also described from Flambouriana on the eastern coast (Chrysanthaki and Baltatzis, 2003).

Tourmaline-Epidote Gneisses At a similar lithostratigraphic position as the garnet-amphibole-gneisses, tourmaline-epidote-gneisses can be found at a small outcrop on the northern side of Agios Dimitrios bay. The tourmalinites occur within the chlorite-epidote schists and overlie the metabasitic rocks. The lithology appears dark and distinctly foliated. The foliation is produced by an alternation between quartz-rich and tourmaline-epidote-rich layers (Fig. 13). Orientation of mica minerals and chlorite create a schistos-

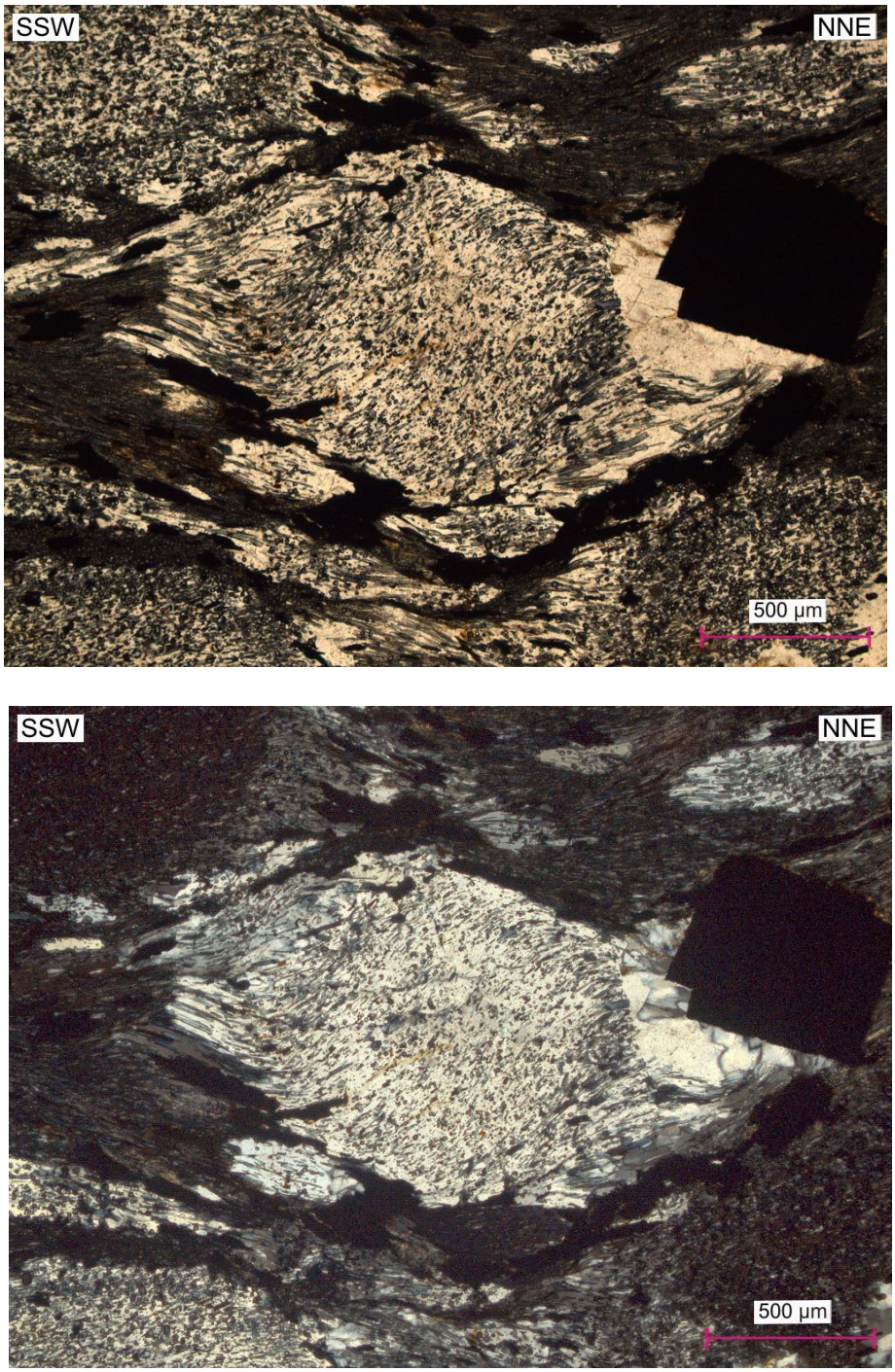

Figure 12: Thin section of amphibole-spessartine gneiss viewed in normal (top) and crossed (bottom) polarized light. Crossite, spessartine and rutile crystals define a foliation within an albite blast. Quartz grows syntectonically onto a magnetite crystal. The matrix surrounding the feldspar blast consists mainly of blue amphiboles, mica and finely dispersed garnets.

ity along subhorizontal planes, on which elongated tourmaline crystals define a SE-NW lineation. Crenulation lineation is parallel to the mineral lineation and dips toward the NE at a shallow angle.
The mineral assemblage is made up of tourmaline (dravite–schoerl), epidote, magnetite, quartz, chlorite, actinolite, and muscovite.

3.3.4 Mylonitic Marble

The mylonitic marble appears as a distinct lithology in the landscape as it weathers out as an approximately 3–5 m thick layer. It is blue-grey in color and is often associated with folded gneiss layers (Fig. 14). Quartz grains on foliation planes define a shallow NNE-dipping lineation. Minor amounts of sericite are aligned with the mylonitic foliation. Beds of the marble dip toward the NW over NE to SE at a low angle, defining a dome-shaped structure. The mylonitic marble shows intense subhorizontal isoclinal folding on all scales. In the thin section, the average grain size of the calcite crystals can be determined as lying between 50 and 100 μm. However, a large grain-size variation can be observed, especially pronounced in a mylonitic foliation with extremely fine-grained to coarser-grained bands of calcite crystals (Fig. 14). Larger calcite crystals exhibit twinning both as thin twin layers and thick twin bands. Quartz occurs as clasts showing top to S-directed shear. Especially remarkable is the fact that some quartz clasts appear to be internally broken instead of acting as rigid clasts within a marble matrix.

3.3.5 Albite-Gneiss

Directly overlying the blue-grey mylonitic marble is an approximately 5 m thick layer of albite-rich gneiss. Layers of albite-gneiss are also often intercalated with the mylonitic marble. These layers within the marble are generally strongly folded, mostly as sub-horizontal isoclinal folds. Further to the south, gneissic layers appear more chaotically folded.
The gneiss is principally composed of quartz, albite, chlorite, calcite, and sericite. Chlorite and sericite minerals define the foliation plane, which is overgrown by albite-blastesis. Major amounts of calcite mineral growth can be observed between the mineral grains and replacing feldspar crystals (Fig. 15).

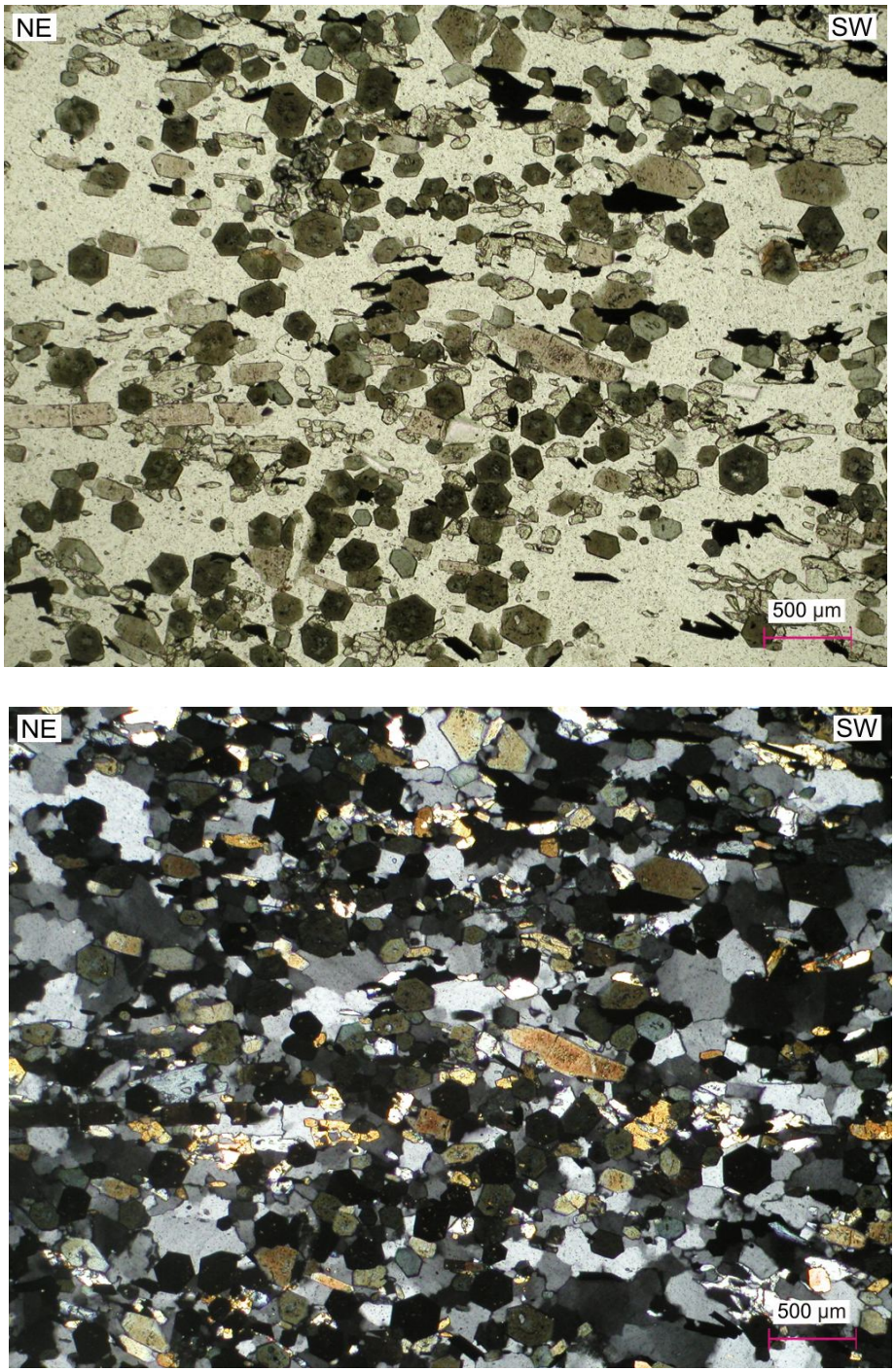

Figure 13: Thin section of a tourmaline-bearing quartzite viewed in normal (top) and crossed (bottom) polarized light. Idiomorphic tourmaline crystals appear green to brown when observed parallel to c-axis and light pink to yellow when observed perpendicular to c-axis. Along with epidote crystals and opaque Fe-oxides, tourmalines occur dispersed in a quartz-rich matrix.

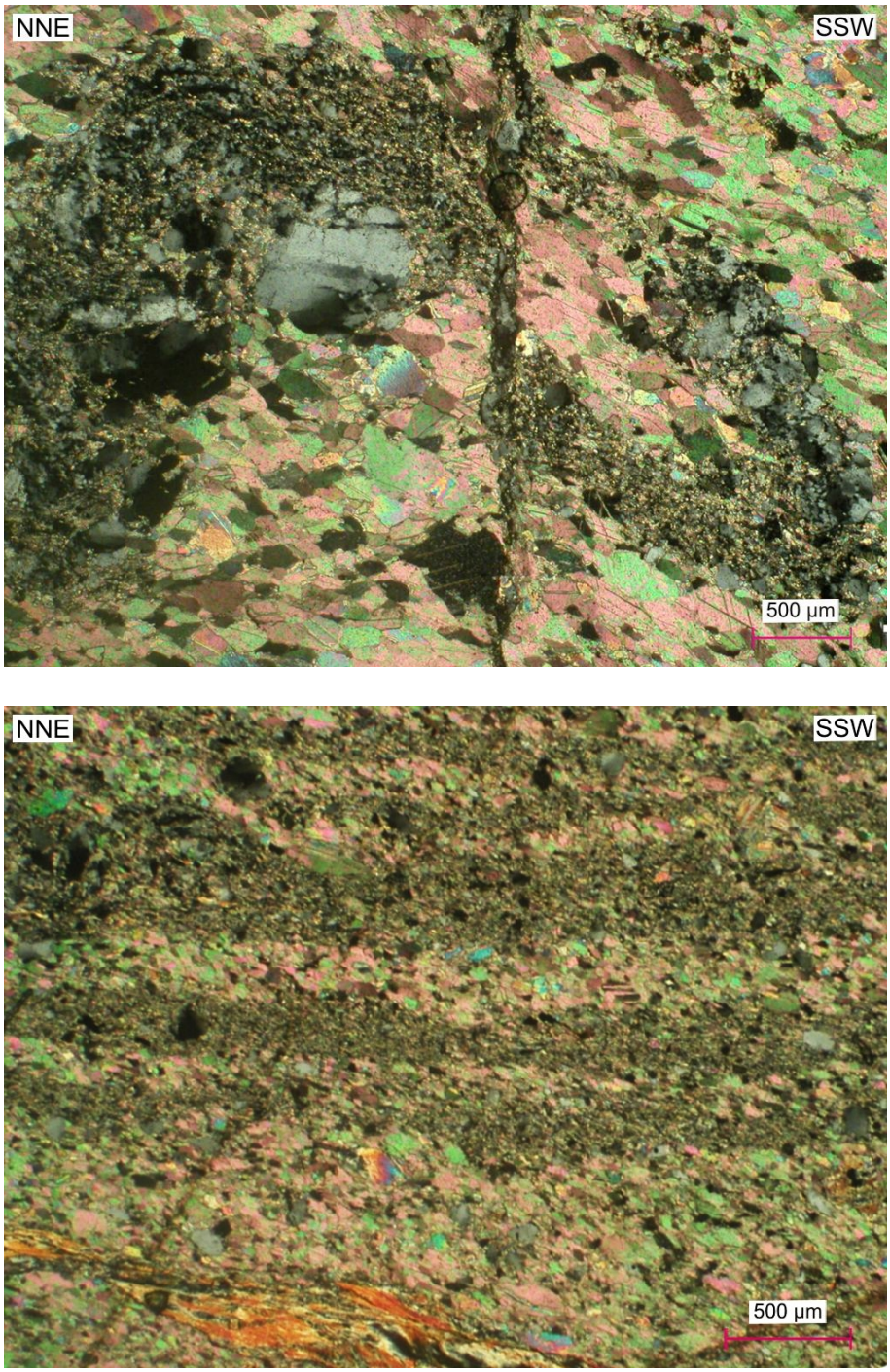

Figure 14: Thin section of mylonitic marble viewed in crossed polarized light. Within the marble folded gneiss layers are commonly found (top). Layers of more and less fine-grained calcite crystals define a mylonitic foliation (bottom).

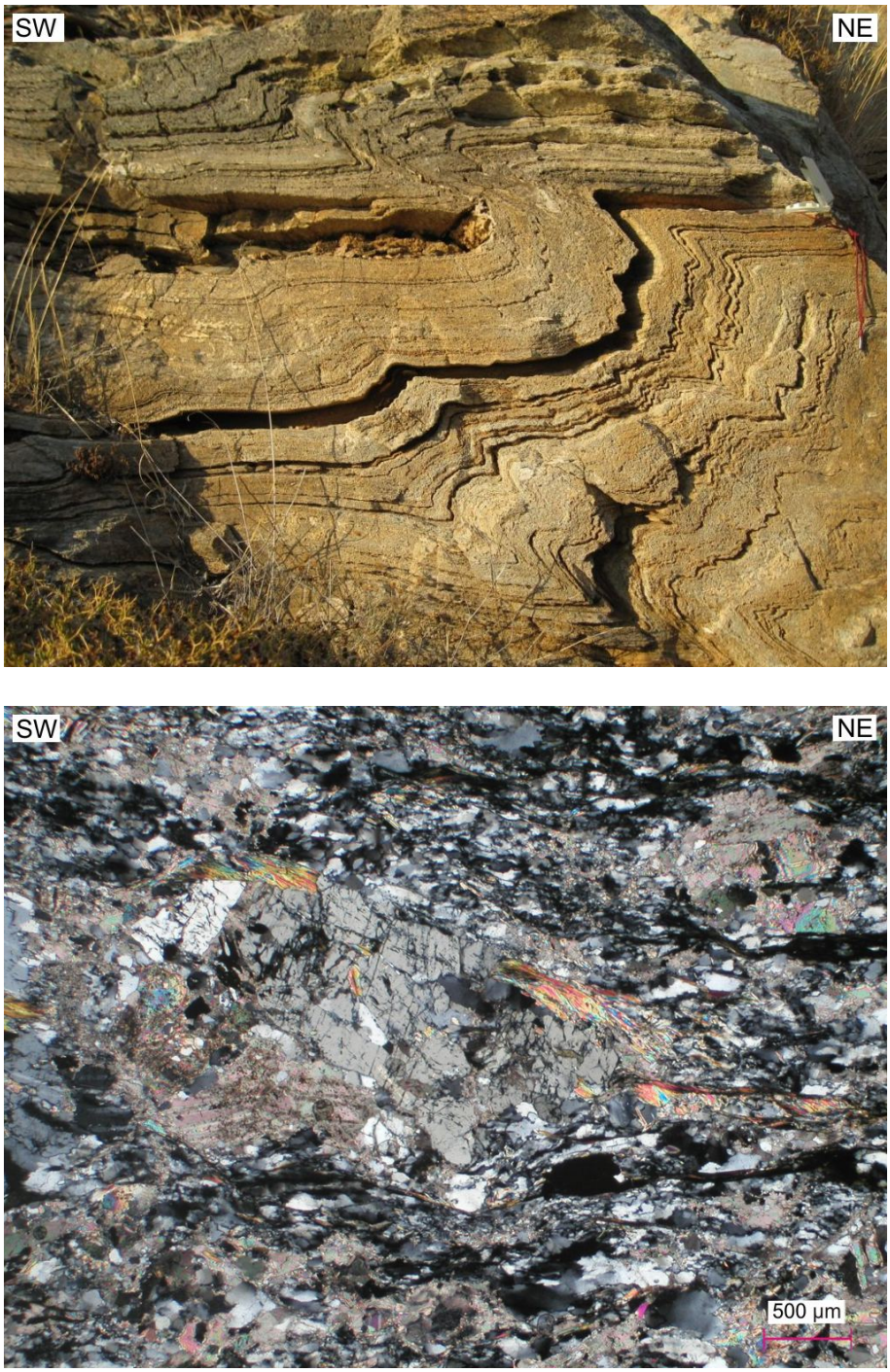

Figure 15: Foliated, folded gneiss (top) and thin section picture of albite-gneiss in crossed polarized light (bottom) showing ubiquitous growth of calcite crystals due to overprint by carbonate-rich fluids.

3.3.6 Carbonate-rich Albite-Chlorite-Sericite Schist

Major amounts of schistous material surround the mylonitic marble and gneiss layers. Additionally, isolated lenses of phyllite also occur overlying the ultramylonitic marbles. The mineral assemblage consists primarily of quartz, albite, chlorite, calcite, and sericite. In contrast to the greenschists, these rocks contain no epidote. Large feldspar crystals are twinned and show poikiloblastic microstructure. The chlorite-schists show distinct foliation (Fig. 16) and mineral lineation (dipping shallowly toward NE). Isoclinal folds, kink bands and sc-fabrics can be observed within this lithology.

Figure 16: Brittle fault offsetting foliation planes of albite-chlorite-schists. Here the albite-chlorite-schists are overlain by epidote-schists (top right).

3.3.7 Impure Marble

Between the chlorite schist and the ultramylonitic marble layer lies a lithology that consists mainly of calcite, quartz, feldspar and chlorite. It can be described as a carbonate-rich gneiss, or as an impure marble. On a hand-piece scale, strongly elongated quartz-lenses can be seen (Fig. 17). Larger broken-up quartz, feldspar and Fe-oxide grains act

as clasts between foliated chlorite, fine-grained calcite and quartzite. Calcite is ubiquitous, but concentrated in layers. A strong, probably protomylonitic, foliation can be observed and is made up of bands of fine-grained quartz and mica. Calcite is often found interspersed between quartz grain boundaries.

3.3.8 Ultramylonitic Marble

Ultra fine-grained mylonitic marbles present a conspicuous horizon. The marble shows a distinct layering with bands of pink to yellow and grey-blue coloring. In thin section-scale a mylonitic layering of coarser- and finer-grained areas can be observed (Fig. 18). The average calcite grain size lies at approximately 10 μm. There is, however, a markable variation in grain size so that certain mylonitic layers are composed of calcite crystals whose size lies below the resolution of the optical microscope. Grain size reduction may have been the consequence of deformation at a temperature lower than necessary for dynamic recrystallization. Fluid activity might have enabled movement at low temperatures by further reducing fault friction.
The ultramylonite consists almost purely of calcite, with only occasional occurrence of small quartz clasts (Fig. 18). Larger clasts are usually made up of calcite crystals. There is only a very rare occurrence of mica. Additionally, the mylonitic layers are cross-cut and offset by coarser-grained calcite veins.
Two species of ultramylonitic marble can be distinguished, which vary in respect of color and position. Whereas the pink- to yellow-colored marbles (Fig. 19) are found to be dipping steeply to the SW, the blue-white marbles show a more shallow angle of dip and are found farther away from the underlying impure marbles.
In certain areas the ultramylonitic marble is also partially overprinted by Fe-rich fluids. This alteration replaces the calcite with an Fe-rich phase, but preserves the quartz clasts and the foliation.

3.3.9 Cataclasites

Cataclastic faults can be observed throughout the southernmost area of Kythnos Island. Especially remarkable, however, is a several decimeters thick zone of cataclasites directly overlying the ultramylonitic marble. Directly adjacent to the ultramylonite, the cataclastic components are almost solely of marble origin. With increasing distance to the

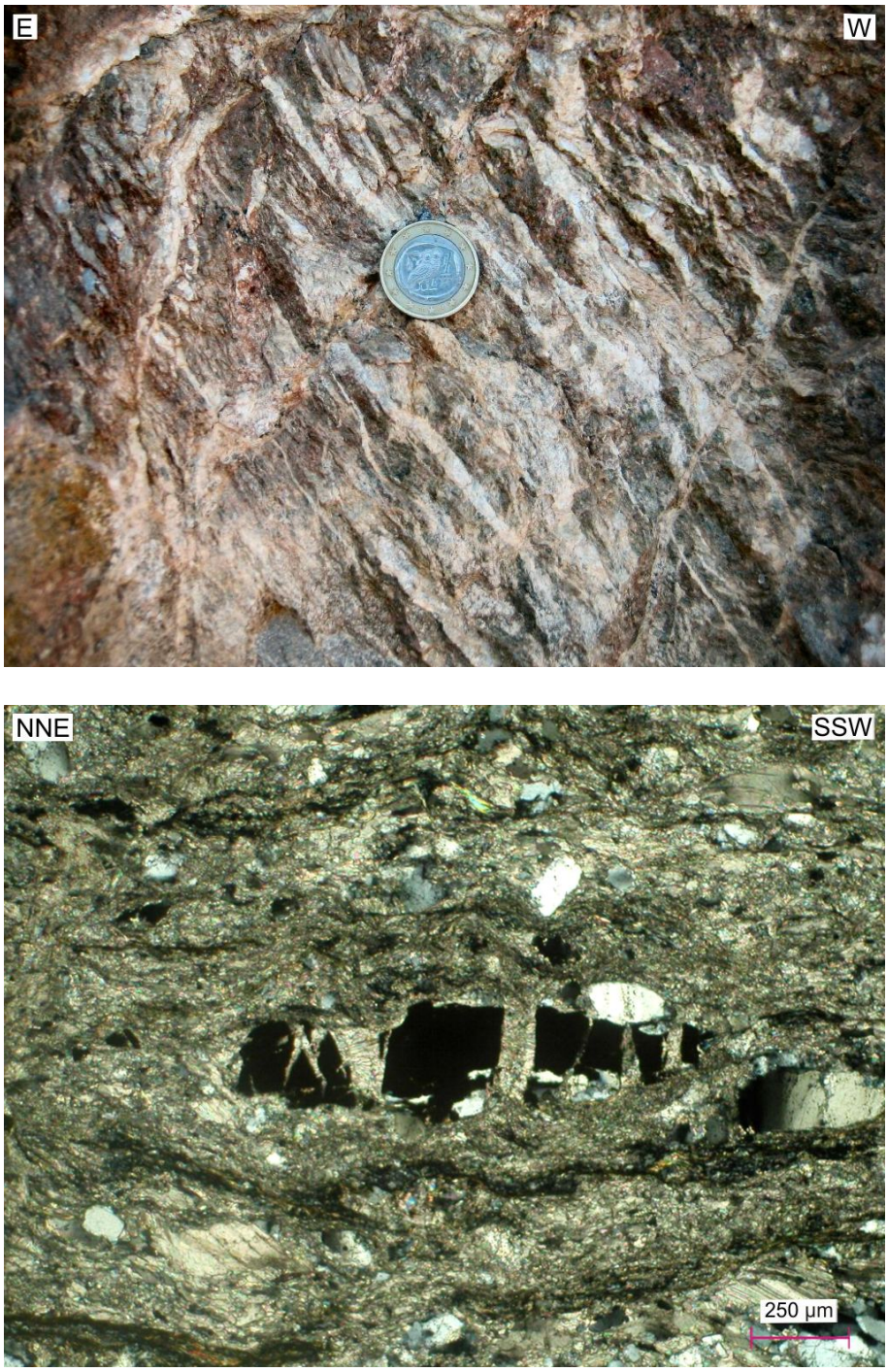

Figure 17: Fine-grained impure marble with large amounts of gneissic-quartzitic lenses. Outcrop picture (top) and thin section image (bottom).

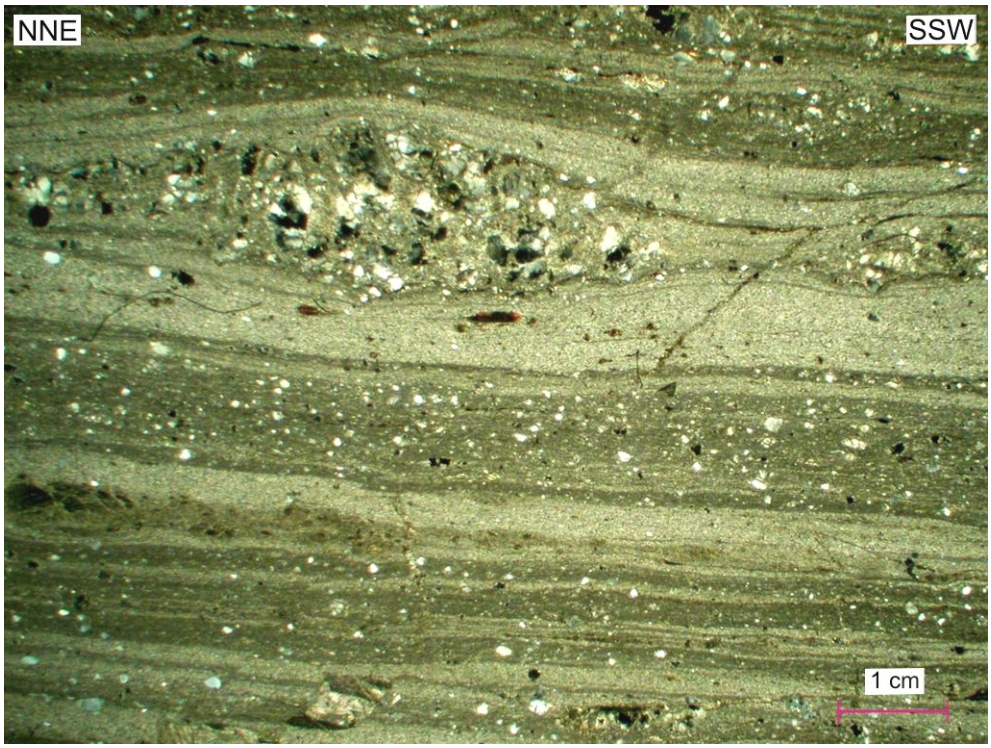

Figure 18: Thin section image of ultramylonitic marble viewed in crossed polarized light. A banding with more or less fine-grained calcite crystals can be determined. Broken-up quartz components act as clasts and dispersed small quartz crystals and mica pervade the marble. Large calcite crystals grow in extension gashes.

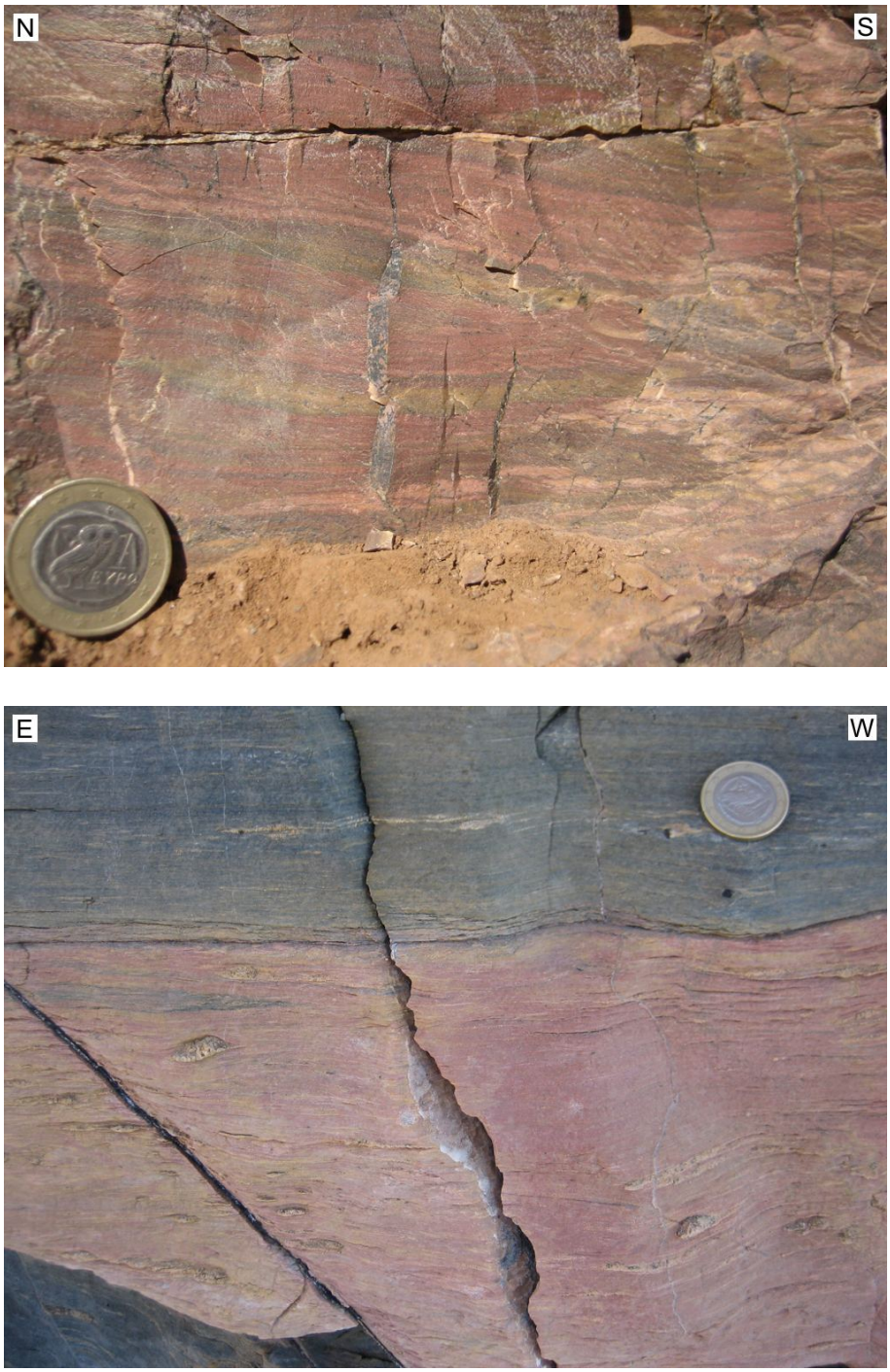

Figure 19: Outcrops of ultramylonitic marble show fine banding and variations in color from pink to yellow (top) to blue (bottom). Occasional inclusions of quartz weather out (right).

ultrafine-grained marble, components show a larger variation in composition and include polycrystalline quartz, gneissic material, and components altered by Fe-rich fluids. In some samples larger components are enveloped in a thin calcite fringe (Fig. 20).
The shape and size of the grains differ remarkably, both within and throughout the samples. Whereas quartz grains are most often angular to subangular, marble components also show rounded shapes.

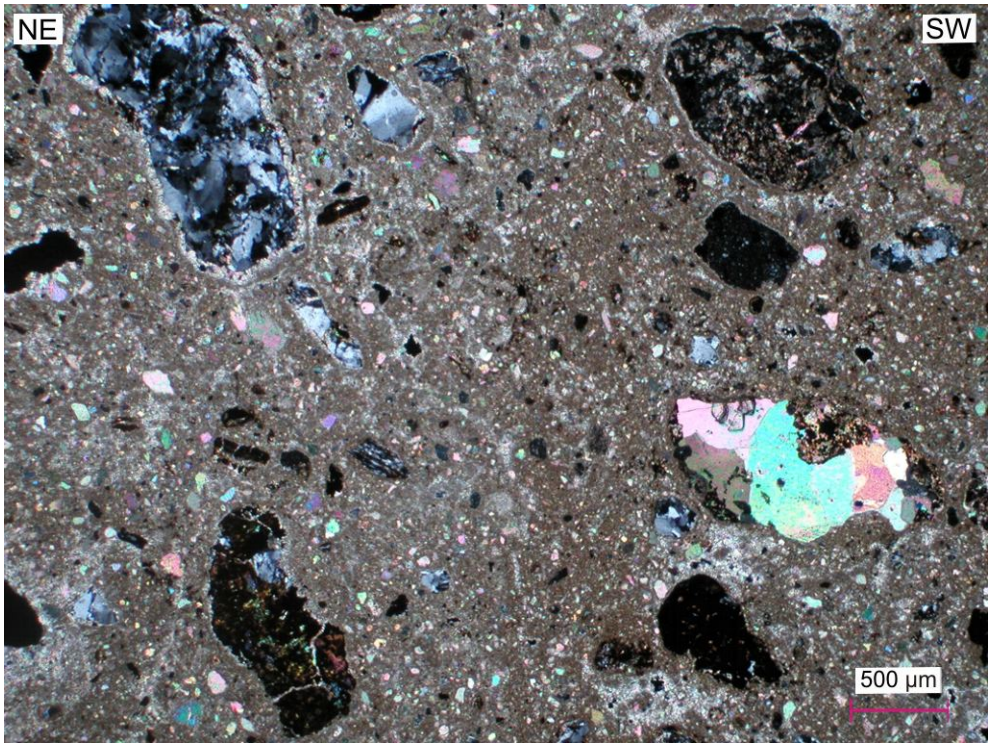

Figure 20: Thin section of cataclasite viewed in crossed polarized light. Components are polycrystalline quartz, calcite and calcite overprinted with Fe-oxides. Some quartz components are enveloped in a rim of fine-grained calcite.

3.3.10 Protocataclastic Quartzites

The southernmost area of Kythnos Island is dominated by strongly brecciated, leached and hydrothermally altered quartzitic rocks. The protocataclastic quartzites crop out only on the southernmost areas of Kythnos Island and were originally described as carbonatized volcanic rocks (DeSmeth, 1975). The rocks are composed mainly of quartz, and contain minor amounts of calcite and muscovite. Some areas show massive hy-

drothermal overprint fluids depositing Fe-oxides and -hydroxides (primarily goethite and hematite).

The degree of deformation and alteration varies throughout the outcrops. Some areas appear as massive quartzites, showing quartz grain boundary triple junctions with 60° angles, a feature commonly put down to statical recrystallization, a process which could imply posttectonic annealing. Mica minerals seem to be concentrated in bands and show a preferred orientation which may point to an original foliation direction (Fig. 21). Locally, the quartz-rich rocks are deformed to ultracataclasites (Fig. 30) and strongly overprinted by Fe-rich fluids.

Figure 21: Thin section of quartzite viewed in crossed polarized light (top) showing foam structure and possible foliation defined by white mica. Outcrop picture of strongly fractured quartz-rich rock (bottom).

3.4 Deformation History

3.4.1 Foliation and Lineation

Deformation is most pronounced in a penetrative schistosity, which is most obvious in phyllite units, showing prominent foliation planes. Most planes of schistosity are found to be dipping shallowly to the NNE in more northern areas and to the SSW in the southernmost regions. This results in an overall dome-shaped structure with the foliation planes dipping in an outward direction (Fig. 22). In proximity to the ultramylonitic marbles, the foliation planes show a steeper southward dip. The schistosity is commonly overprinted by various folding stages.

Mineral and stretching lineations are found to strike rather consistently toward NNE to NE (Fig. 22). Additionally to the persistent NNE-directed lineation, subordinately a SSW direction can also be observed. From the lower-lying strata to the higher ones a drift in lineation direction from NE to NNE can be observed. In the tourmaline-epidote-gneiss both a mineral and crenulation lineation can be observed. Isolated lenses of metabasic rocks show mineral lineation, defined by a preferred orientation of amphibole crystals, also dipping toward NNE.

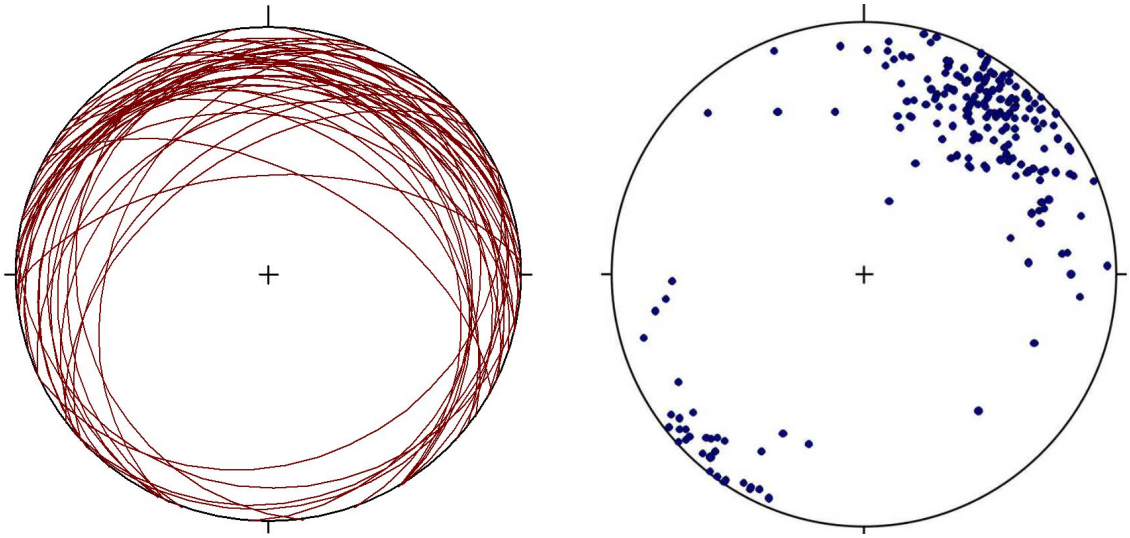

Figure 22: Schmidt's equal area plot of the lower hemisphere showing foliation planes dipping to the NW, N and NE at a low angle (left). Lineations of all types (stretching and crenulation lineation) strike consistently in a NE-SW direction (right).

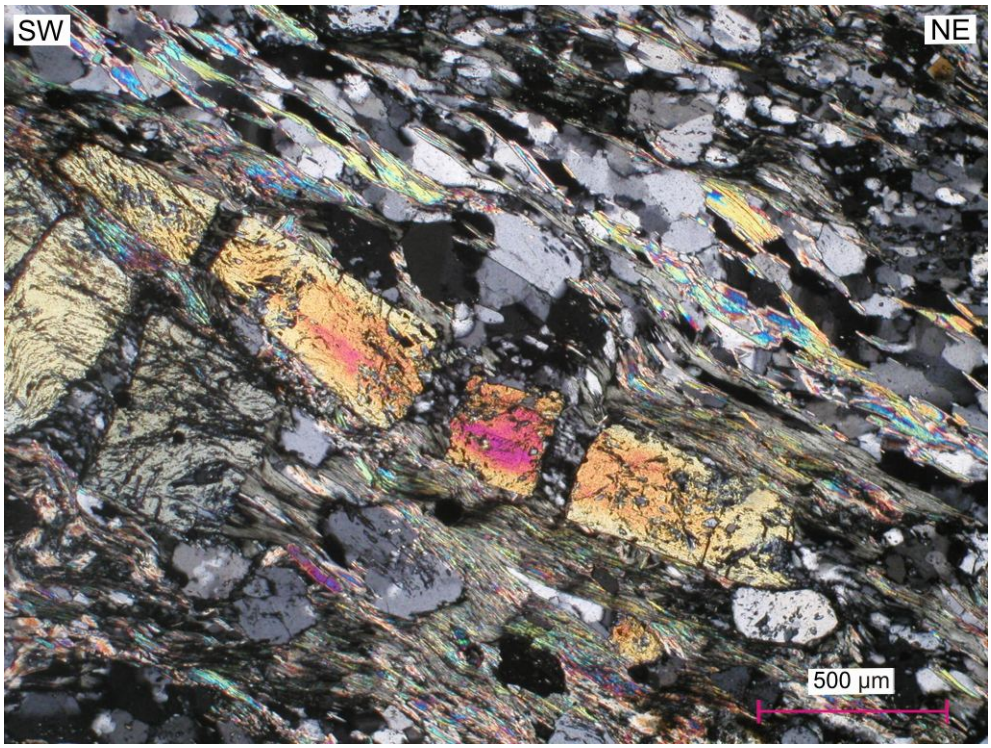

Figure 23: Thin section of greenschist viewed in crossed polarized light. The boudinaged epidote crystal in the center shows remnants of an older, folded, foliation direction and is part of a younger stretching lineation. Younger foliation is also formed by preferred orientation of mica.

Figure 24: Subhorizontal isoclinal folding of a gneiss layer in the marble mylonite. The limb between the two fold hinges has been sheared through, giving evidence for extensional shear postdating isoclinal folding.

3.4.2 Folding

At least two different folding phases can be observed on southern Kythnos (Fig. 25). Especially schists and marbles show widespread isoclinal folding along subhorizontal axial planes and southwest-vergent fold axes. Second order z-, s- and m-fold geometries indicate a larger-scaled isoclinal folding. Isoclinal folds with subhorizontal axial planes, but NW-SE trending fold axes also occur subordinately.

Map-scale open folding is produced as the strata, which lie mostly horizontal throughout the island, dip more steeply to the south in the southernmost regions. This open folding is depicted in the cross-sections drawn by De Smeth (1975). Parallel to the open folding, buckle and thrust folds with a subvertical axial plane can be observed in the ultramylonitic marble. Refold structures are widespread and can be observed when a subhorizontal fold axial plane is overprinted by subvertical axial plane (Figs. 26 and 27).

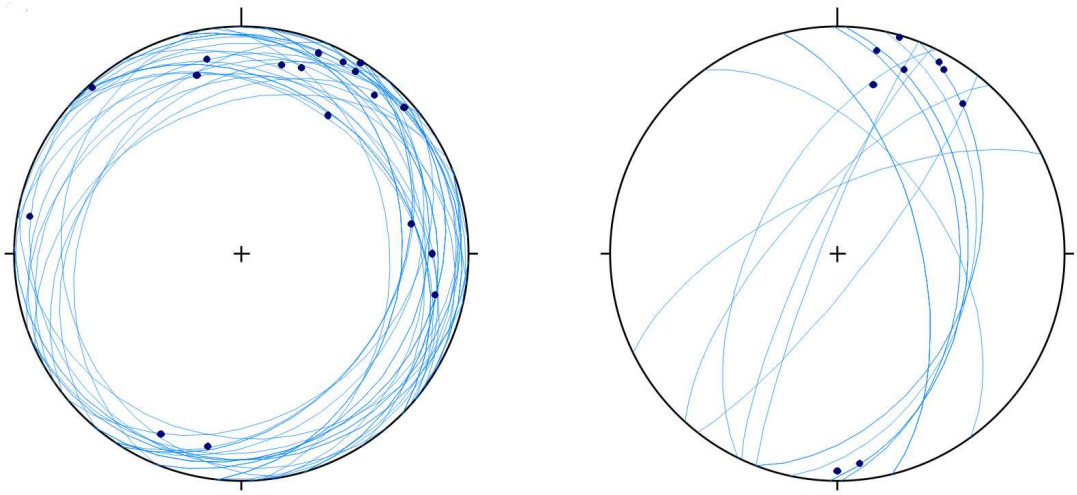

Figure 25: Two principal folding directions as seen in the Schmidt's equal area plot of the lower hemisphere show subhorizontal isoclinal folding with shallow dipping fold axes (left) and upright open folding with fold axes dipping NNE-SSW at a low angle (right).

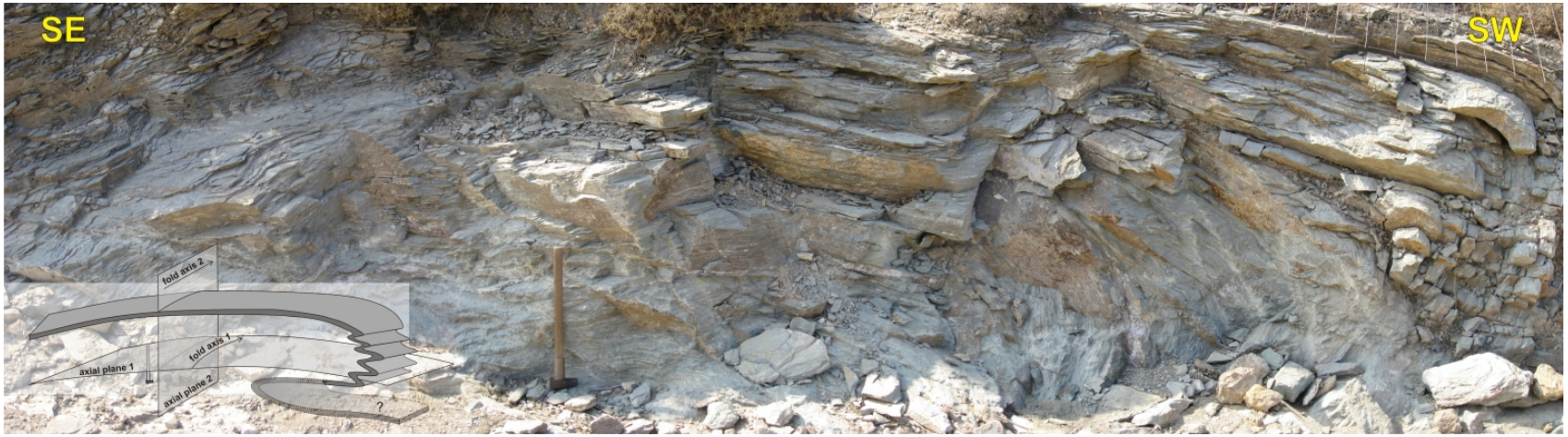

Figure 26: Chlorite schist isoclinally folded along a subhorizontal axial plane and N-S-striking fold axis. The first fold is overprinted by a second folding stage with a subvertical axial plane and fold axis parallel to the fold axis of the first stage.

3.4.3 Boudinage

Boudinages and pinch-and-swell structures of gneiss layers are common within the mylonitic marble (Fig. 28). Layers of gneiss are thinned out in a direction that is consistent with NE-SW-directed extension. On thin section-scale boudinages appear most often in clasts (of magnetite or quartz) within the marbles.
Furthermore, boudinaged epidote crystals in the epidote schist produce a stretching lineation.

3.4.4 Shear Sense Indicators and Mineral Grain Deformation

The rocks of the greenschist-marble unit, which show penetrative schistosity, exhibit scc'-fabrics (Fig. 29) and shear bands both in outcrop- as in thin section-scale. These shear sense indicators point to a general top to SSW-directed deformation. Within the marble layers, quartz and gneiss porphyroclasts also show clast geometries consistent with top to SSW-directed kinematics.

3.4.5 Marble-Ultramylonite Shear Zone

A conspicuous element of the southeastern tip of Kythnos Island is an up to 5 m massive layer of an extremely fine-grained marble. The ultramylonitic marble shows a significant tectonically reduced (in contrast to the coarser yellow-grey marble) grain size produced by dynamic recrystallization. This calcitic marble shows mylonitic foliation consisting of mm- to cm-wide bands of calcite crystals with varying grain sizes (Fig. 18).
The ultramylonite is associated with cataclasite layers cutting steeply toward the SW and discordantly through the existing structures. An up to a meter massive layer of ultracataclastic material represents a boundary between the ultramylonitic marble and an adjacent highly brecciated quartzitic lithology. The ultracataclasites show major variations regarding composition and degree of cataclasis, which enable a distinction between different generations (Fig. 30). Directly in contact with the ultramylonite, the cataclastic components appear to be predominantly calcitic, whereas within the quartzite almost no calcitic material can be observed. However, most components within the cataclasites are polycrystalline quartz grains, calcites, marbles overprinted by iron-rich fluids (Fig. 20). More marble-rich cataclasites show substantial amounts of rounded grains and grains with a thin fine-grained calcitic rim around the components.

Figure 27: Refolded gneiss layer within epidote schists. The first folding stage is along a SE-dipping axial plane and a SW-NE-directed fold axis, which is overprinted by a second folding stage with a subvertical axial plane and a SE-NW-directed fold axis.

Figure 28: Boudins of gneissic material in mylonitic marble indicating NE-SW extension.

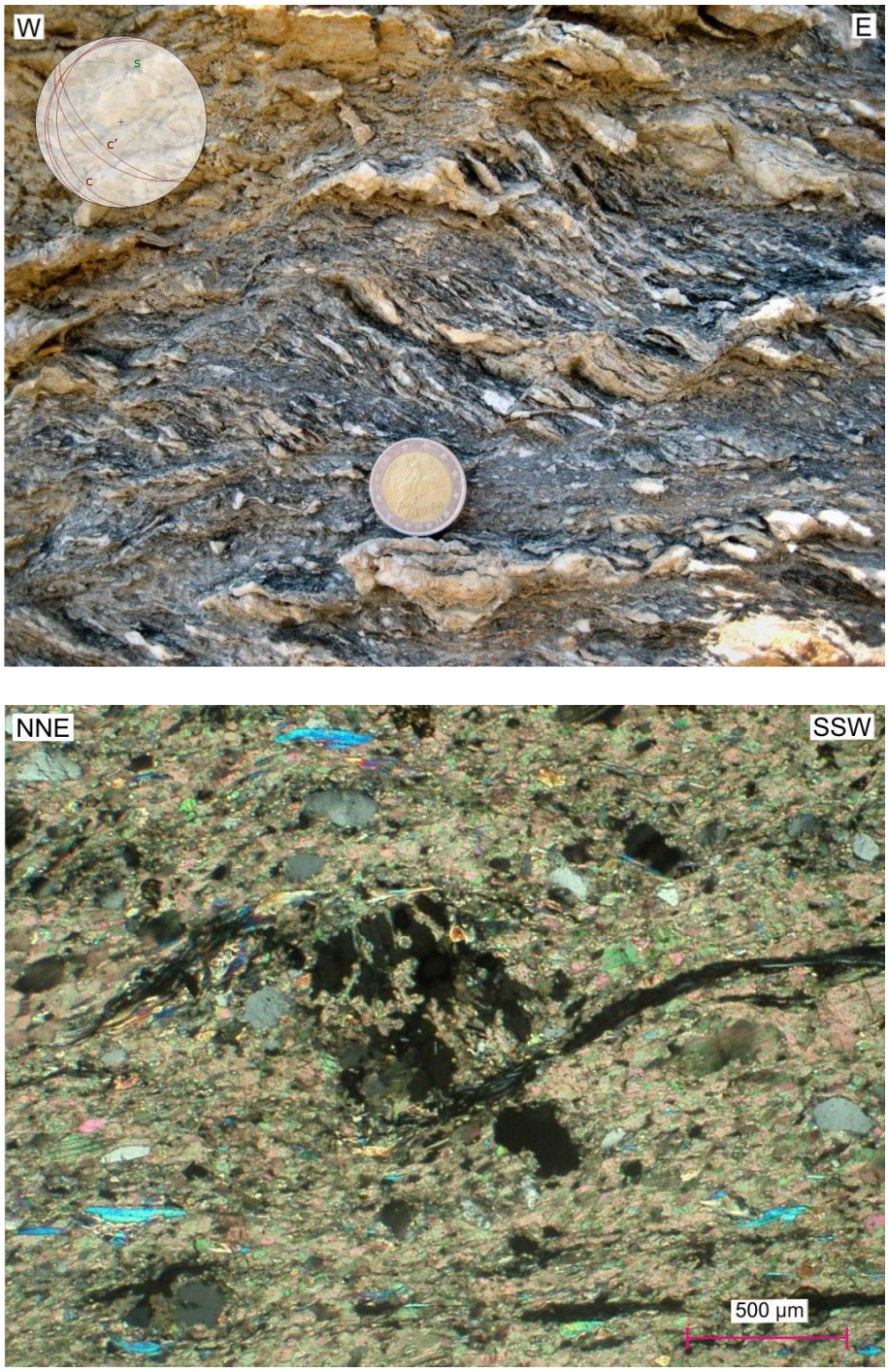

Figure 29: Top to SW-directed movement observed in a shear band in a chlorite-schist exhibiting scc'-fabric (top) and in a δ-clast within Qtz- and mica-rich marble (bottom).

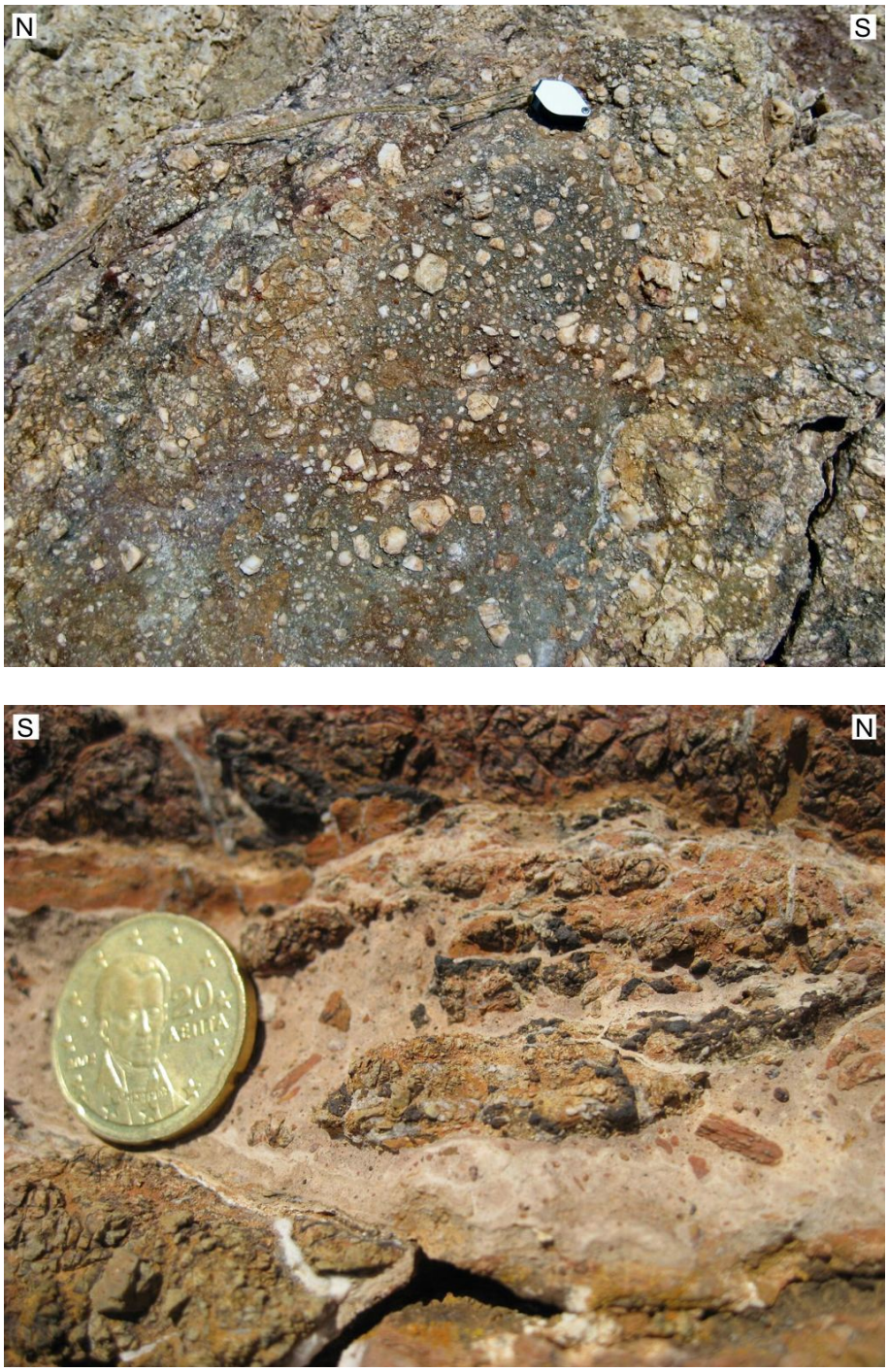

Figure 30: Quartzitic cataclasite with angular quartz components (top). Hydrothermally altered ultramylonitic marble showing cataclastic deformation (bottom).

3.4.6 Brittle-Ductile Deformation

The pre-existing structures within the greenschist-marble unit and the ultramylonitic marble are further overprinted by NW-SE-directed shortening perpendicular to direction of extension, which led to the folding of the ultramylonitic marble layer into an antiform. Within the marble ultramylonite, buckle folds and fault bend folds (Fig. 31) give evidence for this compressional event with a subvertical axial plane and a NE-SW-directed fold axis.

3.4.7 Brittle Deformation

Numerous joints and faults document brittle deformation phases. Vein generations can be distinguished according to their orientation and filling and cross-cutting relationships enable a relative age estimation. These veins are commonly filled with quartz, calcite, Fe-oxides and -hydroxides and baryte crystals. The direction of the final stages of brittle fault generation which are documented on fault planes (Fig. 32) indicate that the whole area under investigation was subjected to normal faulting due to further NE-SW directed extension, both on shallow-dipping SSW-NNE fault planes with down-dip movement and a conjugated high-angle fault system indicating a principal compression direction from the NW and SE and corresponding NE-SW extension.

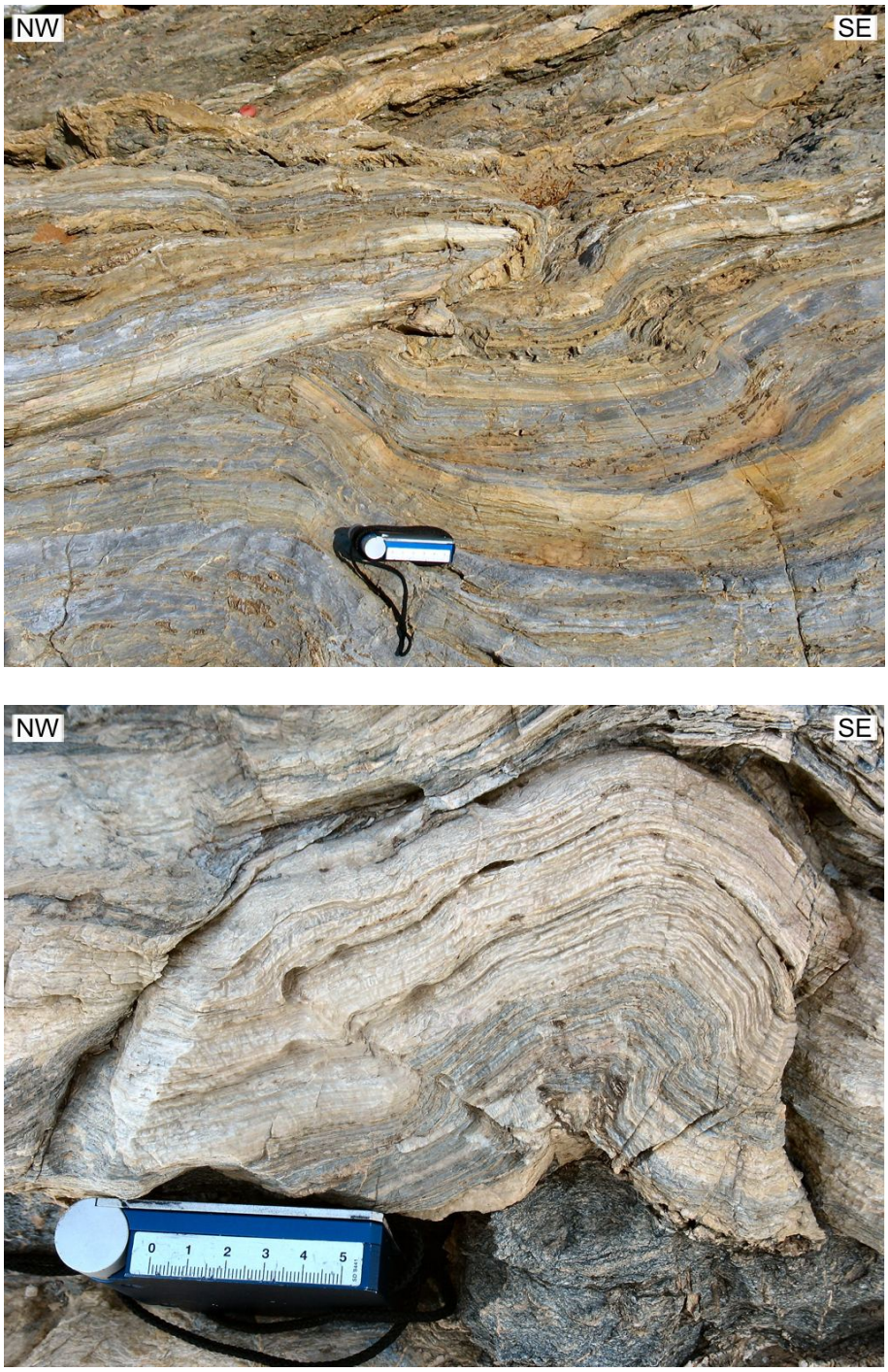

Figure 31: Fault bend fold (top) and buckle fold (bottom) in ultramylonitic marble showing shortening perpendicular to main SSW-NNE extension direction.

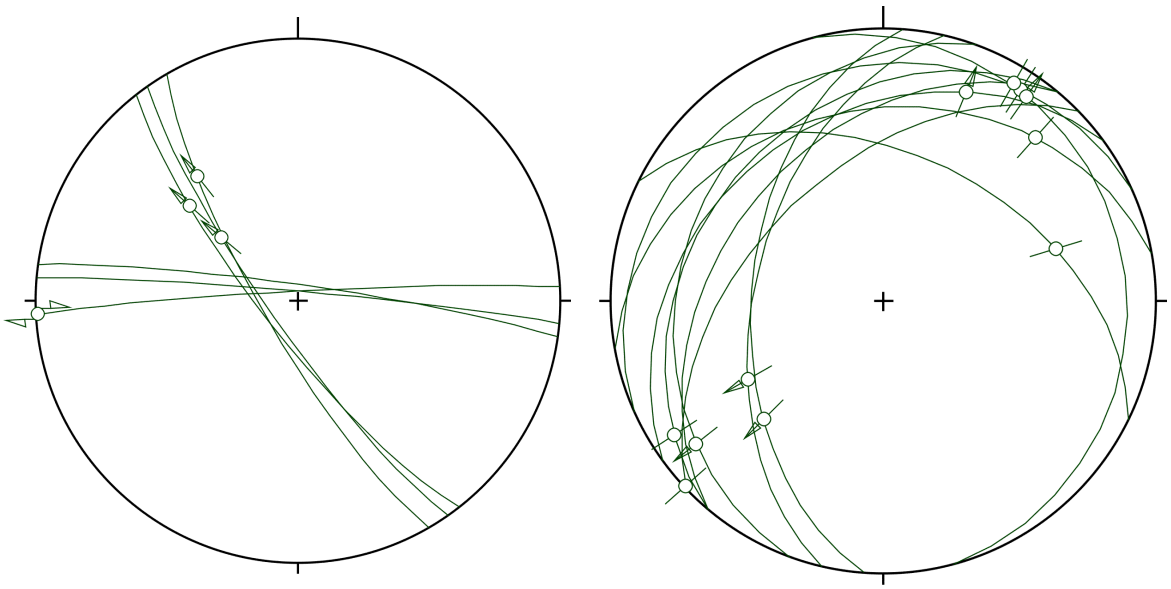

Figure 32: Angelier lower hemisphere plots of brittle fault planes. Conjugate high-angle fault system (left) and shallow dipping brittle fault planes (right) indicating SW-NE extension.

3.4.8 Summary of Deformation History

Lithologies on Kythnos have been affected by various stages of ductile and brittle deformation. The first deformation phase (D1) is marked by a NE-SW-trending lineation and a top to SW-directed sense of shear. Evidence of D1 is pronounced in lower-lying strata of epidote-schists. Subsequent deformation (D2) is characterized by a rotation of the lineation direction toward the N, with mineral lineation trending NNE-SSW, while shear sense is directed top to SSW. These deformation stages show widespread greenschist-facies overprint. Ductile deformation resulted in the development of schistosity and mineral lineation, such as in elongated quartz and feldspar crystals. This occurred alongside subhorizontal isoclinal folding followed by upright open folding.
Under the brittle-ductile transition and post-metamorphic brittle conditions, faulting is dominated by an NNE-SSW-directed extensional regime. During the brittle-ductile transition, fabrics with SSW-directed sense of shear were formed. Further exhumation led to localization of strain first in mylonites, then in cataclasites. The shear zone is characterized by major grain size reduction of calcite crystals and by the brittle behaviour of quartz grains within the ultrafine-grained mylonitic marble. Significant grain size reduction is a common characteristic of shear zones and provides a means of re-

Figure 33: Large-scale normal fault dipping toward SW at the southern end of Kythnos Island. The brittle fault is associated with hydrothermal activity leading to iron ore deposition.

ducing friction. Brittle deformation of quartz grains indicate temperatures lower than 270°C, the minimum temperature for crystal plasticity of quartz (Voll, 1976).
A final brittle overprint is evident in veins and open joints. Extension gashes were formed during various generations, which can be subdivided according to their orientation and the material with which they are filled. The orientation of major brittle structures is consistent with ongoing SSW-NNE-directed extension.
Altogether, the structures on Kythnos Island give insight into deformation events at various stages of exhumation through the middle and upper crust.

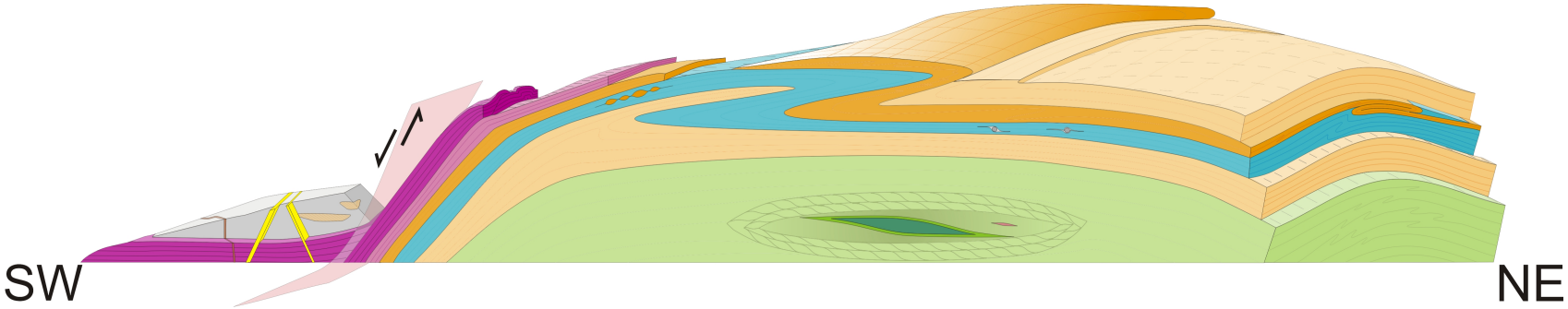

Figure 34: Synoptic diagram of deformation phases and major lithologies.

3.5 Geochemical and Microprobe Investigations

The whole-rock and mineral chemistry of the metabasic rocks and the ferromanganoan metasediments were investigated to provide a comparison with previously published data on this material. The whole-rock composition of the metabasites allow an estimation of the depositional environment and gives information on the possible connection with ophiolitic slices found throughout the Cyclades. For the ferromanganoan metasediments the measurement of the composition of garnet and amphibole was thought to confine metamorphic conditions and to allow comparison of the mineral chemistry of similar lithologies on other Cycladic islands.

Microprobe investigations were carried out on the Cameca SX 100 at the Department of Lithospheric Research at the University of Vienna. A beam current of 20 nA and a voltage of 15 kV were used. A defocused ion beam was used for measurements of amphiboles, due to their high sodium content. With the electron microprobe, compostions of garnet, amphibole, chlorite, epidote and tourmaline were determined from the ferromanganoan metasediments and tourmalinites.

Whole-rock chemistry of major, minor and trace elements was performed on three samples of metabasic rocks from different localities. The major and some minor elements were measured using optical emission spectroscopy (ICP-OES), atomic absorption spectroscopy (F-AAS) and X-ray fluorescence (XRF). Further minor and trace elements were measured by mass spectrometry (ICP-MS). All analyses were carried out at the University of Vienna. The powdered rock samples were used directly for XRF measurements and volatile detection. For measurement using spectrometry the powdered samples were dissolved in either a) a mixture of hydrofluoric acid and nitric acid, or b) with Li-borate (for Si detection).

The atomic emission spectroscopy with excitation by plasma (ICP-OES) was carried out on the "Optima 5300DV". The analytical setup for the spectrometry involved a dwell time of 10 ms, 50 sweeps and one replicate. From the sample 250 mg were dissolved in 250 ml solution, from which the trace elements (Ba, Be, Co, Cr, Cu, Li, Nb, Ni, Pb, Rb, Sr, V, Zn, Zr) were measured. For the major elements (Si, Fe, Al, Ca, Mg, Na, K, Mn, Ti, Ba, Sr, Zr) this solution was diluted to 1/10 of the original concentration.

The mass spectrometer (ICP-MS) is of the type "Elan 6100", and uses inductively coupled plasma (gaseous Ar) for ionization.

Measurements with X-ray fluorescence were carried with a wavelength-dispersive fluo-

rescence spectrometer, PHILIPS PW2400, using a powdered, heated and compressed rock sample.
The elements Na, K, Cu and Zn were additionally measured by atomic absorption spectroscopy, using a flame for thermal excitation.
Loss of ignition (LOI) was determined gravimetrically by heating 5 g of sample at 1000°C for a duration of 5 h. The LOI includes carbonates, which are lost as carbon dioxide, crystal bound water, non-carbonate carbon and sulfur. The actual composition of the LOI was measured on Elemental Analyser Elementar VarioMacro, which analyzes CHNS+O by combustion of liquid and solid samples at 1150°C.
Analytical errors generally lie between 5–10 % but depend on method used and the respective concentration of the element measured. The quality and further the error of the analyses was determined by comparison with internal standards. The precision and thus the error of a single measurement can be approximated by the deviation of the measured standard value from the known standard composition.

3.5.1 Whole Rock Chemistry

Measured element concentrations Concentrations of major elements were measured by ICP-OES (Si, Al, Fe, Ca, Mg, K, Ti, Mn, P), F-AAS (Na, K) and XRF (Si, Al, Fe, Ca, Mg, Na, K, Ti, Mn, P). LOI was measured gravimetrically, the detailed composition of which was determined by CHNS elemental analyser. Minor and trace elements were measured by ICP-OES (Ba, Co, Cr, Cu, Li, Ni, Pb, Rb, Sr, Zn, Zr), F-AAS (Cu, Zn) and ICP-MS (Ba, Co, Cr, Cs, Cu, Ge, Li, Mo, Ni, Pb, Rb, Sb, Sn, Sr, Tl, V, Zn). Rare Earth Elements (Sc, Y, La, Ce, Pr, Nd, Sm, Eu, Gd, Tb, Dy, Ho, Er, Tm, Yb, Lu, Th, U) were measured by ICP-MS. Mean values are given in tables 1 to 3 and are placed alongside previous measurements from lithologies on Kythnos. Ki704 was described in the field as a magnetite-bearing metabasic rock and was sampled south of Agios Dimitrios (Fig. 35).
The sample Ki709 is taken from the same locality but appeared lighter coloured and showed relictic magmatic fabric. Ki713 originates from the North of Agios Dimitrios and was much darker in appearance, but showed the same magmatic fabric. Data from Carl (1993) are also from the Agios Dimitrios area, whereas data by Chrysanthaki and Baltatzis (2003) is from samples taken in the area around Kanala.

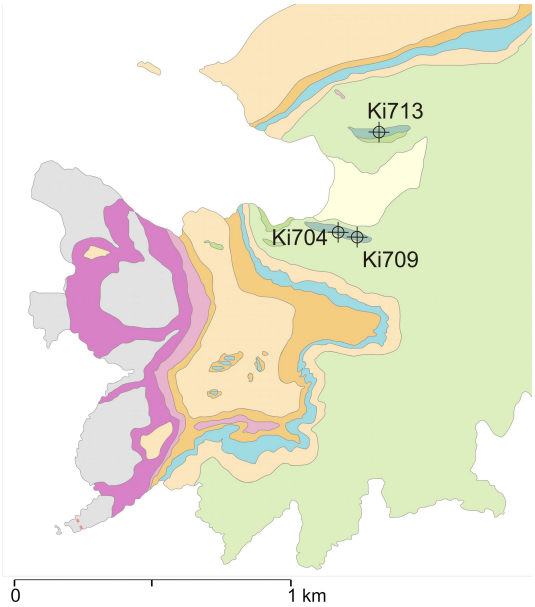

Figure 35: Locations of the samples used for analysis of whole rock chemistry. Sample Ki713 was taken from an outcrop north of Agios Dimitrios, whereas Ki704 and Ki709 were found south of the bay.

Major and Minor Constituents

					Meta-Ultrabasite				Metabasite			Metasediment				
		Ki704[1]	Ki709[1]	Ki713[1]	Ki-36[2]	Ki-41[2]	Ki-62[2]	Ki-37[2]	Ki-42[2]	Ki-107[2]	Ki-134[2]	Ki-69[2]	Ki-100[2]	Ki-125[2]	KP12[3]	K408[3]
SiO_2	[%Ox]	38,45	51,66	40,99	42,1	40,8	39,3	38,2	47,4	50,2	41,5	50,9	47,2	48,2	46,21	46,3
Al_2O_3	[%Ox]	12,33	14,31	8,57	8,95	6,94	8,94	19,5	14,8	15,5	14,1	18,0	16,8	21,2	12,38	13,8
Fe_2O_3	[%Ox]	8,92	11,58	12,79	9,58	12,94	12,9	6,13	8,43	9,30	9,08	11,9	9,87	9,19	10,83	11,90
CaO	[%Ox]	18,81	7,12	5,06	6,36	4,89	3,80	16,6	12,0	5,61	16,4	4,69	8,34	0,40	7,95	8,15
MgO	[%Ox]	3,31	6,28	23,61	23,1	24,2	24,3	12,3	4,59	7,93	4,15	3,84	3,37	7,35	15,30	9,30
Na_2O	[%Ox]	2,87	3,46	0,28	0,52	0,83	0,58	0,80	2,70	4,55	2,85	2,61	2,19	0,43	2,38	3,15
K_2O	[%Ox]	0,52	0,68	0,07	-	0,04	-	0,15	0,55	0,16	0,65	1,82	2,65	5,57	0,66	0,34
MnO	[%Ox]	0,17	0,15	0,17	0,14	0,19	0,17	0,15	0,13	0,13	0,13	0,13	0,06	0,12	0,18	0,17
TiO_2	[%Ox]	1,36	1,76	0,98	0,66	0,74	0,80	0,51	1,05	1,58	1,59	1,55	1,53	1,09	0,77	1,48
P_2O_5	[%Ox]	0,19	0,21	0,14	0,03	0,04	0,07	0,06	0,22	0,10	0,23	0,04	0,18	0,18	0,34	0,09
H2O	[%Ox]	1,69	2,12	6,90	7,76	7,74	8,48	5,24	3,28	3,71	2,80	3,96	3,81	6,94		
CO_2	[%Ox]	11,50	0,18	1,24	0,26	-	-	1,00	3,56	-	7,55	-	4,03	-		
LOI	[%Ox]	12,89	2,47	7,81											2,26	4,80
S	[%Ox]	0,055	0,048	0,056												
N	[%Ox]	0,026	0,003	0,015												
SUM	[%]	99,82	99,67	100,47	99,46	99,35	99,38	100,49	98,71	98,77	101,03	99,45	100,03	100,67	99,26	99,48

Table 1: Summary of major and minor element composition. [1]own data. [2]data from Carl (1993). [3]data from Chrysanthaki and Baltatzis (2003).

Trace Elements

					Meta-Ultrabasite				Metabasite			Metasediment				
		Ki704[1]	Ki709[1]	Ki713[1]	Ki-36[2]	Ki-41[2]	Ki-62[2]	Ki-37[2]	Ki-42[2]	Ki-107[2]	Ki-134[2]	Ki-69[2]	Ki-100[2]	Ki-125[2]	KP12[3]	K408[3]
As	[ppm]	0,6	0,5	6,6												
Ba	[ppm]	29,7	25,4	7,6											21	68
Be	[ppm]	0,35	0,56	0,31												
Bi	[ppm]	0,32	0,01	0,02												
Cd	[ppm]	0,1	0,0	0,08												
Co	[ppm]	30,9	34,2	75,4												
Cr	[ppm]	8,0	48,7	2583	2441	2298	3143	904	253	249	301	142	181	147	919	335
Cs	[ppm]	2,4	1,4	0,1												
Cu	[ppm]	52	22	43											94	187
Ga	[ppm]														14	19
Ge	[ppm]	1,0	1,5	1,3												
Li	[ppm]	8,6	19,2	9,8												
Mo	[ppm]	0,6	0,2	0,2												
Nb	[ppm]				2	-	-	3	1	8	1	-	-	21	15	2
Ni	[ppm]	42	28	804	1151	1013	1122	231	76	97	121	127	84	81	105	103
Pb	[ppm]	4,3	4,4	16,9												
Rb	[ppm]	16,0	7,6	0,03	1	2	1	1	13	9	20	53	48	126	10	5
Sb	[ppm]	0,3	0,3	0,5												
Sn	[ppm]	3,6	1,0	1,9												
Sr	[ppm]	237	98	31	10	13	5	446	343	153	309	499	390	13	213	247
Tl	[ppm]	0,1	0,04	0,003												
V	[ppm]	1,5	1,4	2,2	107	164	149	111	266	283	258	84	131	192	331	367
Zn	[ppm]	122	61	109											79	100
Zr	[ppm]	71	87	77	47	57	67	32	91	126	126	196	126	216	130	154

Table 2: Summary of trace element composition. [1]own data. [2]data from Carl (1993). [3]data from Chrysanthaki and Baltatzis (2003).

Rare Earth Elements

					Meta-Ultrabasite				Metabasite			Metasediment				
		Ki704[1]	Ki709[1]	Ki713[1]	Ki-36[2]	Ki-41[2]	Ki-62[2]	Ki-37[2]	Ki-42[2]	Ki-107[2]	Ki-134[2]	Ki-69[2]	Ki-100[2]	Ki-125[2]	KP12[3]	K408[3]
Sc	[ppm]	28	37	25											57	49
Y	[ppm]	20	29	13	13	21	8	13	23	30	33	20	29	34	32	37
La	[ppm]	5	6	3												
Ce	[ppm]	12	16	8												
Pr	[ppm]	1,8	2,5	1,2	2	4	2	3	4	4	5	6	5	11		
Nd	[ppm]	10	14	7	10	-	15	-	18	10	-	20	-	45		
Sm	[ppm]	2,7	3,8	1,9	3	3	4	-	5	3	2	4	2	9		
Eu	[ppm]	0,9	1,2	0,4												
Gd	[ppm]	3,7	4,6	2,2												
Tb	[ppm]	0,6	0,9	0,4												
Dy	[ppm]	3,6	5,3	2,6												
Ho	[ppm]	0,8	1,1	0,5												
Er	[ppm]	2,1	3,1	1,5												
Tm	[ppm]	0,3	0,5	0,2												
Yb	[ppm]	1,8	2,8	1,4												
Lu	[ppm]	0,2	0,4	0,2												
Th	[ppm]	0,3	0,3	0,2	-	1	-	-	2	-	1	3	-	12	5	
U	[ppm]	0,3	0,1	0,1	1	3	1	-	3	-	4	2	2	3		

Table 3: Summary of Rare Earth Element content. [1]own data. [2]data from Carl (1993). [3]data from Chrysanthaki and Baltatzis (2003).

Interpretation of whole rock chemistry The three samples measured show a great variety in major and trace element composition. Especially major differences in silica content indicate that samples are from both felsic and basic lithologies. However, they all show compositions within the range of meta-ultrabasites to metabasites and metasediments. A large variability in the amount of Mg, Al and the alkaline elements Na and K can be seen. Variation in the Ca content is probably due to differing degrees of overprint with carbonate-rich fluids. This is supported by the fact that also the LOI (composed primarily of CO_2 and minor amounts of H_2O) shows similar strong variation, which correlates with Ca content. Additionally, the samples with highest amount of carbonate also show the highest contents of Sr and Rb. Even though samples Ki704, Ki709 and Ki704 show varying amounts of carbonate content, a comparative amount of non-carbonate CaO remains (approximately 4 %Ox) for all samples. This can be correlated with field observations that overprint with carbonate-rich fluids can be found in widespread areas.

Conspicuous are significant amounts of heavy metals in the sample with very low silica content (Ki713). Especially remarkable are the extremely high amounts of Cr and Ni, which can be taken as an indicator for an originally ultrabasic source rock. Obviously enriched are also Pb, Co and As. The rare earth elements seem to be distributed rather homogeneously.

Altogether this indicates that only sample Ki713 is from a truly metabasitic lithology, showing characteristic low silica and high Mg and heavy metal content. The other samples, however, show either a strong overprint or should be placed within the greenschist facies assemblage. Therefore, as only one sample of a metabasite was measured, conclusions drawn from the whole rock chemistry can only be tentative and for a representative analysis further investigations would be necessary.

3.5.2 Mineral Chemistry

The mineral chemistry composition of garnets, amphiboles, tourmalines and mica was measured in ferromanganoan metasediments and tourmalinites. Samples of ferromanganoan metasediments were taken from central Kythnos and northern Kea. Tourmalinite samples are from southern Kythnos. Representative analyses for mineral composition are given in the appendix. Mineral formulas were calculated using an MS Excel© spreadsheet by Tindle and Webb (1994).

Garnet compositions Garnets are relatively small (with a diameter of up to 50 μm) and are dispersed throughout the foliation. They occur alongside amphiboles, quartz, magnetite, apatite and as inclusions therein (Fig. 36). Showing a high MnO-content around 30%, they are commonly classified as spessartines. The garnet crystals appear to be rather homogeneous so that no compositional variation from core to rim could be observed.

Amphibole composition Amphiboles occur as large elongated crystals within the foliation of the ferromanganoan metasediments and within extension gashes. The alkali-amphiboles can be classified as crossites and magnesio-riebeckites. In a $Fe^{3+}/(Fe^{3+}+Al^{vi})$ versus $Mg/(Mg+Fe^{2+})$ diagram two distinct compositional groups can be identified (Fig. 39). Apart from alkali-amphiboles also Ca-amphiboles (actinolites) and Na-Ca-amphiboles (winchites) can be found. Within the amphibole crystals, compositional variation can be seen in an increase in CaO-content and decrease in Al_2O_3 from core to rim. The compositional variation from core to rim can also be seen as a progression from a crossite to a (Mg-)riebeckite mineral chemistry.

Epidote composition Compositions of epidote crystals were measured in the tourmaline quartzite rock. They show idiomorphic growth and lie within foliation planes. Epidote minerals show hardly any compositional variation. They have a high pistacite component and are thus rich in Fe^{3+}, indicating an oxidizing environment. The formula calculated is as follows: $Ca_2Al_2(Fe^{3+}_{0,87}Mn_{0,07})Si_3O_{12}OH$.

Tourmaline composition Tourmaline crystals show idiomorphic growth and are aligned within the foliation. Minerals are up to 100 μm in diameter and up to a few mm long. They show poikiloblastic cores, in which the inclusions are most commonly made up of the surrounding minerals quartz and magnetite (Fig. 40). A compositional zonation can be observed in which rims show higher Fe content and lower Al than the core. Mineral formula calculations (by A. Ertl. Mg was assigned to the Z-site by using calculations of Bloodaxe et al. (1999). Fe^{3+} was calculated using the method from Lynch and Ortega (1997)) show the rims to be schoerls with the following mineral formula:
$^{X}(Na_{0.91}Ca_{0.04}K_{0.01}\square_{0.04})^{Y}(Fe^{2+}_{1.48}Fe^{3+}_{0.54}Mg_{0.81}Ti^{4+}_{0.06}Mn^{2+}_{0.01}\square_{0.10})$
$^{Z}(Al_{5.26}Mg_{0.74})(BO_3)_3[Si_6O_{18}](OH)_3[O,(OH)]$
$X_Mg = 0.43$; X-site vacancy = 0.04

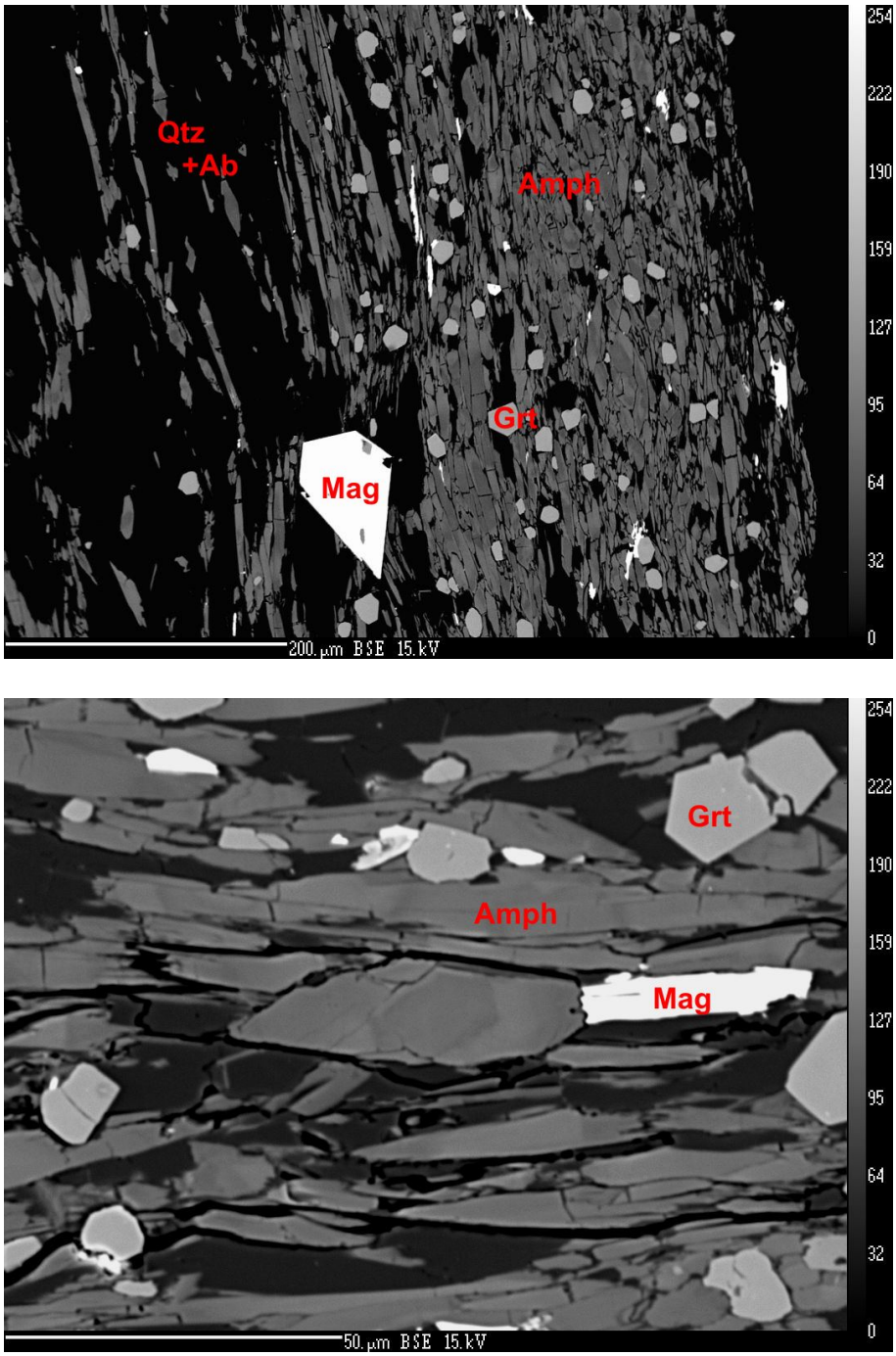

Figure 36: Back-scattered electron imagine of a ferromanganoan metasediment. High back scattering idiomorphic minerals are magnetite and garnet. A layering of amphibole and quartz + albite layers can be observed (top). Garnet and magnetite grow in both these layers. Magnetite is present both within the foliation and as idiomorphic crystals. Amphibole crystals show distinct zoning (bottom).

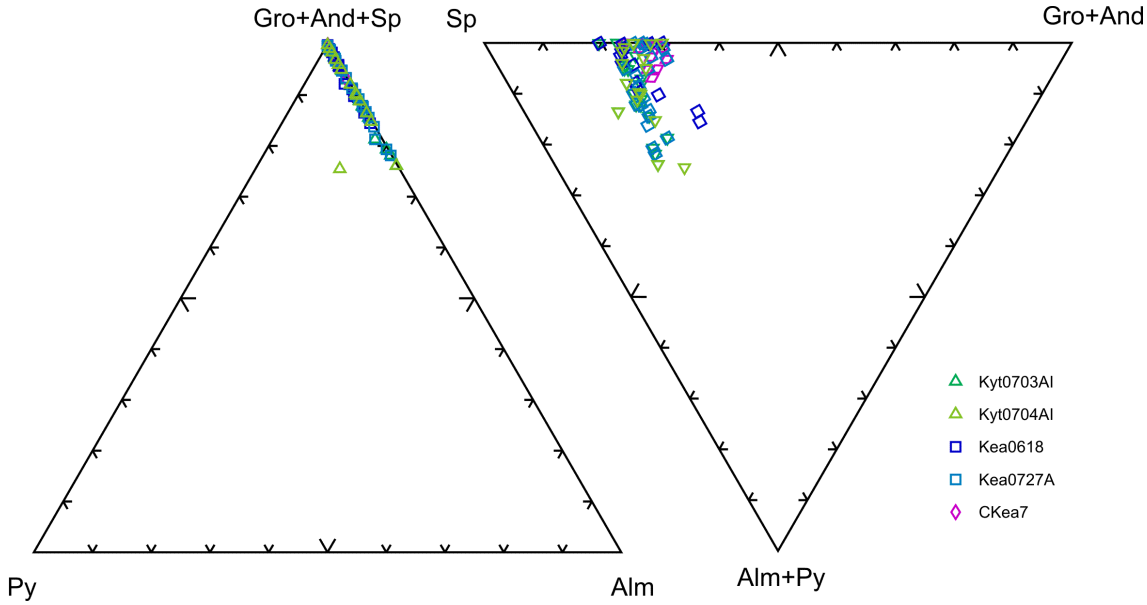

Figure 37: Ternary composition diagram for garnet (after Win et al. (2007)). All samples from Kythnos and Kea show more or less compositional similarities.

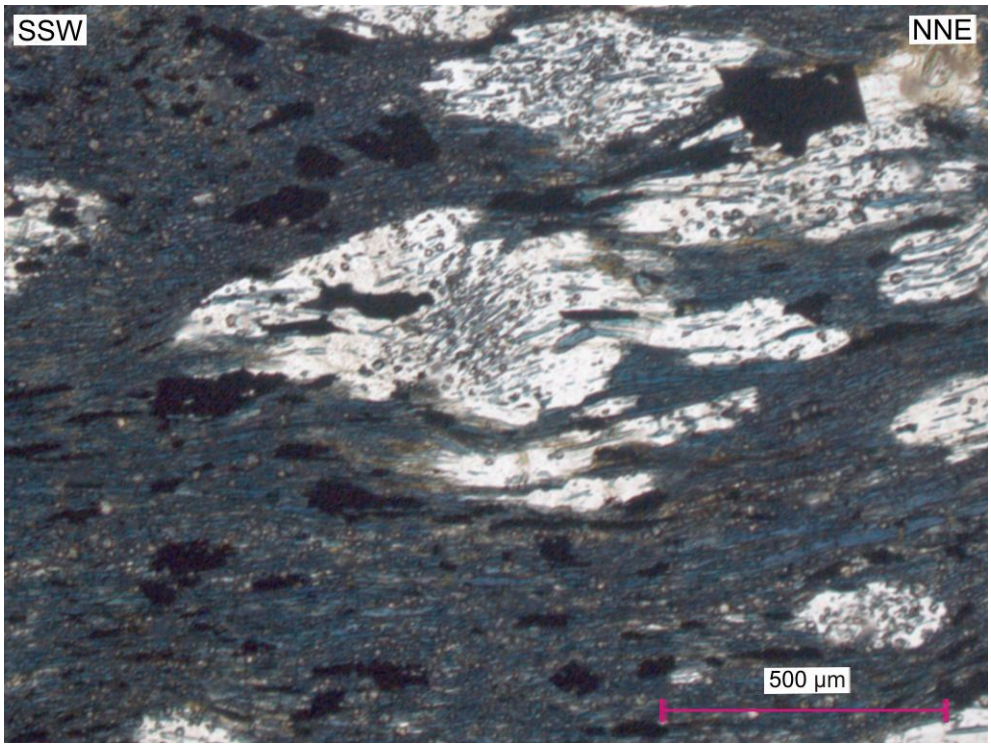

Figure 38: Thin section image of amphibole-rich rock viewed in crossed polarized light.

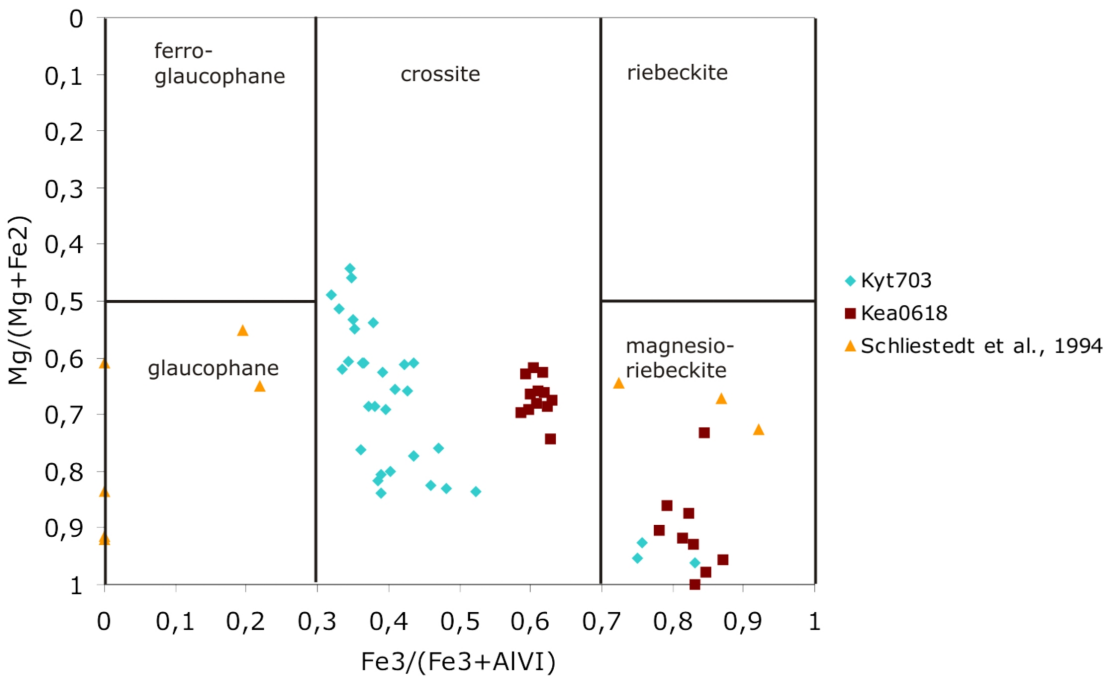

Figure 39: Classification diagram of alkali-amphiboles according to Leake (1978). Measured amphiboles plot in the crossite and the magnesio-riebeckite field.

Tourmaline cores are depleted in Fe and can be classified as (Fe-rich) Dravites with following formula:
$^{X}(Na_{0.88}Ca_{0.01}\square_{0.11})^{Y}(Mg_{1.32}Fe^{2+}_{1.23}Al_{0.21}Fe^{3+}_{0.06}Ti^{4+}_{0.02}Mn^{2+}_{0.01}\square_{0.15})$
$^{Z}(Al_{5.54}Mg_{0.46})(BO_3)_3[Si_6O_{18}](OH)_3[O,(OH)]$
$X_{Mg} = 0.58$; X-site vacancy = 0.11

Interpretation of Mineral Chemistry Data The very distinct mineralogical composition shows little variation throughout the samples. This facilitates a comparison with lithologically similar units on other islands.
Astonishing is the fact that garnets from ferromanganoan metasediments contain almost identical amounts of spessartine. Composition of the amphiboles show an analogous similarity, with all sodic amphiboles plotting in the riebeckite-crossite fields. Along the macroscopic likeness it can be deduced that these layers are of the same origin and possibly even define a distinct marker horizon within the lithostratigraphic section.
Ferromanganoan metasediments, such as piemontite-spessartine-quartzites, spessartine-quartzites and Na-pyroxene-quartzites are described within greenschist facies rocks on

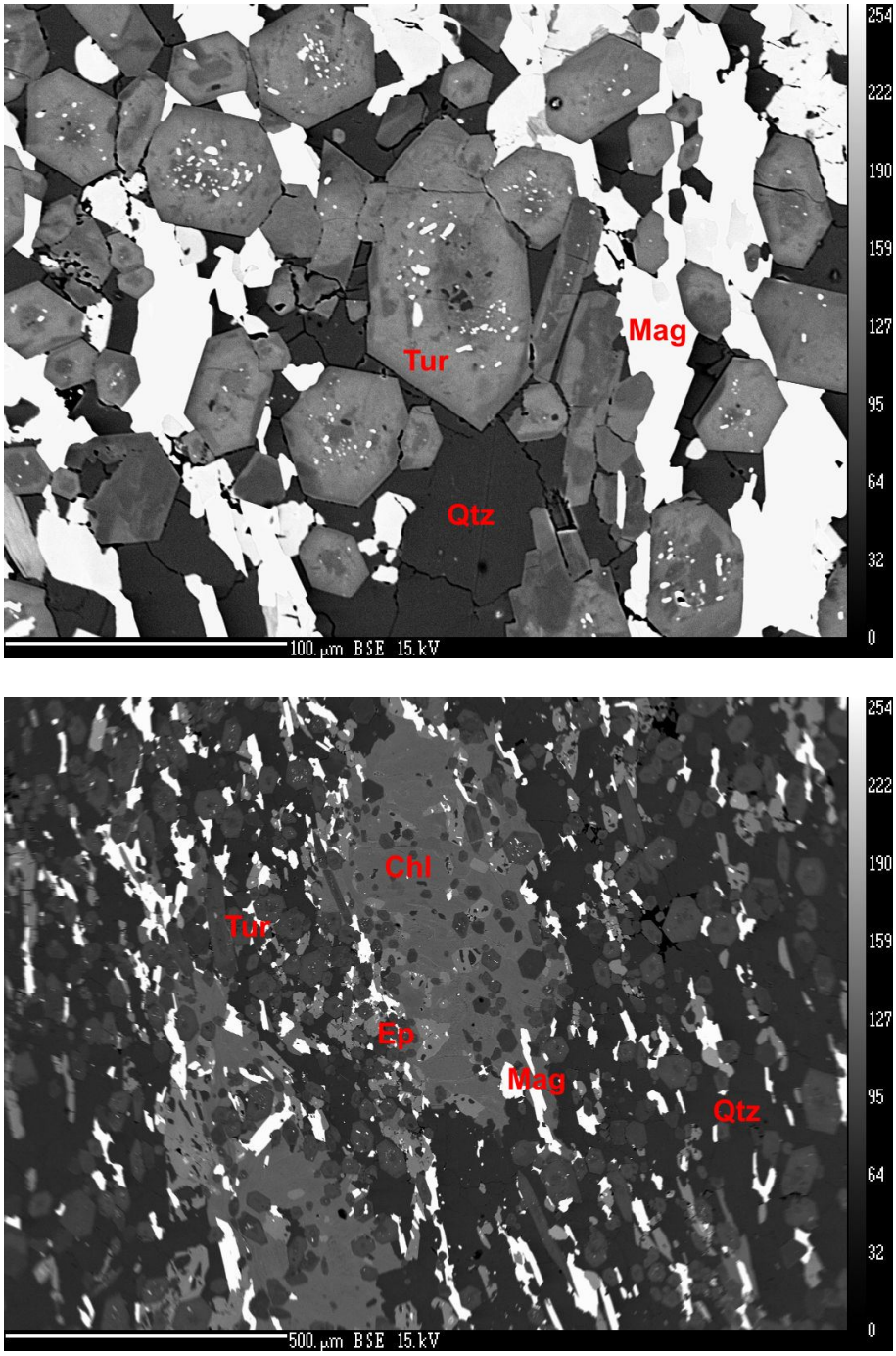

Figure 40: Back scattered electron imagine of tourmaline-magnetite-quartzite. The dark matrix is composed of quartz, within the foliation lie elongated tourmaline, epidote and magnetite crystals. These occur as inclusions within larger chlorite porphyrobalsts (bottom).

the eastern Cycladic island of Andros. These rocks show the garnets to be also mainly abundant in spessartine (X_{Sps} = 0.80–0.92) and the amphiboles Mg-rich crossites to Mg-riebeckites (Reinecke et al., 1985).

Spessartine-rich garnets are typical for low-grade metamorphism in the lower greenschists facies, at $\tilde{3}$00°C, 1–2 kbar (Theye et al., 1996), or 0.5 kbar and 370°C (Hsu, 1968). As garnets in natural rocks, which preferentially incorporate Mn in the form of spessartine component, are formed at significantly lower temperatures than pure almandine, which first appears in metapelites at around 450°C (Bucher and Frey, 1994). Garnet in which spessartine is the principal component is commonly been observed in the lower greenschist facies (quartz-albite-chlorite subfacies) (Schiller and Taylor, 1965), and thus spessartine-quartzites in general are commonly low-grade metamorphic rocks, often found in stratified form (Schiller and Taylor, 1965). They often appear in close association with hydrothermal ore deposits, tourmalinites and Zn- and Ba-rich rock types, as described in an occurrence in the Chilenean Andes by Willner et al. (2001). This is astonishing as such association is also found on Kythnos, on which ferromanganoan metasediments occupy a similar lithostratigraphic position as tourmalinites and both are found in the vicinity of an area showing widespread hydrothermal overprint involving ore deposition and baryte mineralization. Even though the ore formation is confined to veins and brittle faulting, the source rock might have been part of the original depositional sequence and the ores remobilized during metamorphic or hydrothermal activity. According to Chrysanthaki and Baltatzis (2003) the protolith of these sediments was part of an ocean-floor sequence with hydrothermal activity which provided Fe, Mn and trace elements. More detailed characterization of the composition of these spessartine-riebeckite-magnetite lithologies on Kythnos and Kea could further constrain the depositional environment and the metamorphic history of the metasediments.

This distinct lithology represents a prominent marker horizon in the Western Cyclades and provides a linking element for the islands of Kythnos and Kea. Their lithostratigraphic position in respect to to the shear zone gives evidence for crustal linkage and far-reaching acting of low-angle normal faults on a crustal scale.

4 Discussion

A revised geological map and lithostratigraphic column of the southern Kythnos emerged as a product of recent structural and petrological investigations on Kythnos. The remapped area shows that the southern area of Kythnos at Agios Dimitrios is dominated by a major extensional shear zone that caused the development of fine-grained marbles and cataclasites. This small dynamically recrystallized grain size indicates high differential stress and low temperature around the brittle/ductile transition zone (at around 300°C). The extreme thinning and mylonitic foliation points to large displacement values involving high shear strain. The grain size reduction of the mylonitic marble and the partially rounded components in the ultracataclasite may have provided the means for reducing the apparent fault friction enabling movement along an angle lower than the typical 60° (Anderson et al., 1977). Additionally, fluid involvement may have been an important factor involved in friction reduction.

The structure of the fault zone can be correlated to similar major extensional shear zones in the Aegean region, such as major low-angle normal fault detachments on the neighboring islands of Kea and Serifos. However, due to a widespread shortening component perpendicular to the stretching direction, the shear zone in S-Kythnos is bent and buckled, thus showing a range of dip angles. Furthermore, the shear zone includes two distinct ultramylonite horizons, one of which shows a steeper, the other a more shallow dip. To be classified as a low-angle normal fault, the fault zone should have exhibited a dip lower than 30° (Axen, 2007).

The ultramylonite and cataclasite shear zone gives evidence for movement along low-angle fault planes (on some marble mylonite horizons) and high-angle brittle faults, which develop as cataclastic layers and fractures. Ductile movement on mylonite planes and brittle deformation producing cataclasites depict the evolution of the shear zone from the lower to the upper crust. Brittle faults cutting through the mylonitic fault planes show them to be younger. Quartzitic lithologies overlying the ultramylonite shear zone show various degrees of deformation from protocataclasites to rock portions giving evidence for static recrystallization, indicating that strain localized in weaker layers.

Stretching lineation and shear sense indicators show top to the SSW-directed kinematics. This is consistent with deformation direction on the adjacent islands of Kea and Serifos and provides a deviating direction to the previously described top the N to NE direction on the Eastern and Northern Cyclades.

Throughout the Cyclades, lenses of serpentinitic and metagabbroic lithologies can be found in proximity to crustal shear zones. On southern Serifos serpentinite lenses are regarded as the uppermost unit (Petrakakis et al., in press), whereas on Kea (Voit, 2008) they are found near the base of the ultramylonite shear zone. Further northeast, on the islands of Andros (Papanikolaou, 1978) and Tinos (Melidonis, 1980; Katzir et al., 1996), metabasitic lithologies are found in close proximity to the detachment contact between the Cycladic Middle and Upper Unit. On Syros serpentinite lenses and meta-ophiolitic blocks occur in two structural positions; associated with a low angle normal fault zone (Trotet et al., 2001), and as lenses within the greenschist facies Cycladic Intermediate Unit (Hecht, 1984). On Kythnos outcrops of serpentinites and metabasites are situated within the core of a large-scale open fold, lithostratigraphically below the blue-grey mylonitic marble and within the epidote-schists. Their proximity to the normal fault zone exposed at Agios Dimitrios indicates that these lithologies are an integral part of the shear zone. The fact that relics of the magmatic fabric are still preserved locally, and the lack of structural overprint related to the deformation of the fault zone imply that these elements acted as rigid blocks within the shear zone. This is further supported by the fact that the metabasite blocks are enveloped in serpentine-talc-schists, a weaker lithology, which could have accommodated deformation.

According to Schliestedt et al. (1994) the metabasic lithologies show a different thermal and pressure evolution to the surrounding rocks. In contrast to the greenschists, the metagabbroic rocks show no evidence of a high pressure history, equivalent to the M1 metamorphic event. This low degree metamorphic overprint matched with the Uppermost Unit of the Attic Cycladic Crystalline, thus leading to the belief that these metabasic lithologies have to be assigned to the aforementioned Uppermost Unit, placing them on the top of the lithotectonostratigraphic column. However, their structural position on Kythnos contradicts this general positioning scheme, because no major fault separating these metabasic lenses from the surrounding greenschists can be observed. Additionally, on Kythnos laterally continuous marble mylonite layers can be found between the metagabbroic lenses and the shear zone. Therefore, it is proposed that the metagabbroic lithologies on Kythnos are singular ophiolitic blocks that can not be ascribed to a different tectonic unit and must have a common deformation and metamorphic history with the surrounding greenschist facies lithologies.

5 Conclusions

1. Kythnos island represents a major extensional SSW-directed shear zone.

2. The shear zone on Kythnos is characterized by highly strained rocks such as an extremely fine-grained ultramylonitic marble and cataclasites.

3. Stretching and mineral lineations of all lithologies plunge NNE or SSW. Shear sense indicators of structures formed during ductile and brittle conditions indicate general top-to-SSW kinematics.

4. Reduced grain size and broken quartz grains indicate that the shear zone was active at low temperatures.

5. Comparison with major low-angle shear zones on the neighboring islands of Kea and Serifos allows an analogous placement of the Kythnos shear zone, which probably evolved as a low-angle normal fault, but buckled under syn-extensional shortening.

6. Greenschists and marbles show evidence of major folding. A first folding stage involved subhorizontal axial planes and led to widespread isoclinal folding. A later folding phase is concordant with shortening perpendicular to the main extension direction and involves subvertical axial planes. Fold axes are generally parallel to mineral and stretching lineations and plunge in a NNE-SSW direction.

7. High fluid activity of carbonate-rich composition overprints most major lithologies. Localized depostion of ferric oxide and baryte along brittle faults can be observed.

8. Metagabbroic units are found in proximity to the shear zone and are an integral part of the Intermediate Unit of the Attic Cycladic Crystalline.

9. The preservation of an original magmatic microstructure can be ascribed to the metabasites acting as rigid blocks within surrounding weaker serpentine-talc-schists.

10. Whole-rock chemistry of assumed metagabbros show that only minor parts are of metabasic composition. These lithologies are marked by low SiO_2, Al_2O_3 and CaO content and high amounts of Fe_2O_3 and MgO. Also large heavy metal, Ni and Cr, concentrations mark the metabasic lithologies.

11. Mineral chemistry in ferromanganoan metasediments shows garnets with a high spessartine component and amphiboles plotting in crossite to magnesio-riebeckite field.

12. The composition of garnets and amphiboles in ferromanganoan metasediments on Kea and Kythnos show striking similarities. Therefore, this lithology could be used as a marker horizon throughout the Cyclades.

References

E. Alram-Stern. *Die Ägäische Frühzeit: 2. Serie. Forschungsbericht 1975-2003.* Die Frühbronzezeit in Griechenland mit Ausnahme von Kreta. Veröffentlichungen der Mykenischen Kommission, Wien, 2004.

R. Altherr and W. Siebel. I-type plutonism in a continental back-arc setting: Miocene granitoids and monzonites from the central Aegean Sea, Greece. *Contributions to Mineralogy and Petrology*, 35:287–288, 2007.

T.H. Anderson, L.T. Silver, and G.A. Salas. Metamorphic core complexes of the southern part of the North American Cordillera - Northwestern Mexico. *GSA Abstracts with Programs*, 9:881, 1977.

E. Argand. Le tectonique de L'Asie. Comptes Rendus, Congrès Internationale Geologique, (session XIII 922), 1924.

S.S. Augustithis. Thermal springs of Kythnos (Cyclades, Greece); an hydrochemical comparison to some springs of high salinity. In *Proceedings of the international congress on thermal waters, geothermal energy and vulcanism of the Mediterranean area; Volume 2, Thermal waters*, volume 2, pages 555–581, 1976.

D. Avigad. High-pressure metamorphism and cooling on SE Naxos (Cyclades, Greece). *European Journal of Mineralogy*, 10:1309–1319, 1998.

G.J. Axen. Research Focus: Significance of large-displacement, low-angle normal faults. *Geology*, 35:287–288, 2007.

S.R. Barr, S. Templey, and J. Tarney. Lateral growth of the continental crust through deep level subduction-accretion: a re-evaluation of central Greek Rhodope. *Lithos*, 46:69–94, 1999.

V. Bartsch. Die grünschieferfazielle Überprägung im Norden von Kithnos (Kykladen, Griechenland): Geologie, Petrographie und Geochemie. Master's thesis, University of Hannover, 1993.

E.S. Bloodaxe, J.M Hughes, M.D. Dyar, E.S. Grew, and C.V. Guidotti. Linking structure and chemistry in the schorl-dravite series. *American Mineralogist*, 84:922–928, 1999.

M. Bohnhoff, D. Papanikolaou, and G. Stavrakakis. Crustal investigation of the Hellenic subduction zone using wide aperture seismic data. *Tectonophysics*, 343:239–262, 2001.

M. Bröcker and R.T. Pidgeon. Protolith Ages of Meta-igneous and Metatuffaceous Rocks from the Cycladic Blueschist Unit, Greece: Results of a Reconnaissance U-Pb Zircon Study. *The Journal of Geology*, 115:83–98, 2007.

M. Bröcker, D. Bieling, B. Hacker, and P. Gans. High-Si phengite records the time of greenschist facies overprinting: implications for models suggesting mega-detachments in the Aegean Sea. *Journal of Metamorphic Geology*, 22:427–442, 2004.

J.-P. Brun and C. Faccenna. Exhumation of high-pressure rocks driven by slab rollback. *Earth and Planetary Science Letters*, 272:1–7, 2008.

K. Bucher and M. Frey. *Petrogenesis of metamorphic rocks.* Springer, Berlin, 6th edition, 1994.

M. Carl. Petrographische, geochemische und mineralchemische Untersuchungen an Metamorphiten von Süd-Kithnos (Kykladen, Griechenland). Master's thesis, University of Hannover, 1993.

A.I. Chrysanthaki and E.M.M. Baltatzis. Geochemistry and depositional environment of ferromanganoan metasediments on the Island of Kythnos, Cyclades, Greece. *Neues Jahrbuch für Mineralogie – Monatshefte*, 1:1–17, 2003.

P.J. Clarke, R.R. Davies, P.C. England, B. Parsons, H. Billiris, D. Paradissis, G. Veis, P.A. Cross, P.H. Denys, V. Ashkenazi, R. Bingley, H.-G. Kahle, M.-V. Muller, and P. Briole. Crustal strain in central Greece from repeated GPS measurements in the interval 1989-1997. *Geophysical Journal International*, 135:195–214, 1998.

C. Clément, A. Hirna, P. Charvis, M. Sachpazi, and F. Marnelis. Seismic structure and active Hellenic subduction in the Ionian islands. *Tectonophysics*, 329:141–156, 2000.

E.N. Davis. *Geological map of Kea, 1:50,000. Map of Greece.* Geological Survey of Greece, Athens, 1972.

J.B. DeSmeth. Geological Map of Greece 1:50 000, Kythnos Island. *IGME*, 1975.

S. Dürr. Das attisch-kykladische Kristallin. In V. Jacobshagen, editor, *Die Geologie von Griechenland*, volume 19, pages 116–149. Borntraeger, Berlin, 1986.

L.T.C. Endrun, M. Meier, and M. Bohnhoff H.-P. Harjes. Modeling the influence of Moho topography on receiver functions: a case study from the central Hellenic subduction zone. *Geophysical Research Letters*, L12311, 2005.

K.G. Fiedler. *Reise durch alle Theile des Königreiches Griechenland Griechenland in Auftrag der Königl. Griechischen Regierung in den Jahren 1834 bis 1837*, volume II. Friedrich Fleischer, Leipzig, 1841.

M.A. Forster and G.S. Lister. Several distinct tectono-metamorphic slices in the Cycladic eclogite-blueschist belt, Greece. *Contrib. Mineral. Petrol.*, 150:523–545, 2005.

M. Fytikas, F. Innocenti, P. Manetti, A. Peccerillo, R. Mazzuoli, and L. Villari. Tertiary to Quarternary evolution of volcanism in the Aegean region. *Geological Society, London, Special Publications*, 17:687–699, 1984.

N.H. Gale and Z.A. Stos-Gale. Cycladic metallurgy. In J.A. MacGillivray and R.L.N. Barber, editors, *The Prehistoric Cyclades*, pages 255–258. Department of Classical Archaeology, Edinburgh, 1984.

P. Gautier and J.-P. Brun. Crustal-scale geometry and kinematics of late-orogenic extension in the central Aegean (Cyclades and Ewia Island). *Tectonophysics*, 7(2):57–85, 1994.

P. Gautier, J.-P. Brun, R. Moriceau, D. Sokoutis, J. Martinod, and L. Jolivet. Timing, kinematics and cause of Aegean extension: a scenario based on a comparison with simple analogue experiments. *Earth and Planetary Science Letters*, 187:95–104, 2001.

B. Grasemann, K. Petrakakis, C. Iglseder, C. Rambousek, A. Zámolyi, and E. Draganits. The Serifos Metamorphic Core Complex (Western Cyclades, Greece). In A.A. Chatzipetros and S.B. Pavlides, editors, *Proceedings of the 5th International Symposium on Eastern Mediterranean Geology, Thessaloniki, Greece*, volume 1, pages 77–79, 2004.

J. Hecht. *Geological map of Greece 1:50 000, Syros Island.* Institute of Geology and Mineral Exploration (IGME), Athens, 1984.

Ch. Hollenstein, M.D. Mü'ller, A. Geiger, and H.G. Kahle. Crustal motion and deformation in Greece from a decade of GPS measurements, 1993–2003. *Tectonophysics*, 449:17–40, 2008.

L.C. Hsu. Selected phase relationships in the system Al-Mn-Fe-Si-O-H: a model for garnet equilibria. *Journal of Petrology*, 9:40–83, 1968.

C. Iglseder. Fold structures in the tectono-metamorphic evolution of the Serifos Metamorphic Core Complex, Cyclades, Greece. Master's thesis, University of Vienna, 2005.

C. Iglseder, B. Grasemann, K. Petrakakis, M.A. Edwards, A. Zámolyi, C. Rambousek, C. Hörfarter, U. Klötzli, M. Thöni, and E. Draganits. Multistage Plutonism and the Serifos Detachment System (Cyclades, Greece). *Geophysical Research Abstracts, EGU General Assembly 2006*, 8:05118, 2006.

C. Iglseder, B. Grasemann, D. Schneider, A.H.N. Rice, I. Lenauer, M. Müller, G. Mörtl, K. Voit, K. Petrakakis, E. Draganits, and Team ACCEL. Low-angle normal fault mechanics and architecture in the Western Cyclades (Greece). *Geophysical Research Abstracts, EGU General Assembly 2008*, 10:07793, 2008.

C. Iglseder, B. Grasemann, D.A. Schneider, K. Petrakakis, C. Miller, U.S. Klötzli, M. Thöni, A. Zámolyi, and C. Rambousek. I and S-type Plutonism on Serifos (W-Cyclades, Greece). *Tectonophysics*, in press.

V. Jacobshagen. *Geologie von Griechenland.* Borntraeger, Berlin, 1986.

V. Jacobshagen. Orogenic evolution of the Hellenides: new aspects. *Geologische Rundschau*, 83:249–256, 1994.

L. Jolivet. A comparison of geodetic and finite strain patterns in the Aegean, geodynamic implications. *Earth and Planetary Science Letters*, 187:95–104, 2001.

L. Jolivet and C. Faccenna. Mediterranean extension and the Africa-Eurasia collision. *Tectonics*, 19(6):1095–1106, 2000.

L. Jolivet, C. Faccenna, B. Goffe, E. Burov, and P. Agard. Subduction tectonics and exhumation of high-pressure metamorphic rocks in the Mediterranean orogens. *American Journal of Science*, 303:353–409, 2003.

Y. Katzir, A. Matthews, Z. Garfunkel, M. Schliestedt, and D. Avigad. The tectono-metamorphic evolution of a dismembered ophiolite (Tinos, Cyclades). *Geological Magazine*, 133:237–254, 1996.

M. Keiter, F. Tomaschek, and C. Ballhaus. The structural evolution of Kythnos Island (Cyclades, Greece) - a reconnaissance. *Zeitschrift der Deutschen Gesellschaft für Geowissenschaften*, 159:513–520, 2008.

N. Lambrakis and G. Kallergis. Contribution to the study of Greek thermal springs: hydrogeological and hydrochemical characteristics and origin of thermal waters. *Hydrogeological Journal*, 13:506–521, 2005.

B. E. Leake. Nomenclature of amphiboles. *Canadian Mineralogist*, 16:501–520, 1978.

J. Lee and G.S. Lister. Late Miocene ductile extension and detachment faulting, Mykonos, Greece. *Geology*, 20(2):121–124, 1992.

X. Li, G. Bock, A. Vafidis, R. Kind, H.-P. Harjes, W. Hanka, K. Wylegalla, M. van der Meijde, and X. Yuan. Receiver function study of the Hellenic subduction zone: imaging crustal thickness variations and the oceanic Moho of the descending African lithosphere. *Geophysical Journal International*, 155:733–748, 2003.

G.S. Lister, G. Banga, and A. Feenstra. Metamorphic core complexes of Cordilleran type in the Cyclades, Aegean Sea, Greece. *Geology*, 12:221–225, 1984.

E.P. Loehnert. Contribution to the origin of thermal-mineral spring waters on the islands of Milos and Kythnos (Aegean Sea, Greece). *Neues Jahrbuch fuer Geologie und Palaeontologie. Monatshefte*, 7:403–414, 1988.

G. Lynch and J. Ortega. Hydrothermal alteration and tourmaline-albite equilibria at the Coxheath porphyry Cu-Mo-Au deposit, Nova Scotia. *Canadian Mineralogist*, 35: 79–94, 1997.

J. Makris. The crust and upper mantle of the Aegean region from deep seismic soundings. *Tectonophysics*, 46:269–284, 1978.

J. Makris and C. Stobbe. Physical properties and state of the crust and upper mantle of the Eastern Mediterranean Sea deduced from geophysical data. *Marine Geology*, 55:347–363, 1984.

S. McClusky, S. Balassanian, A. Barka, C. Demir, S. Ergintav, I. Georgiev, O. Gurkan, M. Hamburger, K. Hurst, H. Kahle, K. Kastens, G. Kekelidze, R. King, V. Kotzev, O. Lenk, S. Mahmoud, A. Mishin, M. Nadariya, A. Ouzounis, D. Paradissis, Y. Peter,

M. Prilepin, R. Reilinger, I. Sanli, H. Seeger, A. Tealeb, M.N. Toksöz, and G. Veis. Global positioning system constraints on plate kinematics and dynamics in the eastern Mediterranean and Caucusus. *Journal of Geophysical Research*, 105:5695–5719, 2000.

N.G. Melidonis. *The geological structure and mineral deposits of Tinos island (Cyclades, Greece).*, volume 13, pages 1–80. Institute of Geology and Mineral Exploration, Athens, 1980.

M. Okrusch and M. Bröcker. Eclogites associated with high-grade blueschists in the Cyclades archipelago, Greece; a review. *European Journal of Mineralogy*, 2(4):451–478, 1990.

D.J. Papanikolaou. Contribution to the Geology of Aegean Sea : The Island of Andros. *Annales Géologiques des Pays Helléniques*, 29(2):477–553, 1978.

B.C. Papazachos, V.G. Karakostas, C.B. Papazachos, and E.M. Scordilis. The geometry of the Wadati–Benioff zone and lithospheric kinematics in the Hellenic arc. *Tectonophysics*, 319:275–300, 2000.

G. Pe-Piper and D.J.W. Piper. Unique features of the Cenozoic igneous rocks of Greece. In Y. Dilek and S. Pavlides, editors, *Postcollisional tectonics and magmatism in the Mediterranean region and Asia*, pages 259–282. Geological Society of America, 2006.

K. Petrakakis, A. Zámolyi, C. Iglseder, C. Rambousek, B. Grasemann, E. Draganits, and A. Photiadis. Geological Map of Greece, Serifos Island. Institute of Geology and Mineral Exploration, in press.

A. Philippson. *Beiträge zur Kenntnis der Griechischen Inselwelt.* J. Perthes, Gotha, 1901.

B. Putlitz, A. Matthews, and J.W. Valley. Oxygen and hydrogen isotope study of high-pressure metagabbros and metabasalts (Cyclades, Greece): implications for the subduction of oceanic crust. *Contributions to Mineralogy and Petrology*, 138:114–126, 2000.

C. Rambousek. Quantitative Tectonic Studies of a Miocene Low Angle Normal Fault (Serifos, Greece). Master's thesis, University of Vienna, 2007.

T. Reinecke, M. Okrusch, and P. Richter. Geochemistry of ferromanganoan metasediments from the island of Andros, Cycladic Blueschist Belt, Greece. *Chemical Geology*, 53:249–278, 1985.

U. Ring and P.W. Layer. High-pressure metamorphism in the Aegean, eastern Mediterranean: Underplating and exhumation from the Late Cretaceous until the Miocene to Recent above the retreating Hellenic subduction zone. *Tectonics*, 22(3):1022, 2003.

U. Ring, K. Gessner, T. Güngör, and C.W. Passchier. The Menderes Massif of western Turkey and the Cycladic Massif in the Aegean - do they really correlate? *Journal of the Geological Society, London*, 156:3–6, 1999.

E.A. Schiller and F.C. Taylor. Spessartine-quartz rocks (coticules) from Nova Scotia. *The American Mineralogist*, 50:1477–1481, 1965.

M. Schliestedt, V. Bartsch, M. Carl, A. Matthews, and F. Henjes-Kunst. The P-T Path of Greenschist-Facies Rocks from the Island of Kithnos (Cyclades, Greece). *Chemie der Erde*, 54:281–296, 1994.

S.D. Schmid, D. Bernoulli, B. Fügenschuh, L. Matenco, S. Schefer, R. Schuster, M. Tischler, and K. Ustaszewski. Major tectonic units of the Alps, Carpathians, Dinarides and Hellenides. `http://pages.unibas.ch/earth/tecto/publications-/Greece_ALCADIcompressed_12Apr08.pdf`, 2008.

D. Sokoutis, J.-P. Brun, J. van den Driessche, and S. Pavlides. A major Oligo-Miocene detachment in the southern Rhodope controlling North Aegean extension. *Journal of the Geological Society of London*, 150:243–246, 1993.

W. Spakman, M.J.R. Wortel, and N.S. Vlaar. The Hellenic subduction zone: a tomographic image and its geodynamical implications. *Geophysical Research Letters*, 15: 60–63, 1988.

T. Taymaz, Y. Yilmaz, and Y. Dilek. The geodynamics of the Aegean and Anatolia: introduction. *Geological Society, London, Special Publications*, 291:1–16, 2007.

T. Theye, W. Schreyer, and A.-M. Fransolet. Low-Temperature, Low-Pressure Metamorphism of Mn-rich Rocks in the Lienne Syncline, Venn-Stavelot Massif (Belgian Ardennes), and the Role of Carpholite. *Journal of Petrology*, 37(3):767–783, 1996.

A.G. Tindle and P.C. Webb. PROBE-AMPH a spreadsheet program to classify microprobe-derived amphibole analyses. *Computers and Geosciences*, 20:1201–1228, 1994.

C. Tirel, F. Gueydan, C. Tiberi, and J.-P. Brun. Aegean crustal thickness inferred from gravity inversion. Geodynamical implications. *Earth and Planetary Science Letters*, 227:267–280, 2004.

F. Trotet, L. Jolivet, and O. Vidal. Tectono-metamorphic evolution of Syros and Sifnos islands (Cyclades, Greece). *Tectonophysics*, 338:179–206, 2001.

P.A. van der Maar and J.B.H. Jansen. The geology of the polymetamorphic complex of Ios, Cyclades, Greece and its significance for the Cycladic Massif. *Geologische Rundschau*, 72:283–299, 1983.

K. Voit. Structural Geology and Geomorphology of Northern Kea - A crustal scale Viscous-frictional Shear Zone (Western Cyclades, Greece). Master's thesis, University of Vienna, 2008.

G. Voll. Recrystallization of quartz, biotite, feldspars from Erstfeld to the Leventina Nappe, Swiss Alps, and its geological signicance. *Schweizer mineralogische und petrographische Mitteilungen*, 56:641–647, 1976.

A.P. Willner, S. Pawlig, H.-J. Massonne, and F. Hervé. Metamorphic evolution of spessartine quartzites (coticules) in the high-pressure, low temperature complex at Bahia Mansa, Coastal Cordillera of south-central Chile. *The Canadian Mineralogist*, 39:1547–1569, 2001.

K.S. Win, M. Takeuchi, and T. Tokiwa. Changes in detrital garnet assemblages related to transpressive uplifting associated with strike–slip faulting: An example from the Cretaceous System in Kii Peninsula, Southwest Japan. *Sedimentary Geology*, 201: 412–431, 2007.

N. Zacharias, C. Michael, O. Philaniotou-Hadjianastasiou, A. Hein, and Y. Bassiakos. Fine-grain TL dating of archaeometallurgical furnace walls. *Journal of Cultural Heritage*, 7:23–29, 2006.

A. Zámolyi. Tectonic Geomorphology of Serifos (Cyclades, Greece). Master's thesis, University of Vienna, 2006.

Geological Map

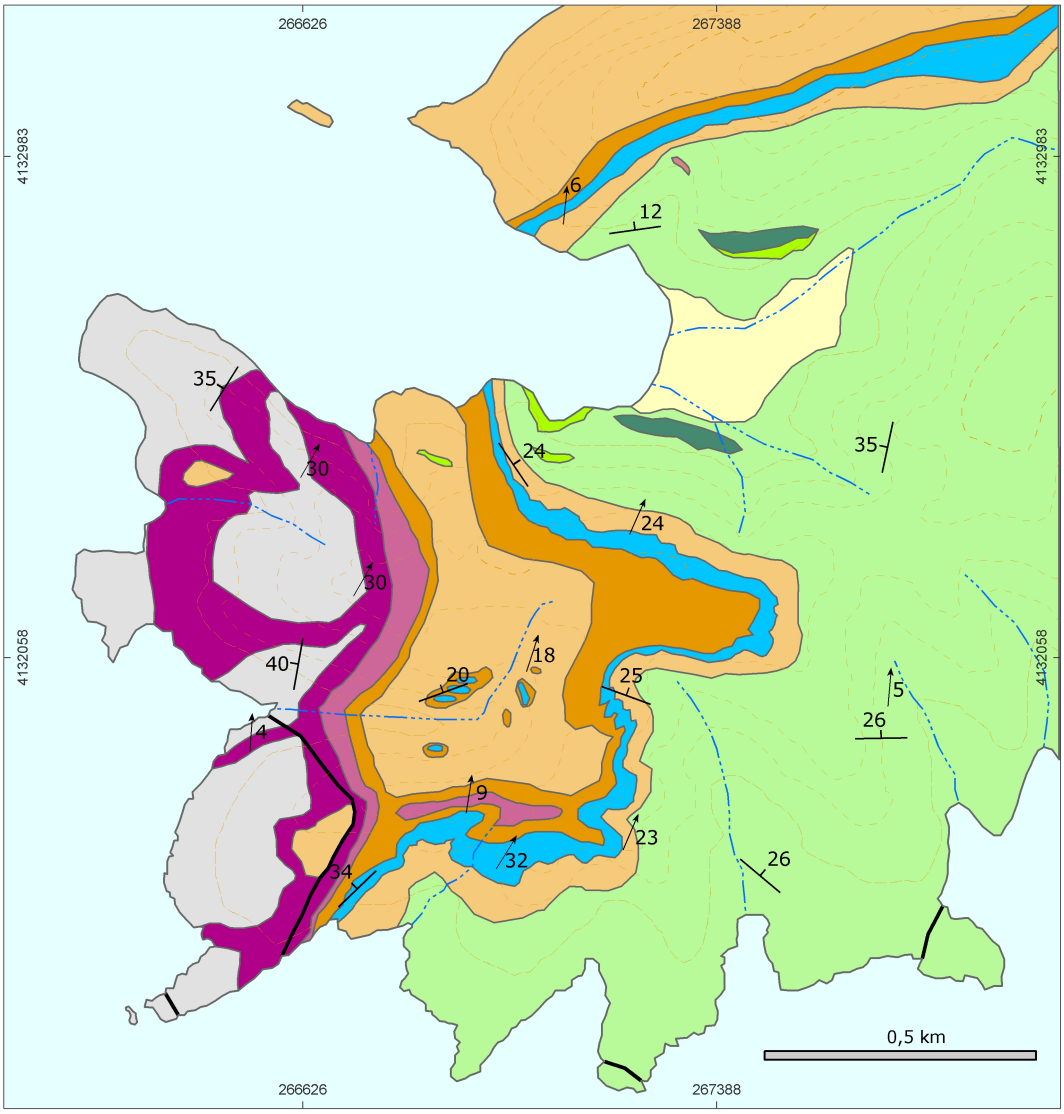

Legend

- Albite-chlorite-sericite schist
- Albite-gneiss
- Chlorite-sericite-actinolite-epidote-albite schists
- Ultramylonitic marble
- Mylonitic marble
- Metabasite
- Tourmaline-magnetite-epidote gneiss
- Quarternary sediment
- Protocataclastic quartzite
- Serpentine-talc schist
- Impure marble
- Fault
- Stream
- Dip of foliation planes
- Lineation
- Contour lines at 20 m interval

Geochemical Data

Summary of Chemical Analysis

			Ki 704						Ki 709						Ki 713					
	Analysis Method		ICP-AES	AAS	ICP-MS	RFA	other	Mean Value	ICP-AES	AAS	ICP-MS	RFA	other	Mean Value	ICP-AES	AAS	ICP-MS	RFA	other	Mean Value
Major and minor constituents	SiO_2	[%Ox]	38,657			38,25		**38,45**	51,199			52,13		**51,664**	40,596			41,38		**40,988**
	Al_2O_3	[%Ox]	12,457			11,96		**12,33**	14,301			14,31		**14,305**	8,586			8,55		**8,568**
	Fe_2O_3	[%Ox]	8,839			9,18		**8,92**	11,640			11,52		**11,580**	12,748			12,83		**12,789**
	CaO	[%Ox]	19,059			17,82		**18,8**	7,179			7,07		**7,125**	5,118			5,01		**5,064**
	MgO	[%Ox]	3,313			3,24		**3,31**	6,274			6,29		**6,282**	23,156			24,07		**23,613**
	Na_2O	[%Ox]		2,867		3,61		**2,87**		3,458		4,6		**3,458**		0,278		0,28		**0,279**
	K_2O	[%Ox]	0,587	0,448		0,51		**0,52**	0,711	0,611		0,71		**0,677**	0,066	0,094		0,06		**0,073**
	MnO	[%Ox]	0,165			0,17		**0,17**	0,148			0,15		**0,149**	0,162			0,17		**0,166**
	TiO_2	[%Ox]	1,372			1,34		**1,36**	1,761			1,75		**1,755**	0,968			0,99		**0,979**
	P_2O_5	[%Ox]	0,195		0,206	0,17		**0,19**	0,207		0,228	0,19		**0,208**	0,132		0,163	0,12		**0,138**
	H2O	[%Ox]					1,692	**1,692**					2,115	**2,115**					6,903	**6,903**
	CO_2	[%Ox]					11,499	**11,50**					0,179	**0,179**					1,243	**1,243**
	LOI	[%Ox]					12,89	**12,89**					2,47	**2,47**	7,81				7,81	**7,81**
	S	[%Ox]					0,055	**0,055**					0,048	**0,048**					0,056	**0,056**
	N	[%Ox]					0,026	**0,026**					0,003	**0,003**					0,015	**0,015**
	SUM	[%]						**99,82**						**99,67**						**100,47**
Trace Elements	As	[ppm]			0,59			**0,6**			0,49			**0,5**			6,55			**6,6**
	Ba	[ppm]	32,4		21,4			**29,7**	27,6		19,0			**25,4**	7,1		8,0			**7,6**
	Be	[ppm]			0,35			**0,35**			0,56			**0,56**			0,31			**0,31**
	Bi	[ppm]			0,32			**0,32**			0,01			**0,01**			0,02			**0,02**
	Cd	[ppm]			0,11			**0,1**			0,02			**0,0**			0,08			**0,08**
	Co	[ppm]	32,8		29,0			**30,9**	37,1		31,2			**34,2**	73,0		77,8			**75,4**
	Cr	[ppm]	8,8		7,1			**8,0**	51,0		46,3			**48,7**	2445,9		2720,5			**2583**
	Cs	[ppm]			2,35			**2,4**			1,45			**1,4**			0,12			**0,1**
	Cu	[ppm]	39,5	62	55,0			**52,3**	11,4	30	25,7			**22,3**	33,5	52	43,7			**43,1**
	Ge	[ppm]			0,99			**1,0**			1,47			**1,5**			1,26			**1,3**
	Li	[ppm]	9,2		8,0			**8,6**	19,5		19,0			**19,2**	10,1		9,5			**9,8**
	Mo	[ppm]			0,65			**0,65**			0,23			**0,2**			0,18			**0,2**
	Ni	[ppm]	42,3		42,5			**42,4**	28,9		26,4			**27,7**	839,6		768,8			**804**
	Pb	[ppm]	4,0		4,5			**4,3**	2,0		5,2			**4,4**	16,3		17,5			**16,9**
	Rb	[ppm]	15,3		16,7			**16,0**	6,8		8,4			**7,6**	-0,5		0,5			**0,0**
	Sb	[ppm]			0,29			**0,3**			0,33			**0,3**			0,49			**0,5**
	Sn	[ppm]			3,65			**3,6**			1,03			**1,0**			1,91			**1,9**
	Sr	[ppm]	241,2		223,5			**236,8**	102,4		85,5			**98,1**	31,7		29,6			**30,6**
	Tl	[ppm]			0,10			**0,1**			0,04			**0,0**			0,00			**0,0**
	V	[ppm]			1,5			**1,5**			1,4			**1,4**			2,2			**2,2**
	Zn	[ppm]	85,0	146	134,6			**122**	50,0	56	76,3			**60,8**	95,0	122	110,9			**109,3**
	Zr	[ppm]	70,7					**70,7**	87,1					**87,1**	77,2					**77,2**
Rare Earth Elements	Sc	[ppm]			27,60			**27,60**			36,88			**36,88**			24,79			**24,79**
	Y	[ppm]			19,81			**19,81**			29,24			**29,24**			13,41			**13,41**
	La	[ppm]			4,72			**5**			6,35			**6**			2,79			**3**
	Ce	[ppm]			11,78			**12**			15,77			**16**			7,83			**8**
	Pr	[ppm]			1,75			**1,75**			2,46			**2,46**			1,21			**1,21**
	Nd	[ppm]			10,13			**10,13**			14,34			**14,3**			6,96			**6,96**
	Sm	[ppm]			2,72			**2,72**			3,83			**3,83**			1,87			**1,87**
	Eu	[ppm]			0,90			**0,90**			1,15			**1,15**			0,43			**0,43**
	Gd	[ppm]			3,70			**3,70**			4,60			**4,60**			2,21			**2,21**
	Tb	[ppm]			0,58			**0,58**			0,86			**0,86**			0,41			**0,41**
	Dy	[ppm]			3,56			**3,56**			5,35			**5,35**			2,56			**2,56**
	Ho	[ppm]			0,75			**0,75**			1,11			**1,11**			0,53			**0,53**
	Er	[ppm]			2,06			**2,06**			3,09			**3,09**			1,48			**1,48**
	Tm	[ppm]			0,29			**0,29**			0,46			**0,46**			0,22			**0,22**
	Yb	[ppm]			1,79			**1,79**			2,83			**2,83**			1,36			**1,36**
	Lu	[ppm]			0,23			**0,23**			0,39			**0,39**			0,19			**0,19**
	Th	[ppm]			0,35			**0,3**			0,31			**0,3**			0,22			**0,2**
	U	[ppm]			0,29			**0,3**			0,11			**0,1**			0,07			**0,1**

Table 4: Summary of chemical analyses of major, minor and trace element for all three samples from Kythnos.

Microprobe Data

Sample	Kyt0703i				CKea7			Kea0618				Kea0727A				Kyt0704Al		
SiO2	36,04	36,02	35,75	36,02	36,31	35,97	36,07	36,30	36,83	36,09	35,93	36,09	36,28	36,35	35,53	36,14	35,82	36,18
TiO2	0,20	0,23	0,24	0,19	0,19	0,25	0,34	0,21	0,14	0,18	0,18	0,33	0,12	0,19	0,39	0,20	0,18	0,20
Al2O3	15,19	14,87	16,43	19,22	18,54	16,99	17,33	18,74	18,22	16,85	18,72	20,67	20,54	20,53	20,35	19,82	19,86	19,68
FeO	7,48	7,20	8,34	8,18	6,04	6,84	7,28	5,96	7,14	6,65	8,24	3,15	4,91	4,28	4,29	7,22	7,40	7,84
MnO	28,51	29,49	27,65	27,87	30,10	28,49	29,84	31,03	29,08	30,38	29,50	32,26	30,88	32,47	33,82	28,75	29,14	28,73
MgO	0,01	0,02	0,03	0,03	0,04	0,03	0,03	0,05	0,24	0,04	0,06	0,05	0,13	0,09	0,02	0,07	0,08	0,10
CaO	6,62	6,38	7,74	7,08	7,93	9,76	8,74	7,35	7,16	8,45	7,22	6,90	6,09	5,44	4,56	6,56	6,59	6,52
K2O	0,00	0,00	0,01	0,01	0,02	0,00	0,00	0,00	0,00	0,00	0,00	0,00	0,01	0,00	0,00	0,01	0,00	0,01
Na2O	0,01	0,01	0,01	0,00	0,06	0,01	0,03	0,03	0,09	0,00	0,00	0,02	0,01	0,00	0,04	0,01	0,00	0,00
Cr2O3	0,00	0,03	0,02	0,02	0,01	0,00	0,01	0,00	0,00	0,03	0,02	0,01	0,03	0,00	0,02	0,00	0,00	0,03
Sum	94,05	94,25	96,22	98,63	99,23	98,35	99,68	99,68	98,90	98,68	99,87	99,47	99,00	99,35	99,02	98,76	99,07	99,30
Si *apfu*	3,130	3,129	3,041	2,980	2,988	2,990	2,971	2,978	3,034	3,000	2,952	2,949	2,978	2,978	2,939	2,980	2,952	2,973
Al^{vi}	0,000	0,000	0,000	0,020	0,012	0,010	0,029	0,022	0,000	0,000	0,048	0,051	0,022	0,022	0,061	0,020	0,048	0,027
Al^{iv}	1,571	1,541	1,664	1,863	1,800	1,674	1,672	1,803	1,781	1,671	1,779	1,943	1,968	1,962	1,928	1,911	1,888	1,887
Ti	0,013	0,015	0,015	0,012	0,012	0,016	0,021	0,013	0,009	0,012	0,011	0,020	0,007	0,011	0,024	0,012	0,011	0,012
Fe^{3+}	0,251	0,276	0,246	0,111	0,166	0,273	0,270	0,163	0,156	0,279	0,186	0,033	0,022	0,023	0,043	0,068	0,089	0,090
Fe^{2+}	0,293	0,248	0,347	0,455	0,249	0,203	0,232	0,246	0,337	0,184	0,381	0,182	0,315	0,270	0,254	0,430	0,421	0,449
Mn	2,097	2,170	1,992	1,953	2,099	2,006	2,082	2,157	2,029	2,140	2,053	2,233	2,147	2,254	2,371	2,008	2,034	2,000
Mg	0,001	0,002	0,004	0,004	0,005	0,004	0,004	0,007	0,029	0,005	0,007	0,006	0,015	0,011	0,002	0,008	0,009	0,012
Ca	0,616	0,594	0,706	0,627	0,699	0,869	0,771	0,646	0,632	0,753	0,635	0,604	0,536	0,477	0,405	0,580	0,582	0,574
X_{Alm}	0,000	0,000	4,835	13,23	4,932	0,931	2,429	5,178	6,812	0,000	8,670	3,594	9,394	7,930	5,517	12,89	11,05	13,01
X_{And}	13,88	15,32	13,00	5,587	8,454	14,07	13,83	8,234	8,082	14,44	9,430	1,673	1,103	1,172	2,183	3,426	4,528	4,518
X_{Grs}	8,651	4,159	11,85	15,48	15,27	15,83	12,50	13,56	13,80	11,47	12,10	18,82	16,90	14,85	11,58	16,04	15,19	14,79
X_{Prp}	0,041	0,087	0,150	0,118	0,156	0,148	0,135	0,227	1,015	0,187	0,238	0,198	0,518	0,377	0,076	0,268	0,320	0,412
X_{Sps}	77,43	80,44	70,16	65,59	71,19	69,02	71,10	72,80	70,29	73,90	69,56	75,71	72,09	75,67	80,65	67,38	68,92	67,27

Table 5: Representative examples of garnet composition. Mineral formula calculated for 12 O.

Sample	Kyt0703					Kyt0704							Kea0618				
SiO_2	54,44	53,36	54,61	54,32	54,55	54,01	51,33	53,46	53,47	53,46	64,95	54,33	54,55	54,76	54,66	53,73	53,85
TiO_2	0,00	0,06	0,03	0,01	0,00	0,07	0,07	0,04	0,01	0,02	0,07	0,00	0,03	0,00	0,03	0,01	0,02
Al_2O_3	5,19	2,84	5,05	4,97	1,59	5,66	5,93	3,93	2,80	1,81	1,76	2,78	3,73	3,18	2,07	1,66	1,22
Fe_2O_3	24,82	26,16	23,46	25,17	20,63	23,01	22,24	24,98	25,55	19,45	14,88	14,15	20,12	21,11	14,62	12,19	9,70
MnO	0,70	1,00	0,80	0,44	2,09	0,49	0,65	0,58	0,69	2,04	1,30	1,95	0,55	0,34	2,63	1,84	4,02
MgO	4,79	5,77	5,52	4,60	10,30	5,79	6,90	5,78	6,22	10,87	7,00	10,57	8,53	8,74	12,96	14,67	15,56
CaO	0,12	0,78	0,28	0,16	2,52	0,32	0,39	0,35	0,79	4,24	2,97	4,29	1,15	1,30	6,42	8,81	11,21
Na_2O	6,24	6,10	6,37	6,32	4,71	6,23	5,66	6,21	6,10	4,09	2,94	1,84	6,01	5,98	3,16	2,34	0,91
K_2O	0,02	0,08	0,01	0,01	0,03	0,07	0,67	0,02	0,06	0,08	0,09	0,15	0,06	0,02	0,05	0,10	0,09
Cr_2O_3	0,00	0,02	0,00	0,01	0,02	0,00	0,08	0,00	0,08	0,07	0,01	0,00	0,00	0,01	0,00	0,04	0,03
Total	96,32	96,19	96,13	96,02	96,46	95,65	93,91	95,35	95,79	96,14	95,96	90,06	94,72	95,44	96,61	95,38	96,60
Si	7,947	7,875	7,924	7,982	7,809	7,888	7,601	7,888	7,898	7,737	9,155	8,370	7,971	7,957	7,818	7,820	7,778
Al^{iv}	0,053	0,125	0,076	0,018	0,191	0,112	0,399	0,112	0,102	0,263	0,000	0,000	0,029	0,043	0,182	0,180	0,207
Al^{vi}	0,840	0,370	0,357	0,842	0,078	0,861	0,635	0,571	0,386	0,047	0,292	0,505	0,612	0,501	0,166	0,105	0,000
Ti	0,000	0,007	0,002	0,001	0,000	0,008	0,007	0,004	0,001	0,003	0,007	0,000	0,003	0,000	0,003	0,001	0,002
Fe^{3+}	1,407	1,732	1,827	1,321	2,024	1,360	1,873	1,641	1,704	1,733	0,000	0,000	1,338	1,447	1,154	0,646	0,496
Fe^{2+}	1,623	1,496	1,288	1,773	0,445	1,450	0,881	1,440	1,453	0,621	1,755	1,823	1,121	1,118	0,595	0,837	0,676
Mn	0,086	0,125	0,112	0,055	0,253	0,060	0,081	0,072	0,087	0,250	0,155	0,255	0,068	0,041	0,319	0,227	0,492
Mg	1,043	1,270	1,414	1,008	2,199	1,261	1,522	1,271	1,370	2,346	1,471	2,427	1,858	1,893	2,763	3,184	3,349
Ca	0,019	0,123	0,118	0,025	0,387	0,050	0,062	0,056	0,126	0,657	0,449	0,707	0,180	0,203	0,984	1,374	1,734
Na	1,765	1,747	1,645	1,801	1,308	1,765	1,625	1,776	1,748	1,148	0,803	0,549	1,703	1,685	0,877	0,660	0,254
K	0,003	0,016	0,008	0,002	0,006	0,013	0,127	0,005	0,012	0,015	0,016	0,029	0,011	0,004	0,010	0,018	0,016
Total	16,787	16,886	16,770	16,828	16,701	16,827	16,814	16,836	16,886	16,820	16,102	16,666	16,894	16,893	16,871	17,052	17,004
Name	crossite	riebeckite	magnesio-riebeckite	crossite	winchite	crossite	magnesio-riebeckite	riebeckite	riebeckite	winchite	antho-phyllite	antho-phyllite	crossite	magnesio-riebeckite	winchite	actinolite	actinolite

Table 6: Representative examples of amphibole composition. Calculation based on 23 oxygen atoms per formula unit.

Sample	Kea0727A						Ki7061		
SiO2	26,22	25,90	26,78	36,06	37,30	26,58	25,85	26,24	25,88
TiO2	0,10	0,06	0,04	0,63	1,17	0,06	0,06	0,05	0,01
Al2O3	19,90	19,65	20,29	16,59	17,00	18,99	20,07	19,87	19,24
FeO	26,82	26,81	25,66	17,46	18,40	22,72	23,85	25,04	23,52
MnO	0,87	0,71	0,78	1,19	0,56	1,49	0,88	0,86	0,80
MgO	13,91	13,30	12,82	12,78	10,67	14,65	16,70	16,00	17,25
CaO	0,02	0,04	0,01	0,07	0,05	0,11	0,01	0,06	0,03
Na2O	0,01	0,00	0,03	0,02	0,05	0,00	0,00	0,04	0,00
K2O	0,07	0,09	0,02	7,42	8,64	0,15	0,00	0,05	0,00
Cr2O3	0,00	0,00	0,00	0,00	0,00	0,11	0,00	0,00	0,02
Total	87,90	86,55	86,43	92,22	93,85	84,85	87,41	88,21	86,75
Si	5,541	5,568	5,688	6,842	6,942	5,723	5,436	5,549	5,475
Al iv	2,459	2,432	2,312	1,158	1,058	2,277	2,564	2,451	2,525
Al vi	2,516	2,565	2,799	2,695	2,838	2,566	2,421	2,508	2,290
Ti	0,015	0,010	0,007	0,090	0,163	0,009	0,009	0,008	0,001
Fe3+	0,093	0,112	0,288	0,207	0,288	0,191	0,000	0,034	0,000
Fe2+	4,646	4,709	4,271	2,562	2,576	3,900	4,239	4,184	4,259
Mn	0,156	0,129	0,140	0,191	0,089	0,272	0,156	0,158	0,144
Mg	4,381	4,262	4,061	3,615	2,959	4,701	5,235	5,043	5,439
Ca	0,004	0,008	0,003	0,014	0,010	0,026	0,010	0,003	0,007
Na	0,007	0,002	0,021	0,012	0,034	0,002	0,000	0,030	0,001
K	0,037	0,048	0,012	3,591	4,103	0,081	0,013	0,000	0,000
F	0,160	0,109	0,054	0,096	0,047	0,109	0,000	0,000	0,000
Cl	0,007	0,007	0,007	0,006	0,006	0,007	0,000	0,000	0,000
OH*	15,832	15,884	15,939	15,898	15,947	15,884	16,000	16,000	16,000
Name	ripidolite	ripidolite	bruns-vigite	diaban-tite	diaban-tite	pycno-chlorite	ripidolite	ripidolite	ripidolite

Sample	Ki7061		
SiO2	37,10	37,29	36,94
TiO2	0,08	0,08	0,03
Al2O3	23,04	22,38	21,29
FeO	12,11	13,45	14,73
MnO	0,39	0,96	1,36
MgO	0,02	0,02	0,01
CaO	23,01	22,43	21,72
Na2O	0,00	0,00	0,01
K2O	0,01	0,00	0,01
Cr2O3	0,02	0,03	0,00
Total	95,77	96,65	96,09
Si	2,964	2,975	2,988
Al	2,169	2,104	2,030
Ti	0,005	0,005	0,002
Fe	0,809	0,897	0,996
Mn	0,026	0,065	0,093
Mg	0,002	0,002	0,002
Ca	1,969	1,917	1,882
Na	0,000	0,000	0,002
K	0,001	0,000	0,001
Cr	0,001	0,002	0,000

Table 7: Representative examples of chlorite (left) and epidote (right) composition. Mineral formula calculation based on 28 O for chlorite, and on 12 O for epidote.

List of Tables

1 Summary of major and minor element composition 59
2 Summary of trace element composition 60
3 Summary of REE content 60
4 Summary of chemical analyses 81
5 Garnet composition 82
6 Amphibole composition 83
7 Chlorite and epidote composition 84

List of Figures

1 Major geological units in Greece 11
2 Overview Cyclades 13
3 Faulting in the Eastern Mediterranean 15
4 Seismicity of the Eastern Mediterranean 16
5 Satellite image of mapping area 19
6 Geological Map of Kythnos Island 21
7 Lithostratigraphic columns 22
8 Thin sections of orthopyroxene in metabasite 24
9 Thin section of brown hornblende in metabasite 25
10 Metabasitic lithologies 26
11 Greenschists 27
12 Thin section of ferromanganoan metasediment 28
13 Thin section of tourmalinite 30
14 Thin section of marble mylonite 31
15 Albite gneiss 32
16 Albite-chlorite-mica-schist 33
17 Impure marble 35
18 Thin section of marble ultramylonite 36
19 Outcrop image of marble ultramylonite 37
20 Thin section of cataclasite 38
21 Thin section and outcrop image of quartzite 40
22 Plot of foliation planes and lineations 41

23 Foliation in Ep-schist 42
24 Isoclinal folding 43
25 Plots of fold directions 44
26 Refold structure in chlorite schist 45
27 Refold structure in epidote schist 47
28 Boudinage 48
29 Shear sense indicators 49
30 Marble ultramylonite shear zone 50
31 Buckle fold and fault bend fold 52
32 Plots of brittle fault planes 53
33 Large-scale normal fault 54
34 Synoptic diagram of deformation phases and major lithologies 56
35 Map of sample locations 59
36 BSE image of ferromanganoan metasediment 63
37 Garnet composition diagram 64
38 Thin section of sodium amphiboles in ferromanganoan metasediment . . 64
39 Classification diagram of alkali-amphiboles 65
40 BSE image of tourmalinite 66

Address and Contact Information

Personal address: Glasergasse 20/5, 1090 Vienna, Austria
Telephone: 0043 699 10269322 (mobile)
E-mail: iris.lenauer@univie.ac.at
Date and place of birth: April 16th, 1985 in Noordwijk (Netherlands)
Citizenship: Austria

Education

1989–2003: Primary and secondary education at Port Dickson Dutch School (Malaysia), Primarschule Gals (Switzerland) and Geelong Grammar School (Australia), Bundesgymasium Neusiedl am See (Austria) and Sir-Karl-Popper-Schule (Vienna, Austria)
2003: High school graduation with distinction at Sir-Karl-Popper-Schule, Vienna
2003-2008: Study of Earth Sciences at the University of Vienna
2007 Bachelor's degree with work on
(a) Field Geology during a Mars Analogue Simulation Experiment in the Utah Desert
(b) Comparison of Martian Meteorites with Terrestrial Equivalents

Work Experience

2008–2009: Student assistant for e-learning at the University of Vienna
2005–2007: Student tutor at the University of Vienna for the lab exercise "Chemistry for geologists"
2006: Internship at the geology lab at OMV (Vienna)
2003: Internship at the accounts department at Domus Facility Management, Bank Austria-Creditanstalt (Vienna)
2003–2007: Voluntary service in environmental projects with the ÖAV (Austrian Alpine Organization)

Abstracts

Lenauer, I., Mörtl, G., Iglseder, C., Grasemann, B., & Edwards, M. (2008). Field evidence for a major normal fault on Kythnos Island (Western Cyclades, Greece). Geophysical Research Abstracts 10, EGU2008-A-03218.

Lenauer, I., Mörtl, G., Grasemann, B., & Iglseder, C. (2008). Structural investigations along a low-angle normal fault zone (Kythnos, Greece). 01-03 July, 2008, International Meeting of Young Researchers in Structural Geology and Tectonics (YORSGET), abstract volume, Trabajos de Geología, Oviedo, Spain.

Further Skills

IT: MS Office, Corel Draw, Tectonics FP, ArcGIS, GoCAD/AutoCAD, LateX

Languages: German (native speaker), English (fluent), French, Italian, Russian (basic)